Alternative Amphiphilic Antifouling Strategies Using Fluorous Moieties

Jules Thenin

University of Glasgow

Thesis submitted in fulfilment of the requirements for the degree of Master of Research (MScR), 2025.

School of Chemistry

College of Science and Engineering

University of Glasgow

Declaration

The work described in this thesis was carried out at the University of Glasgow between 2023 and 2025, under the supervision of Dr. William Peveler and Dr. Alasdair Clark. All work submitted is my own, unless stated to the contrary, and has not been previously submitted for any degree at this or any other university.

Jules Thenin

August 2025

Abstract

Nonspecific adsorption of chemical species onto sensing surfaces, commonly referred to as fouling, poses a significant challenge in biosensing, particularly for label-free detection methods. Fouling can compromise both the accuracy and selectivity of these techniques by interfering with the sensor's ability to distinguish target analytes from background species.

To address this issue, the development of antifouling surface chemistries has emerged as a promising strategy to reduce or eliminate unwanted interactions. However, many existing antifouling agents fail to provide consistent protection against a broad spectrum of proteins. In this thesis, a series of antifouling molecules incorporating a pentafluorobenzyl moiety were designed to create amphiphilic surfaces as a less harmful alternative to traditional polyfluoroalkyl substances. These molecules were successfully functionalized onto gold nanostructures to form self-assembled monolayers.

Localized surface plasmon resonance, a label-free analytical technique, was employed to evaluate the antifouling performance of the functionalized surfaces. All tested surfaces demonstrated improved resistance to fouling by bovine serum albumin compared to unmodified gold. Additionally, a mixed monolayer incorporating both antifouling molecules and anti-BSA antibodies was fabricated to serve as a biosensing interface. This mixed surface was designed to selectively detect target analytes via antibody recognition while repelling nonspecific protein adsorption through the antifouling component. Although the experimental data were inconclusive, the PFB-based mixed surface exhibited antifouling behaviour comparable to that of a control surface functionalized with polyethylene glycol.

Acknowledgements

I would like to thank my primary supervisor Dr. William Peveler for providing me with the opportunity to work within their laboratory, as well as their support and patience throughout my work. In addition, I'd like to extend thanks to all the current and past members of the Peveler group, Isla, Ross, Celeste, etc.

Specifically, thank you to Liam Wilson, a key member of the Peveler group, for their help, advice and supervision. In addition, a special thanks to Daniel Osborne for his guidance and assistance in synthesising compounds used in my work.

A great deal of help was provided by my secondary supervisor Dr. Alasdair Clark and all current and past members of the Clark Group, in particular, Justin Sperling who greatly assisted in all LSPR experiments and data acquisition, as well as former member Calum Cuthill, who was the principal designer for the software used for all LSPR data acquisition and management.

Definitions/Abbreviations

BSA	Bovine serum albumin
ELISA	Enzyme-linked immunosorbent assay
LFA	Lateral flow assay
QCM	Quartz Crystal Microbalance
BLI	Biolayer interferometry
MCL	Microcantilever-based sensor
UV	Ultraviolet
SPP	Surface plasmons polariton
LSP	Localized surface plasmon
SPR	Surface plasmon resonance
TIR	Total internal reflection
FO-SPR	Fiber Optic Surface Plasmonic Resonance
LSPR	Localized surface plasmon resonance
SAM	Self assembled monolayer
PEG	Polyethylene glycol
DNA	Deoxyribonucleic acid
LOD	Limit of detection
ATR-FTIR	Attenuated total reflection Fourier transform infrared spectroscopy
FITC	Fluorescein isothiocyanate
PFAS	Per- and polyfluoroalkyl substances
PFB	Pentafluorobenzene
CFL	Codium fragile
LPSE	Lipopolysaccharide from E. coli
LPSS	Lipopolysaccharide from Salmonella Minnesota
THF	Tetrahydrofuran
DCM	Dichloromethane
HPLC	High-Performance Liquid Chromatography
NMR	Nuclear Magnetic Resonance
EtOAc	Ethyl acetate
LED	Light-emitting diode
AIBN	Azobisisobutyronitrile
PTFE	Polytetrafluoroethylene
PBS	Phosphate-buffered saline
RI	Refractive Index
CMOS	Complementary Metal-Oxide-Semiconductor

Table of Contents

List of Figures

1 Introduction

1.1 Fouling and Antifouling

Fouling is when unwanted cells or large molecules, including inorganic, or organic molecules, adsorb onto a surface.[1,2] The fouling process occurs when molecules initially bind to a surface through electrostatic forces and Van der Waals interactions. This unwanted or non-specific adsorption is often encountered in biosensing, where unintended binding of molecules beyond the scope of the sensor, stick and reduce over-all sensitivity. Non-specifically bound molecules fixed to a surface can develop into films that eventually irreversibly bind to that surface.[3]

Numerous applications have been negatively impacted by this phenomenon. Within marine and shipping industries, fouling has caused considerable issues, specifically by increasing the drag on vessels and hindering ships' structural integrity.[4,5] In biomedical applications, fouling of bacteria and proteins has increased the rate of infections with medical implants. The degradation of medical implants has been shown to increase as fouling increases.[6] Similarly, within optical and electrochemical sensors, especially label-free methods, fouling has the potential to cause false positives as well as irrepeatability.[7]

Many fields of study have therefore explored methods of fouling prevention or 'antifouling' to reduce or prevent issues arising from fouling. Though the phenomenon of fouling has been known for decades in the field of chemical sensing,[7-9] as new applications for surface-based sensors are developed, new antifouling strategies must also be created. Sensor technologies have required a diverse range of antifouling strategies depending on the target analytes and detection methods used.

1.2 Protein Sensing

The study of proteins and their interactions with each other as well as with other molecules is fundamental in understanding biological systems, disease and the development of modern medicine. Some sensing methods which can be used to gain this fundamental understanding rely on surfaces to take their measurements. However, as discussed in Section 1.1, proteins tend to non-specifically bind to many different surfaces.[10,11] Van der Waals forces, hydrophobic interactions, steric repulsion, electrostatic repulsion, hydrogen bonding and surface topography effects govern the nonspecific binding of proteins. Commonly investigated

media in biosensing, like blood and serum, have over 1000 unique proteins at various concentrations, ranging from >50 mg/mL of human serum albumin down to <10 pg/mL for rarer proteins like interferon γ.[12] The surfaces of proteins and other large biomolecules are complex and can have various properties. Even a single protein can incorporate hydrophobic, hydrophilic, negatively charged, and positively charged portions.[10,13] This complex surface morphology (Figure 1) makes proteins readily available to bind to any surface, as a protein's surface morphology allows it to modulate its orientation to better match a surface's morphology.[14]

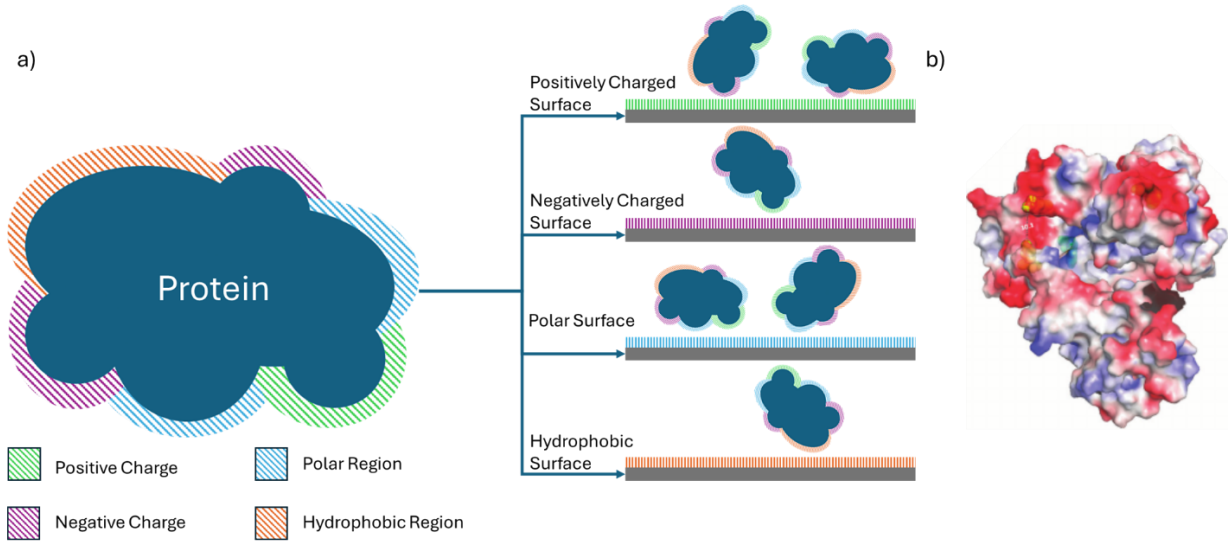

Figure 1. Representation of a protein's complex surface morphology, where a) is a diagram showing how a protein's complex surface can bind to a variety of different surfaces and b) is a charge map of a bovine serum albumin (BSA) protein collected by Goovaerts et al. using electrostatic surface potential calculations, where red is negatively charged portions and blue is positively charged portions of the protein.[15]

Kalasin et al. described an example of the modular orientation of proteins that can increase fouling.[11] Specifically, Kalasin et al. showed how fibrinogen, a protein essential to the clotting of blood which has an overall net negative charge, may have small positively charged portions that can induce binding onto a surface that has an overall negative charge.[11] The complexity of a protein's surface becomes even more confounding when taking into account how proteins tend to unfold. As interactions start to pull on a protein once they adsorb onto a surface, the structures of the protein can unravel, increasing the protein's surface area and exposing differently charged portions which normally would not be able to interact. High energy and charged surfaces like metals cause the denaturing and unfolding of proteins, exposing a protein's hydrophobic core that then can irreversibly bind to the surface.[16] Hydrophobic surfaces cause a similar issue, as hydrophobic interactions are essential to the structuring of proteins and can cause a protein's structure to change and denature. Once a protein would denature, the exposed core can irreversibly bind to a hydrophobic surface.[13] Metal's tendency to electrostatically attract and unfold proteins has been a significant issue for detection methods that rely on metallic surfaces.[10]

The ability to measure and determine protein interactions in a fast, reusable, and inexpensive process is a key goal in modern analytical science, and a huge number of potential methods have arisen. Though this ideal goal has been difficult to achieve, various methods have been used to detect proteins.[17] To get a more complete understanding of how proteins are measured in different biochemical applications, a broad understanding of methods used to detect proteins, even those which do not rely on the use of surfaces for detection, must be described. Many of these methods used for sensing have had several limitations depending on how they are used.

1.2.1 Detection Strategies of Proteins: An Overview of Standard Techniques

Enzyme-linked immunosorbent assay (ELISA), one of the most common methods of protein detection, has been widely used in hospitals worldwide.[17] Enzyme immunoassays like ELISA provide quantitative analysis by inducing a colour change through an enzyme-linked conjugate and substrate reaction with antibody-antigen binding.[17,18] These interactions are highly selective, enabling the detection of trace analytes in complex media. However, labelled detection methods, such as some forms of ELISA, can require multiple antibody bindings per analyte, which can alter its native structure and affect biomolecular studies.[19] Label utilization also increases cost, posing a disadvantage compared to label-free sensing techniques.[17]

Lateral flow assays (LFA) operate by using capillary action, allowing a liquid sample to travel across a membrane-based strip, where labelled antibodies bound to target analytes and generate visible or measurable signals.[20] The sensor consists of several components mounted on a plastic backing, including a sample pad, conjugate pad, nitrocellulose membrane, and absorption pad, each containing pre-immobilized reagents and antibodies.[20,21] Upon sample introduction, a colour change caused by the accumulation of nanoparticle-labelled antibodies bound to a target, indicates the presence of the target protein.[21] LFA is advantageous due to its low cost, simplicity, rapid detection, and broad applicability. However, it is mostly limited to qualitative measurements. In addition, non-specific binding has a major impact on LFA. Biomolecules non-specifically binding to a surface can compete with a desired analyte, resulting in the need of more target analyte to obtain a signal, lowering the sensitivity and causing false negatives. In a similar fashion, different proteins can compete for antibody binding sites, causing false positives.[20,21]

Quartz crystal microbalance (QCM) is a highly sensitive, label-free molecular detection technique based on the piezoelectric effect.[22] It detects mass changes at the antibody-

immobilized surface by measuring the quartz crystal's resonant frequency shifts. This real-time method can detect differences in the sub-nanogram range.[23] However, QCM performance can be affected by variations in viscosity and temperature of the medium used. Additionally, nonspecific binding remains a challenge for QCM. Much like LFA, non-specific binding has prevented subsequent binding of a target protein to its imprinted cavities, which can reduce a sensors sensitivity and selectivity.[22,23]

A similar method to QCM are microcantilever-based sensors (MCLs), which are the simplest micro-electromechanical systems, offering high sensitivity for detecting chemical, physical, and biological targets.[24] MCLs function by measuring changes in surface mass or stress via shifts in cantilever resonant frequency.[25] A cantilever, a small fixed and free-moving beam-like structure, acts as a mechanical transducer, enabling label-free, rapid, and cost-effective detection. MCLs have the potential for miniaturization and portability, though MCLs have issues regarding signal interference in liquids, and cross-reactivity. Additionally, MCLs are susceptible to false positives, as nonspecific binding of proteins onto the cantilever's surfaces can cause unintended changes to the sensors surface mass.[24,25]

A high throughput and label-free method that has been used for the biosensing of proteins is biolayer interferometry (BLI). BLI is a disposable, real-time optical technique based on antibody-antigen interactions.[26,27] BLI measures interference patterns from white light reflected by two surfaces at the biosensor tip: a reference and a ligand-functionalized sample surface. As the sample flows over both surfaces, a comparison between the two surfaces enables accurate detection of analyte binding to the coated biomolecule in real time. BLI has been utilized in vaccine research and development as, unlike other methods, BLI is not affected by mass-transport limitations or artefacts caused by chemical microheterogeneity on a biosensor surface. However, BLI struggles with low sensitivity, especially compared to methods like surface plasmonic resonance (see below in Section 1.2.3). A key foundational issue regarding BLI is how it is limited to detecting larger biomolecules. Furthermore, BLI is susceptible to nonspecific binding, as nonspecific binding onto sensing surfaces can cause steric hindrance, where too much of the sensing surface becomes occupied by biomolecules. The saturation of a surface can leave no physical space for the needed conformational change, resulting in a false reading for low analyte abundance.[26,28]

Electrochemical biosensors are devices which utilize two parts, the first being chemical detection methods which produce an electrical signal to monitor analyte concentration: methods like voltammetry, potentiometry and impedance spectroscopy. The second part essential to electrochemical biosensors is a biological recognition element, like an enzyme, antibody, or nucleic acid, which can selectively interact with a target analyte.[29] These sensors offer high sensitivity, specificity, rapid detection, and minimal sample preparation. Electrochemical biosensors can also be miniaturized for portable, cost-effective

applications.[29,30] However, nonspecific binding has a major effect on electrochemical biosensors, specifically by increasing the background noise of devices. The increase of background noise reduces the signal-to-noise ratio, which lowers the limit of detection of electrochemical devices.[16]

1.2.2 Plasmonic Sensing

Another form of sensing which has been utilized heavily since the 1990s for protein detection is plasmonic sensing. Plasmonic sensing is another label-free method which relies on plasmons; resonant modes that involve the interactions between electromagnetic fields and free-moving electrons.[7,31] Plasmons derive from plasma, a media that possesses freely mobile electrons. Metals are used in plasmonic applications because their free electrons behave collectively like a plasma. The oscillation that occurs in plasmons has a resonate frequency, which depends on the number density of mobile charge carriers, their charge, their mass and their relative permittivity of free space.[32] This bulk plasmon frequency, ω_p^2, can be described by

$$\omega_p^2 = \frac{ne^2}{\varepsilon_0 m}$$

where n is the number density of mobile charge carriers, e is their charge, m is their mass, and ε_0 is the relative free space permittivity.[33]

Many different factors, including the nearby passing of an electron can influence this bulk frequency.[32] As the properties of the equation above change, an example being due to the metallic media itself, changes can be seen in the bulk frequency. The resonance frequency of all metals is unique due to this property, and some metals, like silver and gold, have bulk frequencies in the visible and UV range.[32,34] As plasmonic sensing is focused on resonant modes, it is important to note that there are two variations of plasmonic modes. The first are localized surface plasmons (LSPs), which occur when free electrons within a metallic nanoparticle or nanostructure oscillate collectively, resulting in strong light confinement at nanoscales. The second type are surface plasmons polaritons (SPPs), which are waves that propagate at the metal-dielectric. SPPs occur at a much larger scale when compared to LSPs, with the propagating waves extending over tens of micrometres in the parallel (in-plane) direction, along the metal–dielectric interface. [31,32,35,36] SPPs have been explored as a way of providing tighter integration of optical signals compared to methods relying on the use of dielectric light guides.[37]

1.2.3 Surface Plasmon Resonance Sensing

Surface plasmon resonance (SPR) is a physical phenomenon in which SPPs, coherent electron oscillations at a metal–dielectric interface, coupled to an electromagnetic wave.[27,38] Sensing methods have been developed by exploiting SPR, which can enable the detection of molecular binding events. The SPPs which allow for resonance can be defined by this wavevector,

$$k_{spp} = \frac{\omega}{c}\left(\frac{\varepsilon_d \varepsilon_m(\omega)}{\varepsilon_d + \varepsilon_m(\omega)}\right)^{\frac{1}{2}}$$

where ε_d is the isotropic, real and positive dielectric constant of the dielectric medium and ε_m is the frequency dependent complex dielectric constant of the metal.[39] When resonance occurs and energy is efficiently transferred from the incident light to SSPs propagating along the metal–dielectric interface, a sharp dip in reflected light intensity can be observed. This dip arises because the coupled energy is no longer reflected but instead used to excite the plasmon mode, reducing the reflected signal at the resonance angle or wavelength.[27] This resonance condition is extremely sensitive to changes in the local refractive index, which can be described (if assuming ε_d is comparable to relative permittivity and the medium is non-magnetic) by the equation

$$n = \sqrt{\varepsilon_d}$$

where n is the local refractive index. When molecules bind to receptors immobilized on the metal film, they change the local dielectric environment, shifting the resonance angle or wavelength.[40] This shift is monitored in real time as a change in the reflectivity profile, allowing for quantitative analysis of the presence, concentration, and kinetics of the binding molecules.[38]

To achieve resonance and properly excite the surface plasmons, the wavevector of the surface plasmons (k_{sp}) must be matched with the wavevector of the incident light (k_x).[27,39] In order to achieve the matching of wavevectors, a technique called total internal reflection (TIR) is used. To attain TIR, the light sources used must be directed using p-polarized light through a dielectric material (such as glass) at an angle greater than the critical angle (the minimum angle needed to create TIR).[27,38] At an angle greater than the critical angle, the light generates evanescent waves, which are electromagnetic waves that form at the interface between two media when total internal reflection occurs. This evanescent wave decays exponentially as they move away from the interface. These waves extend about one wavelength into the metal-dielectric boundary, effectively increasing the wavevector of the incident light.[27] The enhanced wavevector allows for better coupling with surface plasmons, facilitating SPR. By utilizing TIR, k_x is increased and is described by the following:

$$k_x = k_0\sqrt{\varepsilon_d}\sin(\theta) = \frac{2\pi}{\lambda}\sqrt{\varepsilon_d}\sin(\theta)$$

Where ε_d and θ are the dielectric constant of the dielectric material and the angle of incidence, respectively, using this strategy, if k_x and k_{sp} can be set to the same value, surface plasmons will be excited and resonate.[27] The surface plasmon excitation appears as a dip within the reflectance spectrum.[27,38] When the surrounding medium of the surface plasmons changes, so does the refractive index; this results in an alteration in k_{sp}, which shifts the observable dip in the reflectance spectrum. This visible shift of the dip within the reflectance spectrum due to a change in the dielectric medium is the fundamental principle which governs SPR.[27,41]

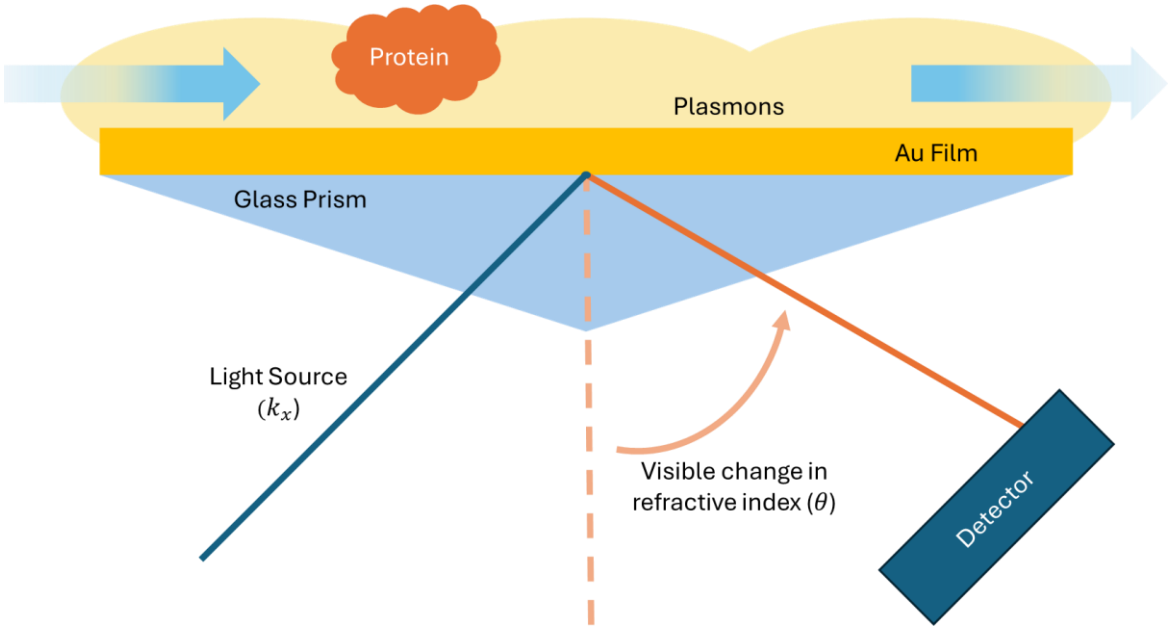

Figure 2. The general set up of a SPR sensor, utilizing a gold film and a glass prism as the dielectric medium. The presence of an adsorbed biomolecule can be observed by a change in reflectance spectra caused by a change in refractive index.

There are several different variations of SPR. As described previously, k_x is reliant on θ as well as λ, thus either of these can be used to tuned k_x. The most common method for tuning k_x is changing the incident angle to stimulate the SPPs (Figure 2). This method is called angle-based SPR (q-Modulation), which typically uses a glass prism and is utilized in most commercial SPR devices.[27,42] Alternatively, instead of a prism, a method named Fiber Optic Surface Plasmonic Resonance (FO-SPR) is a variation of SPR that utilizes an optical fibre instead of a prism. FO-SPR has an advantage over traditional SPR since FO-SPR can result in smaller and easier to implement sensors.

1.2.4 LSPR Sensing as an Alternative to SPR

Local surface plasmon resonance (LSPR) is a distinct yet related phenomenon to SPR and has been used to enhance sensing sensitivity when compared to traditional SPR techniques.[27,31] LSPR, unlike SPR, relies on using LSPs to visualize a change in the resonance condition of nanoparticles, which can be observed using reflectance, transmission or scattering.[43] Instead of utilizing a bulk metallic surface – as in the case of SPR - nanoparticles or nanostructures which are smaller than the wavelength of the resonating plasmons are used.[27] SPR relies on propagating SPs at a metal-dielectric interface and is typically detected as a dip in reflectance spectra using a prism-based setup.[39] In contrast, LSPR occurs in nanostructures that allow light to pass through or around them (Figure 3), but at the resonance wavelength, the collective oscillation of surface electrons leads to strong absorption and scattering of light, reducing the amount of light transmitted. As a result, resonance appears as a dip in the transmission spectrum.[31]

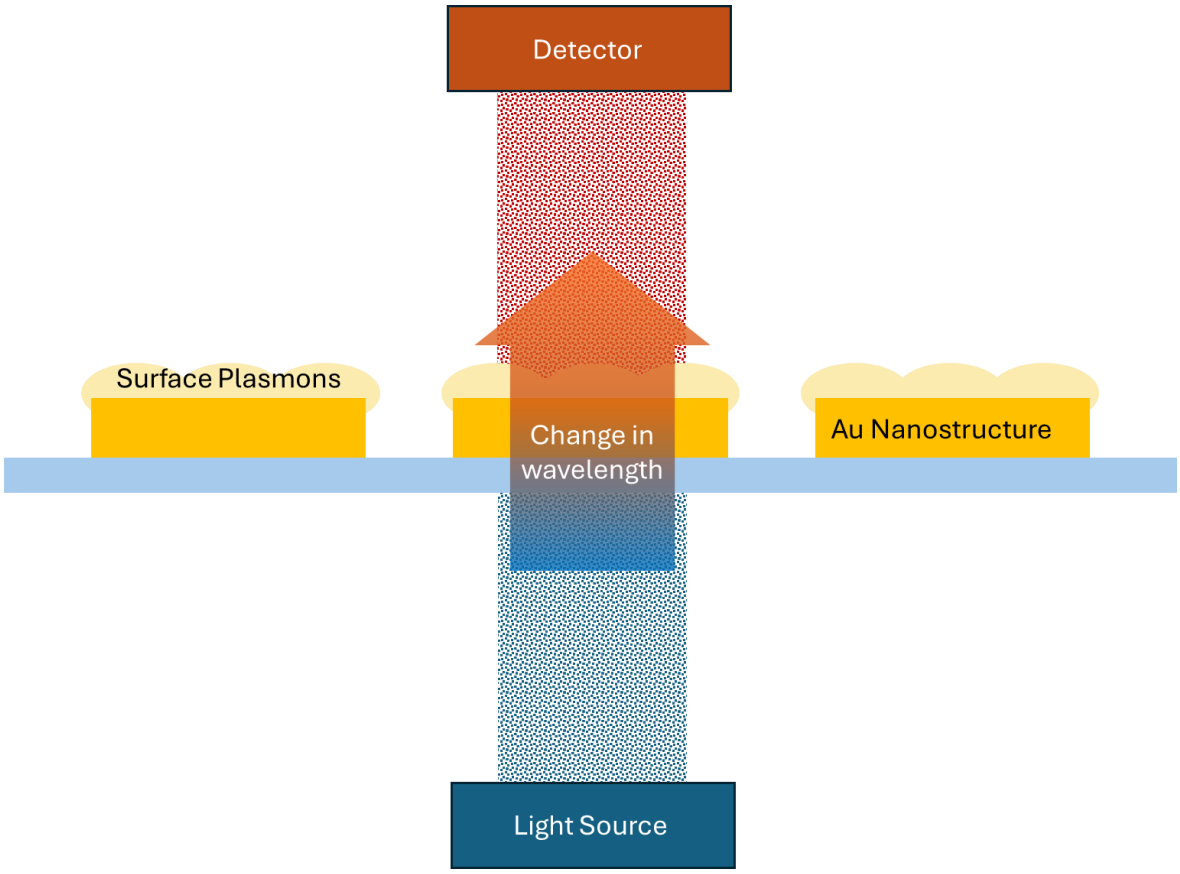

Figure 3. Schematic of a typical LSPR sensor setup. This configuration uses gold nanostructures to induce plasmon resonance without the need for a glass prism. The presence of an analyte is detected through a shift in the resonance wavelength, observed as a change in the transmission minimum. A detector on the other side of the nanostructures is used to find this change.

The use of nanostructures makes LSPR significantly more sensitive than traditional SPR, owing to the shorter electromagnetic field decay length and stronger near-field enhancement associated with the localized plasmonic modes. The localized surface plasmons in nanoparticles generate fields that decay over just ~10 nm when compared to ~200 nm in SPR, allowing for highly selective detection of molecules close to the surface.[31] This tight confinement also leads to greater electromagnetic field intensity at the nanoparticle surface, amplifying the response to binding events and enabling single-molecule sensitivity. [27,31,32] The frequency of the LSPs depend on the nanostructures' size, geometry and composition. The LSPR peak wavelength (λ_{max}) is described as,

$$\lambda_{max} = \lambda_p \sqrt{2n_m^2 + 1}$$

Where λ_p is the wavelength corresponding to the plasma frequency of the bulk metal, and n_m represents the refractive index.[31] This dramatically simplifies LSPR when compared to SPR, as LSPR does not require the matching of the incident light wave vector and plasmonic wave vector. Since the wavevectors do not need to be matched, using glass prisms or optical fibres is not necessary, which decreases the complexity and the cost of LSPR devices compared to SPR.[31,32,36] Furthermore, LSPR is less temperature sensitive than SPR. These differences have caused LSPR to be optimal for more diverse applications, as it can be incorporated into more portable systems and better utilized in the creation of sensing arrays. A key difference to highlight regarding LSPR is its shorter sensing distance, as SPR has a sensing distance of around 1000 nm, whereas LSPR has a sensing difference of around 10 nm. At greater distances, the sensitivity of LSPR decreases due to the reduced penetration depth of the evanescent field, however LSPR's sensitivity at those lower distances is much greater.[31]

1.3 Self-Assembled Monolayers and their use in Plasmonic Sensing

LFA, QCM, BLI, MCL's, electrochemical biosensors, SPR and LSPR are all reliant on surfaces to function and to engineer specificity. Metallic surfaces are commonly utilized for these methods of sensing, and a great benefit to metallic surfaces is their modifiability, with surfaces being easily tailored for a specific application by the formation of a self-assembled monolayer (SAM).[44,45] SAMs are a method for creating organized and complex surface chemistries. They form through a self-organizing process in which molecules covalently, yet reversibly, adsorb onto a metal surface. These molecules pack closely together, with their packing arrangement governed by a hierarchical system of supramolecular interactions.[46,47]

Gold (Au), has been the most utilized in biosensing methodologies due to its noble character, which has ensured stability and resistance to oxidation and other reactions.[32,48,49] Thiols can easily form SAMs at gold interfaces due to the Au-S's strong covalent soft-soft bonding.[50,51]

The most widely studied SAMs are Au-alkane thiolates, which have been utilized in various fields. Alkanethiols have been seen to bind to a surface in a two-step process, the first being the faster initial adsorption of the thiol to the gold surface and the second being a slower restructuring process that eventually achieves optimal molecular packing. During each of these steps, several factors (time, solvent and molecular structure) have been shown to affect the formation of a SAM significantly.[45,48,52,53]

Time has been a significant factor in the creation of SAMs.[49] Ganesh et al. found that if SAMs were given more time to assemble, it improved alkoxycyanobiphenyl thiol monolayer characteristics.[52] There is a large amount of variation regarding the amount of time needed to form SAMs, as more volatile adsorbents could take a matter of minutes to form a SAM. In contrast, less volatile molecules could take hours to even days to properly form.[45,52] More specifically, regarding the properties of the molecules used to form SAMs, shorter-chain thiols exhibit a faster initial adsorption onto surfaces due to their higher mobility and volatility.[54] In contrast, thiols with longer alkyl chains, though slower to adsorb initially, promote more effective molecular reorganization and alignment over time due to stronger Van der Waals interactions associated with larger molecules, resulting in the formation of more uniform and well-ordered monolayers.[55]

The concentration of thiol molecules plays a significant role in the formation of SAMs. Higher concentrations (typically in the mM range) accelerate the initial adsorption process, leading to rapid surface coverage.[56] However, the slower secondary phase of SAM formation, involving molecular reorganization and alignment, occurs over several hours and is largely independent of thiol concentration.[57] This indicates that while high concentrations promote fast adsorption, they do not necessarily enhance the quality or uniformity of the final monolayer.

Solvents also have significant impacts on the formations of SAMs, as the rate of adsorption, the packing density, and the final structure of the monolayer can be affected by the solvent's polarity or viscosity.[45] The most common solvents used for alkanethiols are both ethanol and methanol. These polar solvents have been shown to form denser monolayers faster. Dimethylformamide has also been utilized for molecules that are harder to dissolve in alcohols, though more time is required to produce efficient SAMs than with ethanol and methanol.[45,53] Some less commonly used solvents for SAM formation include water, although it is rarely employed on its own. Yan et al. demonstrated that effective and uniform hexadecanethiolate SAMs could be formed in an aqueous micellar solution.[58]

The parts of the molecules used in SAMs that contribute most to structural integrity are known as spacers. Spacers reduce steric hindrances, optimize molecular orientation and therefore increase binding efficiency, overall improving SAM structure and organization.[59] Within alkanethiols, the alkane portion is considered the spacer (Figure 4). It is where most of a SAM's

stability stems from, as this hydrophobic portion aggregates onto the surface, helping in the self-organization of the monolayer.[46,47,49,60]

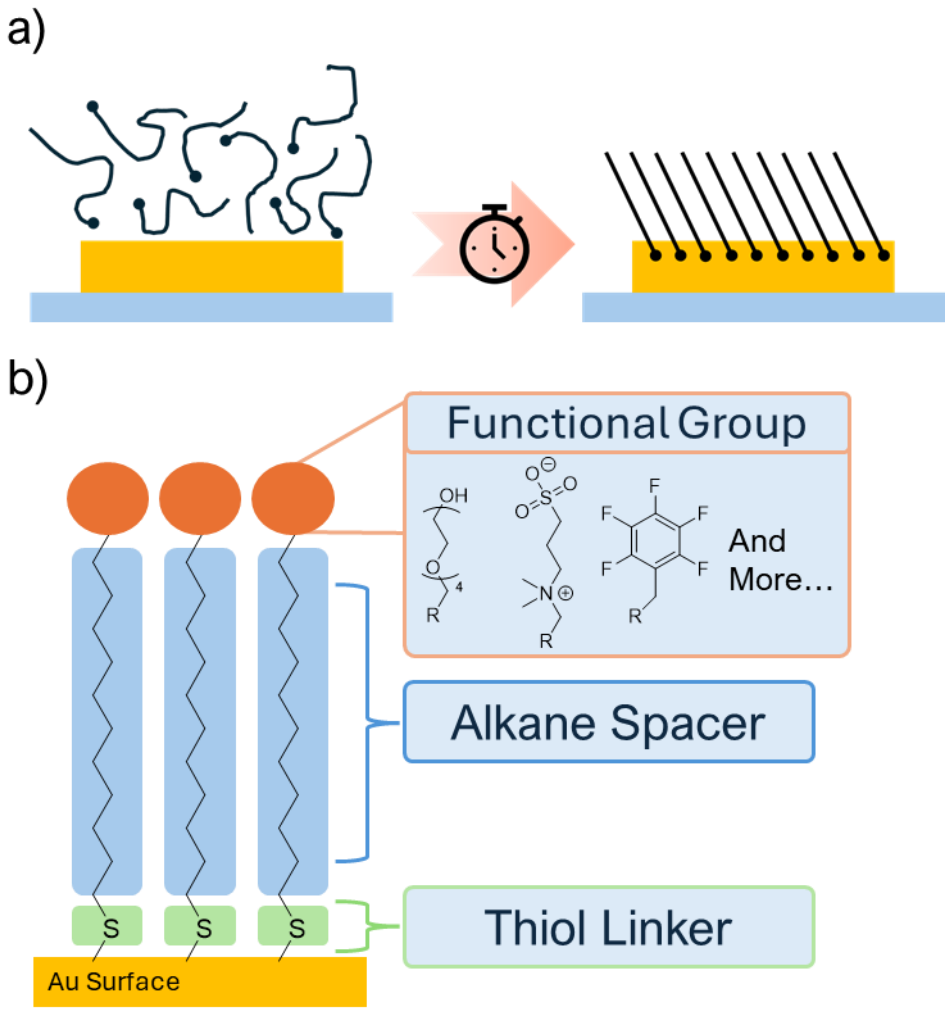

Figure 4. Key characteristics of SAMs, a) the self-alignment of SAMs moderated by time. b) A visual for the different portions of the molecules used to create SAMs, including a thiol linking the molecule to the gold surface, the 11 carbon alkane spacer, as well as functional groups (PEG, zwitterionic and pentafluorobenzyl molecules).

Furthermore, the alkane portion has led to stable monolayers in various environments; Xu et al. provided evidence that alkanethiol SAMs are densely packed and stable in water or hexadecane once formed.[45] The most effective SAMs that utilize alkanethiols are >10 carbons long, as longer chains have stronger Van der Waals interactions between each other, which help with SAMs' formation process, stability and density.[47,49]

Polyethylene glycol (PEG) and other glycolic molecules have also frequently been used as spacers, especially when incorporated alongside alkanes within SAMs to enhance molecular orientation and structural stability.[61,62] The hydrophilic nature of PEG contrasts with the hydrophobic properties of alkane chains, which creates opposing interactions that drive the organization of the monolayer.[46,47,49,60,62] During SAM formation, these interactions have

promoted the separation of hydrophilic and hydrophobic regions, ensuring that the hydrophilic PEG segments preferentially associate while minimizing unfavourable exposure to the hydrophobic alkane components. This phase separation contributes to the overall structural integrity and functional optimization of the SAM.[46,47,49,60,62] Another functionality of spacers has been their use to elevate the targeting body away from the surface of the monolayer for biosensing applications.[59,63] By separating the targeting molecule above a SAM, it provides room for the desired analyte to react and adsorb to the functionalized targeting molecule, reducing the steric hindrance on the surface.

The incorporation of a targeting molecule onto a SAM is essential to engineer selectivity, and the way targeting molecules have been engineered into SAMs have been through tail groups. A tail group is a terminal functional group (Figure 4) of the molecule used within a SAM, and is the portion of the SAM exposed to the surface.[49,64] Much of a SAM's versatility results from the use of different tail groups, which have allowed SAMs to be utilized in so many biosensing applications.[49,63,65] Tail groups play a major role in the creation of detection surfaces but have also been utilized to create both antifouling surfaces and detection surfaces.[66]

Carboxyl groups have been commonly used as a tail group within SAMs.[61] Carboxyl groups have been used to help with the immobilization of DNA, antibodies and biotin (for avidin linkage) onto SAMs by reacting the carboxyl group with N-hydroxysuccinimide (NHS) to form an activated ester.[49,67] This NHS ester can subsequently react with free amine groups in biomolecules, such as those found in lysine residues, thereby anchoring them to the SAM. Amines can also be used as a tail group and can be used to incorporate many of the same biomolecules mentioned above using a similar NHS reaction with a carboxyl group on a target molecule.[48]

Biotin-based affinity strategies represent one of the most widely utilized approaches in biosensor design due to the exceptionally high binding affinity between biotin and tetravalent (strept)avidin, as these have a dissociation constant of $K_d = 10^{-15}$ M.[61,68] This strong interaction has facilitated the development of modular biosensor design. The process typically involves the functionalization of a molecule which incorporates biotin, and a thiol used to bind onto a gold surface, followed by the attachment of tetravalent (strept)avidin to the created biotin-functionalized monolayer. Once the surface has been coated with streptavidin, it serves as a platform for the selective detection of a target biomolecule which has been modified to contain biotin (Figure 5).[61]

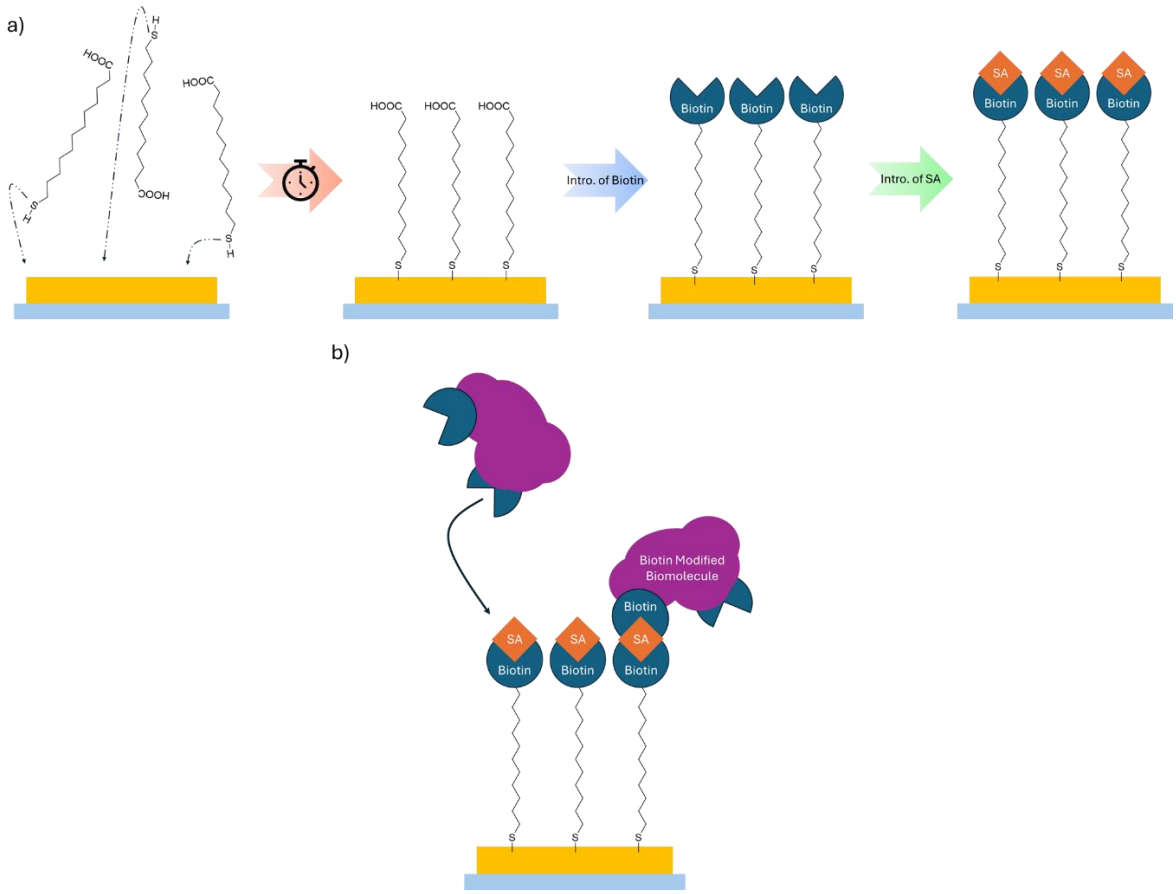

Figure 5. a) Process of creating a biotin-based affinity sensing surface, starting with the creation of a SAM utilizing a carboxyl containing molecule, followed by the introduction of biotin, and lastly the introduction of (strept)avidin (SD). b) Biotin layer sensing a biotin modified target biomolecule via biotin's affinity to SD.

Employing this method, Dutra et al. utilized a biotin-SAM-based sensing methodology that used SPR to detect cardiac troponin T with a linear range from 0.03 up to 6.5 ng/mL and a detection limit of 0.01 ng/mL.[69] The use of biotin-based affinity strategies has been extensively applied in biosensing applications for several decades, offering a robust and specific mechanism for biomolecular immobilization. The utilization of an adsorbent used to bind to a surface, a spacer, and a tail group has led to a heavily modular system which has allowed SAMs to be used in a variety of different fields and biosensing methodologies.

In biosensing two common variations of SAMs have been utilized, pure and mixed monolayers (Figure 6).[49] The former is where one molecule is used for the creation of a monolayer, whereas mixed monolayers have a layer of at least two different thiols that can vary in ratio and a random ordering.[49]

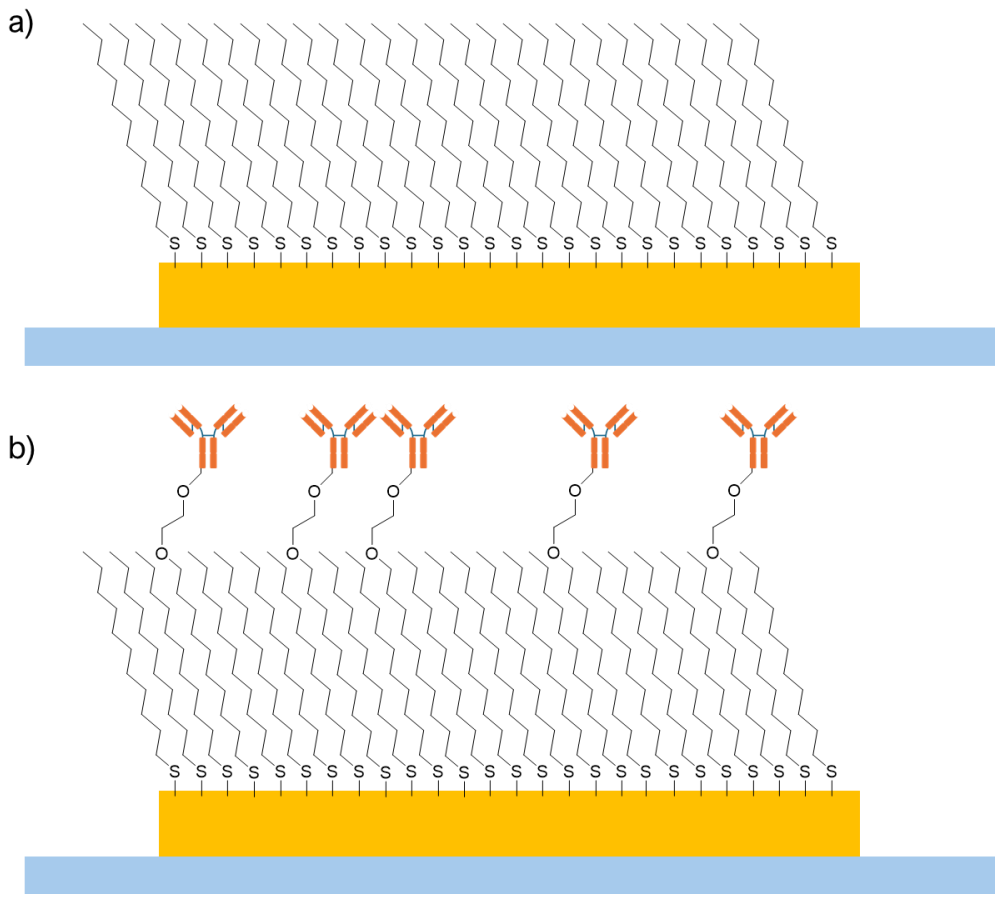

Figure 6. The difference between a) pure monolayer and b) mixed monolayer utilizing an antibody and a spacer.

There have been particular reasons for utilizing either a pure or mixed monolayer; pure monolayers have been used to create simpler and denser monolayers, which are optimal for creating resistant and stable coatings.[49,70] Mixed monolayers are optimal for the creation of surfaces that improve biomolecule accessibility by both modifying the density and by separating targeting groups (antibody, biotin, etc.) above the monolayer, ameliorating their ability to bind to their target.[48] Mixed monolayers have also allowed for more modular surfaces that can be modified to have a desired hydrophilicity or targeting efficiency. Due to this high modularity, mixed monolayers have been employed to create surfaces that enable both detection and antifouling simultaneously. Their combined antifouling properties and accessibility to biomolecules make them particularly useful in the development of biosensors. Liu et al. created a mixed monolayer that utilized an antifouling agent, and an antibody bound to the monolayer by a carboxyl group.[71] The created mixed monolayer surface was utilized with SPR to detect cardiac troponin T and could resist fouling from proteins 85% more efficiently than bare gold. The surface created a strong linear correlation ($R = 0.991$, $P < 0.0009$) at concentrations lower than 50 µg/mL of cardiac troponin T, with a 100 ng/mL LOD. The ease of creating SAMs has allowed sensors that rely on metallic surfaces to become more variable, diversifying the types of target analyte that methods such as LSPR and SPR can detect.

1.4 Antifouling Strategies and their Importance with LSPR

Various analytical techniques have been employed to evaluate the effectiveness of antifouling strategies in surface chemistry. Attenuated total reflection Fourier transform infrared spectroscopy (ATR-FTIR) is a label-free, non-destructive technique that analyses molecular vibrations to study chemical composition, protein secondary structure, and biomolecular interactions by measuring infrared adsorption at a crystal-sample interface.[72] Ellipsometry is another optical technique which measures changes in polarized light reflection to determine thin-film thickness. Ellipsometry has often been used to compare the thickness of accumulated biomolecules on surfaces.[16,73] Finally, fluorescence microscopy is a method that utilizes the fluorescence of dyes incorporated into biomolecules to measure their accumulation. Regarding the study of antifouling, fluorescence microscopy has commonly used fluorescein isothiocyanate (FITC)-labelled BSA to visualize and track protein accumulation regarding antifouling.[74-76]

All label-free methods of sensing, including plasmonic sensing, have had serious drawbacks when it comes to protein sensing, as mentioned in Section 1.2, proteins can foul and denature onto the surfaces used to take measurements resulting in higher background noise and lower sensitivity, in turn limiting reusability and leading to false positives.[7,31] The selectivity of label-free methodologies entirely relies on the repulsion of non-target species, as LSPR and SPR cannot accurately differentiate one species' presence from another without surface functionalization.[41,77] The ability to differentiate species can be achieved by repelling all unwanted interactions. A typical LSPR protein sensor (Figure 7) incorporates an antibody affixed via a tail group to its gold surface, as well as a way to prevent the fouling of unwanted species.

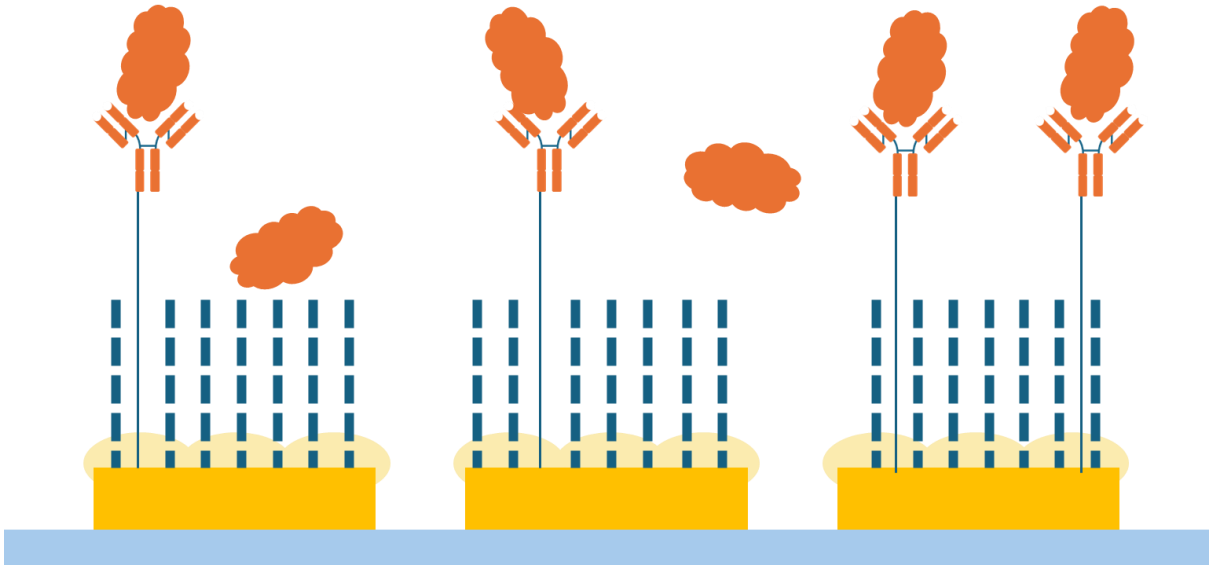

Figure 7. A simplification of an LSPR based sensor which utilizes an antibody to capture a target analyte, as well as a method of antifouling, represented by the dashed lines.

Blocking is the most employed method of preventing fouling. Blocking involves incorporating a protein (commonly BSA) onto a surface. These surface-affixed proteins can then "block" the interactions with other unwanted species.[78] Jeyachandran et al. demonstrated that BSA blocking was efficient by utilizing ATR-FTIR and calculating a percentage of blocking efficiency by comparing the amount of protein coverage on a blocked surface versus the amount of protein coverage on an unblocked surface. However, the efficiency varied depending on the surface functionalized. BSA achieved a 90–100% blocking efficiency on hydrophobic surfaces, while on hydrophilic surfaces, it ranged from 68–100%.[79] This percentage range was dependent on the fouling protein used (concanavalin A, immunoglobulin G, staphylococcal protein A). The main limitation with the use of blocking, especially for LSPR, has been the increased size associated with BSA. Jachimska et al. have shown that a BSA molecule's length was 8.3 nm in the compact state (N form at pH 4–9) and 26.7 nm in the extended state (F-form).[80] As mentioned in Section 1.2.4, LSPR's sensing distance of ~10 nm means such antifouling methods compromise LSPR's ability to function. To prevent antifouling surfaces from affecting an LSPR sensor's ability to take proper measurements, alternative surface chemistries that rely on less bulky chemistries must be investigated.

An alternative method has been the use of antifouling molecules incorporated into thiol SAMs themselves. By attaching antifouling molecules to a surface, these designed molecules prevent the fouling that would occur to that surface during measurement.[7,47,81] PEG, as arguably the most common example, resists fouling by hydrogen bonding with water, creating a layer of water upon the sensor's surface. This layer of water prevents the nonspecific binding of proteins to a surface. Prime et al. found using ellipsometry that a PEG monolayer made of a molecule composed of 6 ethylene glycol units was able to resist all fouling from fibrinogen (a protein essential to blood clotting) and chymotrypsinogen (a digestive enzyme).[62] However,

even if PEG has frequently been labelled as the "golden standard" for resisting nonspecific binding of proteins, proteins can often still adsorb onto the surface they cover.[82–84] PEG often has high resistance to the adsorption of hydrophobic proteins, but less resistance to more hydrophilic species.[76] Additionally, PEG can be sensitive to biological conditions and has been shown to decay due to oxidative stress induced by charged ions and molecules which can cause the creation of radicals within the PEG molecules.[7,85–87]

A commonly used alternative to PEG are zwitterionic molecules. Zwitterionic materials are characterized by having both cationic and anionic groups, making them electrically neutral and yet highly hydrophilic. These molecules work by hydrogen bonding with water to create a hydration layer that exclude fouling species, like PEG.[7] A significant advantage over PEG is that zwitterionic molecules have electrostatic properties, which allows for a denser hydration layer.[88] Xing et al. employed the use of a zwitterionic polymer coating to reduce the fouling on a silicon wafer. Using SPR it was found that less than 5 ng/cm^2 adsorbed onto the surface, whereas the bare surface had ~250 ng/cm^2 of BSA adsorbed onto it. By utilizing fluorescence microscopy and fluorescently dyed BSA protein (FITC-BSA), it was found that the zwitterionic polymer reduced the adsorption from BSA by 98% when compared to a bare surface.[75] In a similar way, Joshi et al. investigated the antifouling ability of a zwitterionic polymer designed to reduce fouling on gold nanostructures used for a portable version of an imaging SPR sensor. It was found using SPR that the zwitterionic polymer was able to reduce fouling by 90% from a BSA solution (1 mg/mL) when compared to bare gold. However, the zwitterionic surface in complex solution (milk 10% diluted), which contains a diverse mixture of fat, ions and proteins, was unable to reduce fouling.[89] Zwitterionic materials have had some difficulties. Specifically, zwitterionic materials have struggled maintaining their resistance to fouling regarding a change in the pH of the medium, the ionic strength and the temperature.[7,90] Furthermore, both PEG and zwitterionic molecules have the issue of size, as they relied on the creation of a hydration layer in order to antifoul. As stated previously, the sensing distance of LSPR is around 10 nm, so antifouling systems that are too bulky can limit the ability of LSPR to detect species properly.[31]

1.5 Fluorine's Use in Antifouling Chemistries

Fluorinated molecules have been incorporated and used in organic chemistry extensively over the last few decades and have been integral to modern pharmaceutical chemistry and material sciences. The fluorous effect is a term that describes a trend that was observed using fluorinated molecules first by a PhD student at the University of Aachen, M. Vogt. The observed trend is that fluorous molecules tend to associate with other fluorous species while repelling non-fluorous species.[91,92] Antifouling surfaces have utilized this trend; arguably the most famous use is the non-stick surfaces found on pots and pans. The fluorous effect occurs

due to the strong electronegativity of fluorine, which results in fluorine creating a strong dipole while in a molecular system. This strong dipole is highly resistive to spontaneous change, resulting in these dipoles being poor at participating in Van der Waals interactions.[93,94]

Fluorine has been utilized to create amphiphilic and omniphobic surfaces.[93–95] Omniphobic surfaces are surfaces which repel all chemical species, which also involves the repelling of liquids and solvents from interacting with a given surface. The repulsion of all species seems appealing; however, for biosensors, especially those that rely on antibody-antigen interactions, omniphobicity can prevent the immobilization of desired species. Shakeri et al. showed that using fluorinated SAM infused with a fluorinated liquid lubricant successfully created a foul-resistant omniphobic surface.[95] In addition to omniphobic surfaces, amphiphilic surfaces have been created by incorporating fluorinated molecules. Amphiphilic surfaces incorporate both hydrophobic and hydrophilic portions. Amphiphilic surfaces allow for a more modular surface as often the surfaces in question can have their ratio of hydrophobic to hydrophilic portions finely tuned. Gentilini et al. designed fluorinated PEG chains to protect gold nanoparticles from degradation and undesired surface interaction, which exhibited strong amphiphilic character confirmed by FTIR Spectroscopy.[96]

1.5.1 The Utility of Fluorinated SAMs

Fluorinated alkane chains have been incorporated into SAMs for antifouling surfaces.[97,98] Fluorinated SAMs can often provide changes in friction,[97] wettability,[99,100] work function,[97,101] capacitance,[100] and in some cases temperature resistance.[98,102] The C-F bond that is found in these fluorinated chains are the strongest bond found in organic chemistry (105.4 kcal/mol), compared to the C-H bonds (98.8 kcal/mol).[103] This leads to several advantages regarding stability, and studies have shown a high resilience to harsh conditions, including resistance to high changes in pH.[98] The use of fluorinated SAMs has resulted in surfaces that have been easily customized for different applications, are highly resilient to aggressive chemical environments, and have been shown to resist fouling against proteins. However, fluorinated SAMs have had several downsides associated with them. Evidence has been found that the strong dipole-dipole interactions in fluorinated SAMs can cause inconsistencies with the packing and density of the SAMs, which can cause disparities in a fluorinated SAM's ability to antifoul.[98]

1.5.2 Downsides and Controversies Surrounding Fluorine Usage

The strength of C-F bonds results in compounds which utilise many fluorine atoms becoming "ultra-stable".[98] These fluorinated molecules have extremely long lifetimes due to their resistance to natural degradation,[104] raising many concerns. A common example are per- and polyfluoroalkyl substances (PFAS), synthetic compounds that utilize at least one perfluorinated methyl group or a perfluorinated methylene group within its structure.[104] PFAS have been used for commercial applications ever since the 1950s, and since then, there have been concerns regarding their extreme environmental persistence,[105] which has resulted in PFAS gaining the moniker "forever chemicals". This persistence has caused the contamination of air, groundwater, soil and more.[104] PFAS's resistance to degradation has led to bioaccumulation in various organisms, including humans, and PFAS have been detected in blood and other bodily tissues.[104–106] Linked to this bioaccumulation, PFAS have been linked to toxic effects, including carcinogenicity, alterations in development, immunotoxicity, and reproductive toxicity.[104] This toxicity and resistance to biodegradation has led to restrictions and proposed bans on the use of PFAS.[105] However, as the unique properties of these molecules are still in need, alternatives like chlorine-substituted fluorinated compounds and polyfluoroalkyl ether thiol alcohols have been introduced.[106] Though several issues regarding these alternatives have been found, mainly it is often unknown whether these novel alternative molecules will have similar effects on the environment as PFAS.[106,107]

An alternative that has been investigated in recent times has been fluorinated aromatic structures.[107] It has been shown that fluorinated aromatics, such as fluorobenzene, have more pathways towards degradation than conventional PFAS. Carvalho et al. found that some fluorinated aromatic compounds could be biodegraded via a pathway mediated by microbes utilizing dioxygenases.[107] The tested pathway created a reactive intermediate that eventually led to spontaneous defluorination of fluorobenzene and 4-fluorophenol.[107] It is important to note that even if this research provides evidence that fluorinated aromatic compounds have more viable routes towards degradation than PFAS, much research regarding their environmental effects is still needed to determine how safe these molecules are.[108] This thesis investigates the use of such a compound, but within the context of plasmonic surfaces, where very low levels (in the nanogram scale) of fluorinated molecules are used. These minuscule amounts of fluorinated molecules make LSPR and similar forms of sensing that use antifouling surfaces an optimal discipline to utilize and determine the functionality of these fluorinated alternatives to PFAS.

1.6 Pentafluorobenzyl Moiety

A molecule of interest that contains a high amount of fluorine with only the length of a few angstroms is a pentafluorobenzyl (PFB) moiety. This molecule has been used in the past to create antifouling surfaces, focusing on creating a surface that is resistant to biofouling in marine industries.[76,109–114] Biofouling in this scenario is when an organism sticks to a structure via a protein-based "glue",[76] and this sticking can eventually result in inefficiencies and damage to underwater structures.[114] For a biofouling surface to be optimal, it must be stable and non-toxic and prevent fouling from a wide range of proteins.[76,111,114] These all have been attractive qualities regarding plasmonic sensor design. In addition, the PFB moiety has been used to create amphiphilic surfaces in these marine industries. As mentioned in Section 1.5, amphiphilic surfaces, including SAMs, tend to antifoul better than surfaces that are just hydrophobic or hydrophilic.[93,94]

The PFB moieties are not as effective at antifouling against non-polar proteins compared to other antifouling coatings due to their hydrophobic nature. However, when incorporated into mixed monolayer systems, they tend to increase the antifouling ability of the system they are incorporated into.[76] Surfaces that can resist both polar and non-polar proteins have been developed utilizing the PFB moiety, providing a versatile ability to antifoul against an extensive range of proteins.[76] Pollack et al. developed a surface coating that utilized portions of the hydrophobic pentafluorobenzyl moiety within a hydrophilic polymer. The created surface resisted protein nonspecific binding from BSA 60% better than a control surface (Sylgard 184 polydimethylsiloxane).[111] Gudipati et al., in a similar process to Pollack, developed a polymer that incorporated hydrophobic pentafluorobenzyl moieties as well as hydrophilic PEG portions and then compared their created surface to other surfaces. They found that one of their created surfaces HBFP-PEG45 which was composed of 55% pentafluorobenzyl portions and 45% PEG, overall was able to effectively prevent nonspecific binding of a wider variety of proteins than either species on their own (Figure 8).[76]

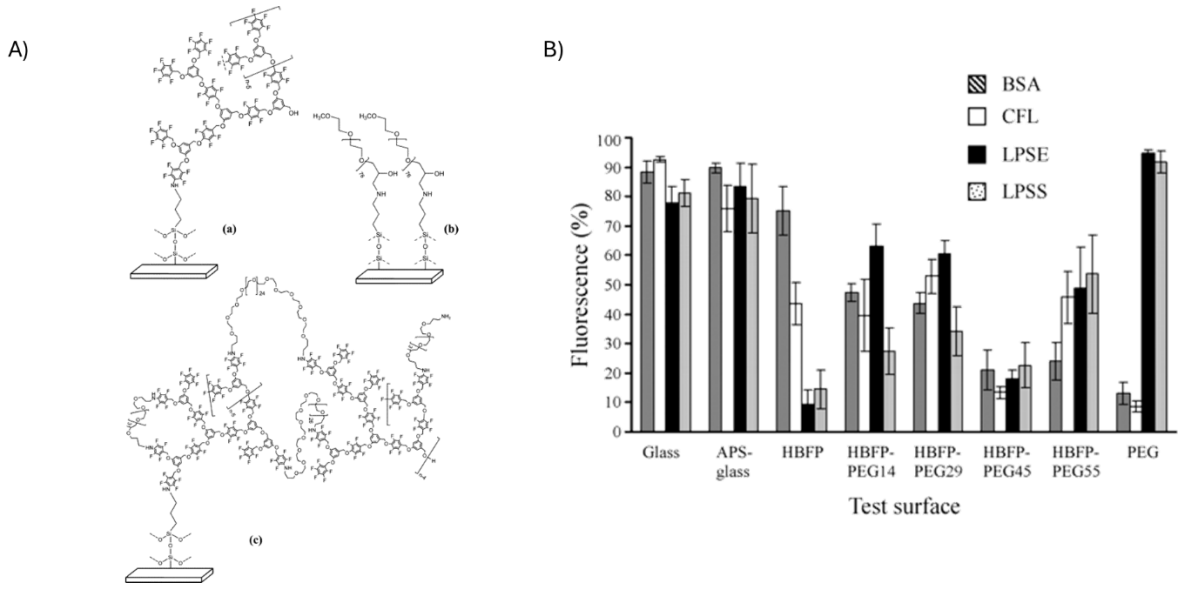

Figure 8. (Gudipati et al.) a) Diagram of the designed and tested polymers which contained PFB. b) Adsorption of bovine serum albumin (BSA), a lectin from codium fragile (CFL), lipopolysaccharide from E. coli (LPSE), and lipopolysaccharide from salmonella minnesota (LPSS) on the coatings of the cross-linked Pentafluorobenzyl and PEG (HBFP-PEG) was measured using fluorescence microscopy. Surfaces tested where 100% pentafluorobenzyl coating (HBFP), a mixed coating of the HBFP containing 14% PEG (HBFP-PEG14), a mixed coating of the HBFP containing 29% PEG (HBFP-PEG29), a mixed coating of the HBFP containing 45% PEG (HBFP-PEG45), a mixed coating of the HBFP containing 55% PEG (HBFP-PEG55), a 100% PEG surface, a bare glass coating, and a glass coated with 3-aminopropyl)triethoxysilane. The fluorescence measurements (% coverage) were used to quantify adsorption, where 100% = complete coverage of the tested surface and 0% = no adsorption. The HBFP-PEG45 coating exhibited the most substantial resistance to all biomacromolecules tested compared to other compositions.[76]

Another point of utility when considering the creation of PFB antifouling surfaces has been their utility within SAMs. The aromaticity of PFB is advantageous for SAM formation, as aromatic rings have been shown to enhance the stability and thermal resistance of SAMs.[115] Kang et al. in a study aimed to determine structural characteristics of novel SAMs showed that, when compared to aromatic SAMs utilizing benzene rings, PFB-containing SAMs had nearly 2.3 times higher molecular density.[116] Though this paper did not utilize the pentafluorobenzyl moity in a sensing or an antifouling application, their finds of an increase in surface density would lend itself to the creation of better antifouling surfaces.

1.7 The utility of PFB in LSPR Chemical sensing.

Many applications of PFB have been focused on antifouling in marine industries. This thesis aims to explore the use of PFB within chemical sensing by designing an antifouling SAM that could be easily synthesized and function against a wide variety of proteins. The surfaces are tested using LSPR sensing, however, it is important to note that the molecules created can be applied to various sensing methodologies and applications. Three molecules were successfully

synthesized and incorporated into SAMs. These were compared to control surfaces (PEG and bare Au). Finally, a mixed SAM was created with one of the designed molecules alongside an antibody containing molecule, expecting to test and determine the PFB surface's ability to detect a given protein while utilized within a sensor.

2 Experimental

2.1 Synthetic Procedures

2.1.1 Preparative Techniques

Chemicals and solvents were purchased from commercial suppliers and used without additional purification unless otherwise stated. Anhydrous solvents (toluene, tetrahydrofuran (THF), dichloromethane (DCM)) were obtained by passage through Pure Solv solvent filtration systems, and solvents were transferred by syringe. Reactions were conducted within sealed microwave vials using Asynt hotplates equipped with a mineral oil bath and controlled using an Asynt temperature probe. All glassware and stir bars were dried with a heat gun or stored in the oven and allowed to cool under an inert atmosphere prior to use. Reactions were carried out under nitrogen in an inert or dry atmosphere.

2,3,4,5,6-Pentafluorobenzyl bromide was purchased from Thermo Scientific. 11-Bromo-1-undecene was purchased from Alfa Aesar. Thioacetic acid was purchased from Aldrich. Daniel Osborne synthesized 3,6,9,12-Tetraoxatricos-22-en-1-ol (PEG4-11-undecane) and 26-[(Methylthio)carbonyl]-3,6,9,12,15-pentaoxahexacosanoic acid at the University of Glasgow.

2.1.2 Purification Techniques

Flash Column Chromatography was performed manually using self-pack columns (d = 40 mm or 70 mm) filled with silica gel (60 Å, 40-63u). All solvents used were reagent grade and were as received from suppliers unless otherwise stated. A Buchi Rotary Evaporator was used to remove solvents and volatile compounds.

2.1.3 Analytical Techniques

Thin Layer Chromatography was implemented as a tool to monitor reactions and to determine the solvent systems for flash column chromatography. Self-cut Supelco silica gel coated aluminium plates (0.2 mm particle size, 60 Å pore-size). Plates were visualized using both ultraviolet (UV) light (λ_{Max} = 255 nm or 365 nm) or using potassium permanganate ($KMnO_4$) stain and heated from a heat gun (~1 min).

Nuclear Magnetic Resonance (NMR) Spectrometry – Proton (1H), Carbon (13C) and Fluorine (19F) were recorded in deuterated solvents, unless otherwise stated, using standard pulse methods on an AVANCE III 400 Bruker (1H = 400 MHz, 13C = 101 MHz). Chemical shifts are expressed in parts per million (ppm, δ scale) and are referenced to residual protonated solvent (e.g. in $CDCl_3$ 1H = 7.26 ppm, 77.2 ppm). Coupling constants, J, are quoted to the

nearest 0.1 Hz are multiplicities are described as singlet (s), doublet (d), triplet (t) quartet (q), quintet (quin), sextet (sxt), septet (sept), broad (br) and multiplet (m). For ^{13}C NMR measurements of the pentafluorobenzyl moity in all molecules, several signals were not observed. This was due to splitting caused by the fluorines on the ring.

Mass Spectrometry (MS) was performed on a Bruker microTOFq Mass Spectrometer using electrospray ionisation (ESI) in positive mode (ESI+).

S-[(2,3,4,5,6-pentafluorophenyl)methyl] ester (1-Ac)

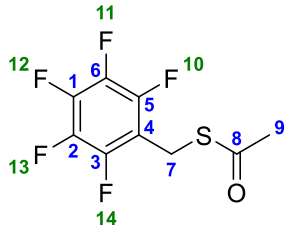

Synthesis was adapted from Sohn et al.[117] For synthesis of **1-Ac**, anhydrous K_2CO_3 0.826 g (4.51mmol, 1.47 equiv.) was added to a dry microwave vial with a stir bar. The vial was sealed and flushed with N_2 using a balloon and needle. Dry THF (9.6 mL) was added to the vial via a syringe. 2,3,4,5,6-Pentafluorobenzyl bromide was gently heated to melt the starting material, and 0.463 mL (3.07 mmol, 1 equiv.) was added to the vial via syringe, followed by the addition of thioacetic acid 0.319 mL (4.51 mmol, 1.47 equiv.). This reaction mixture was continuously stirred and left to react overnight (18h) at RT.

The crude reaction mixture was mixed with water (20 mL) and then extracted into DCM (2 x 10 mL), and the combined organic layers were washed with brine (50 mL) and dried ($MgSO_4$) and concentrated via a rotary evaporator. The crude material was purified with flash column chromatography (10% EtOAc in hexanes) to give a clear yellow oil. 0.512 g, Yield 40.0% .**^{1}H NMR** (400 MHz, $CDCl_3$) δ 4.20 (2 H, t, *J* = 1.7 Hz, C7-H), 2.36 (3 H, s, C9-H); **^{19}F NMR** (376 MHz, $CDCl_3$) δ -141.11, -154.99, -161.84; **^{13}C NMR** (101 MHz, $CDCl_3$) δ 193.5, 30.3, 20.3 (Solvent $CDCl_3$ Peak 77.4); **HRMS (ESI)** m/z $[M-H]^+$ calcd. for $C_9H_5F_5OS^-$ 254.9909; found 254.9905. **Rf** 0.34 (10% EtOAc in Hexane)

^{1}H NMR

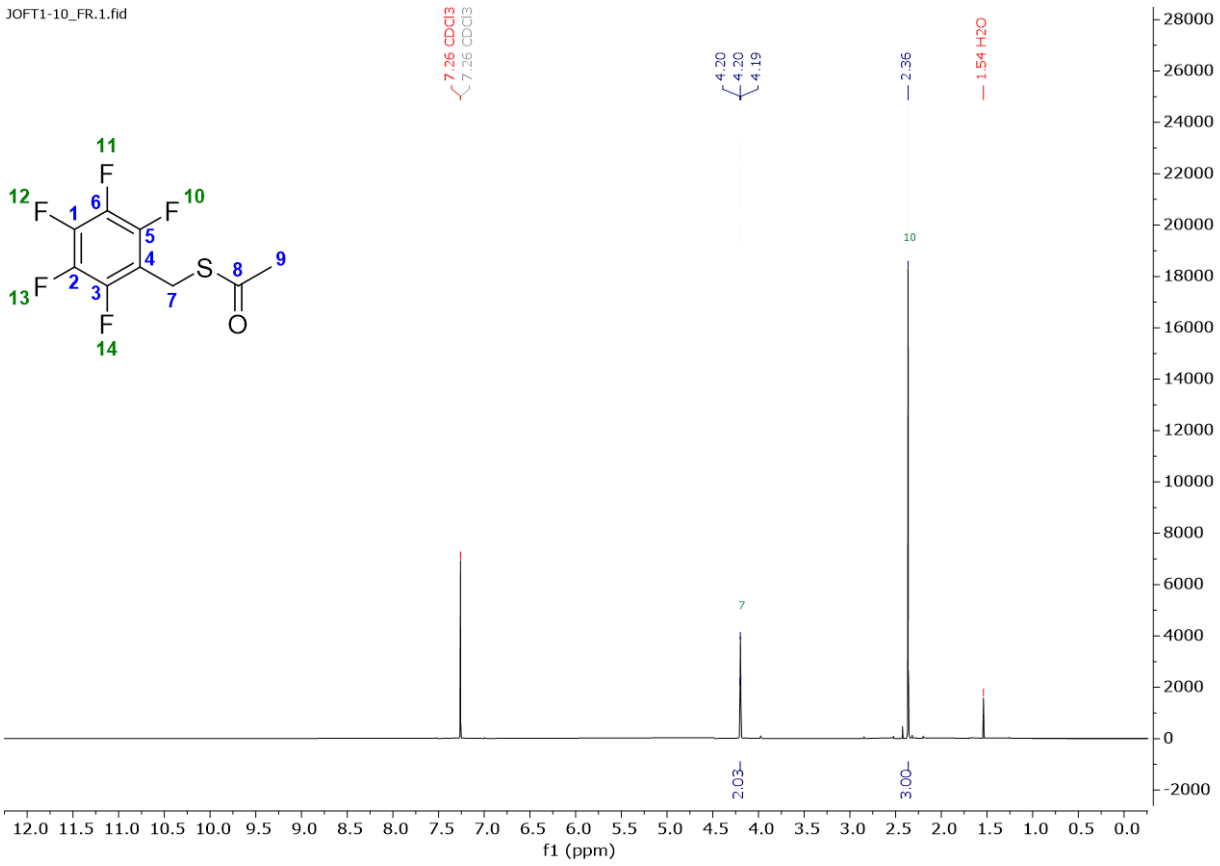

^{19}F NMR

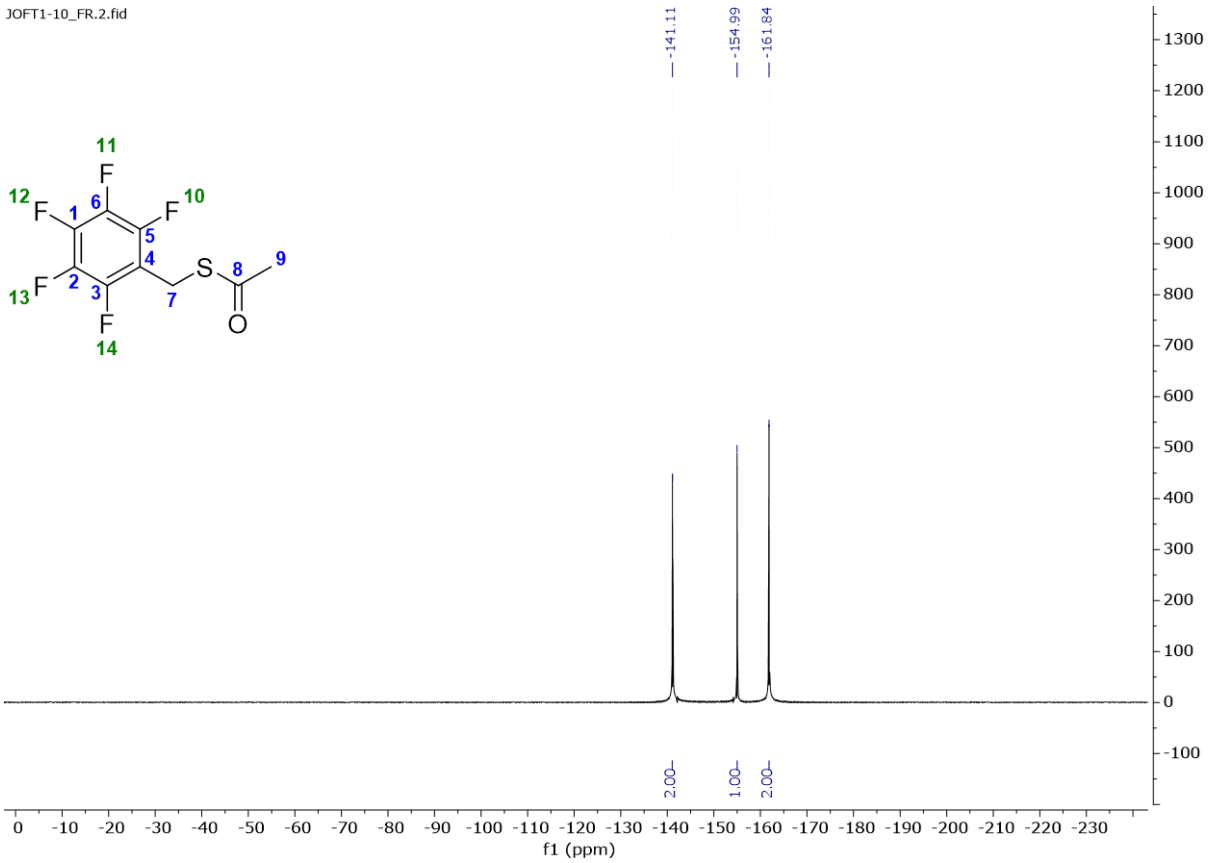

^{13}C NMR

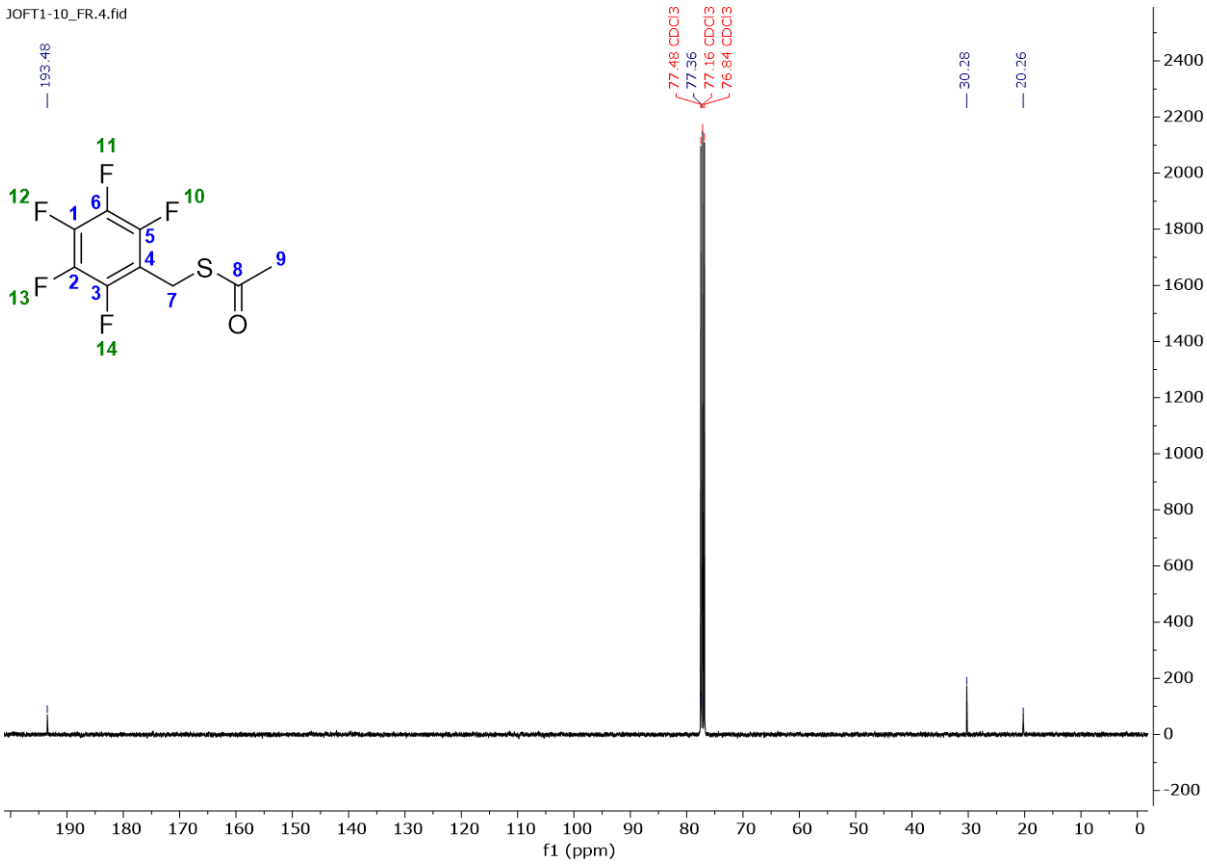
JOFT1-10_FR.4.fid
193.48
77.48 CDCl3
77.36
77.16 CDCl3
76.84 CDCl3
30.28
20.26
11
F
12
F
1
6
F
10
5
4
S
8
9
13
F
2
3
7
O
F
14
f1 (ppm)

11-[(2,3,4,5,6-Pentafluorophenyl)methoxy]-1-undecene (2)

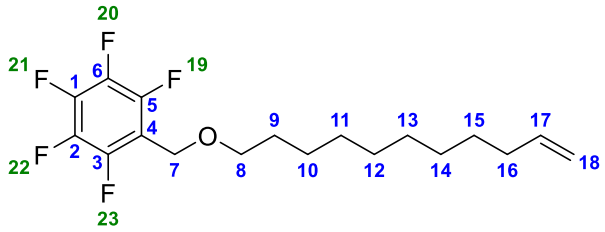

To a microwave vial equipped with a stir bar, KOH (0.0988 g, 1.76 mol, 1 equiv) was added Bu_4NI (0.0325 g, 0.0880 mol, 0.05 equiv). The vial was then flushed with nitrogen via a balloon and needle, followed by the addition of THF (1.5 mL). To this solution, 10-undecene-1-ol (0.300 g,1.76 mmol, 1 equivalent) and then pentafluorobenzyl bromide (0.460 g, 1.76 mmol, 1 equiv) was added to the mixture. The mixture was then heated to 60 °C and stirred overnight (18 h).

The crude reaction mixture was added to water (20 mL) and extracted into EtOAc (80 mL x 3). The combined organic layers were washed with brine (100 mL), dried over $MgSO_4$ and concentrated on a rotary evaporator. Purification was achieved with flash column chromatography using a gradient (petrol ether with 0-6% EtOAc). 0.320 g, Yield 52.0%. **^{1}H NMR** (400 MHz, $CDCl_3$) δ 5.81 (1H, ddt, *J* = 17.0, 10.2, 6.7 Hz, C17-H), 5.02 – 4.90 (2H, m, C18-H), 4.57 (2H, t, *J* = 1.9 Hz, C7-H), 3.48 (2H, t, *J* = 6.6 Hz, C8-H), 2.09 – 1.98 (2H, m, C16-H), 1.57 (2H, m, *J* = 6.6 Hz, C9-H), 1.22–1.40 (12H, m, C10-15-H); **^{19}F NMR** (377 MHz, $CDCl_3$) δ -142.94, -154.08, -162.11. **Rf** 0.125 in (10% EtOAc in Hexane).

^{1}H NMR

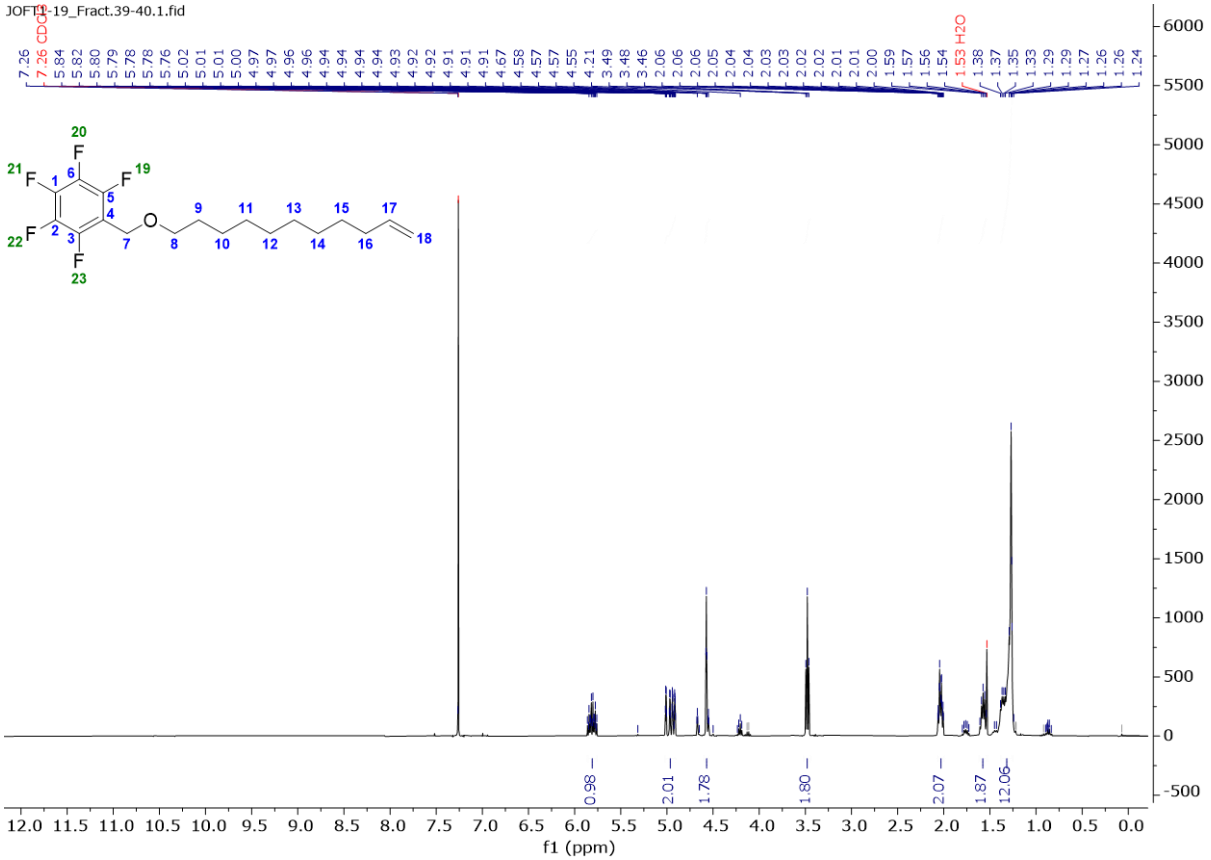

^{19}F NMR

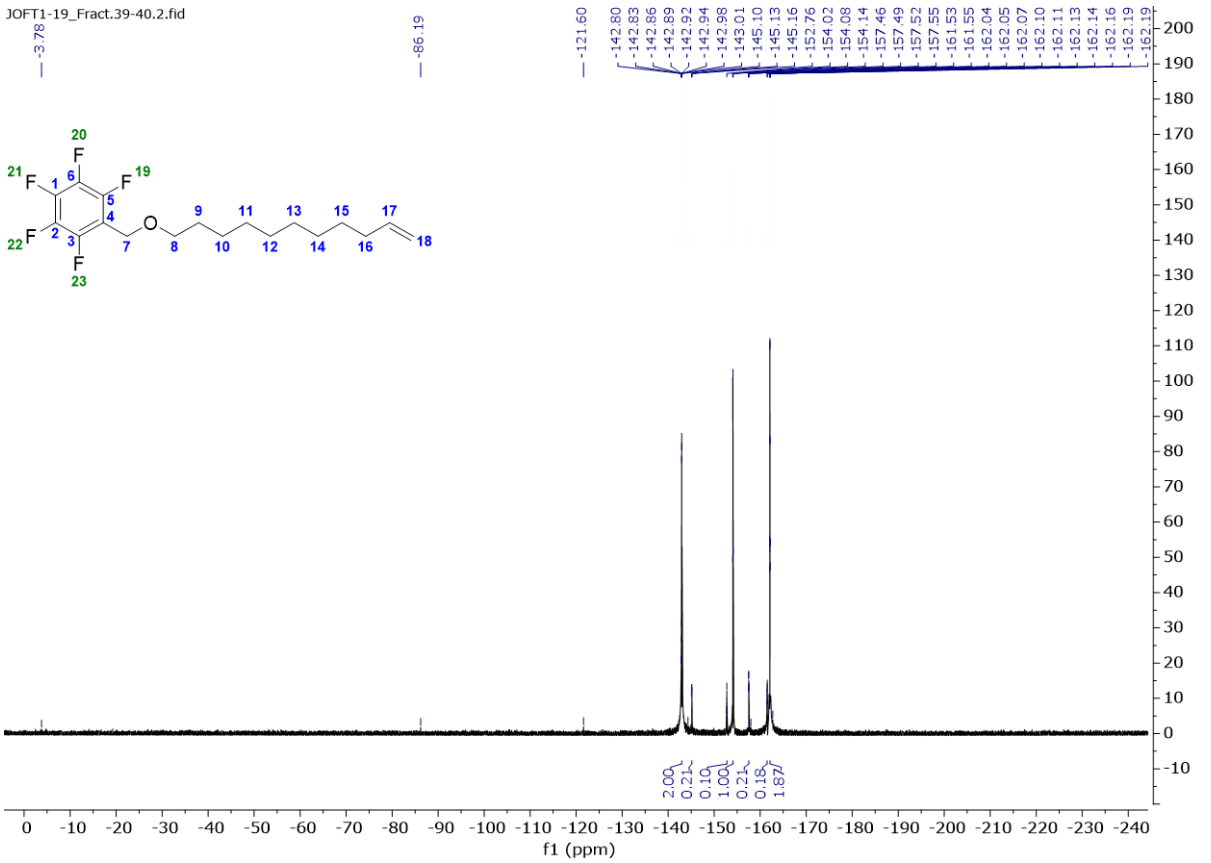

C-Methyl 12-[(2,3,4,5,6-pentafluorophenyl)methoxy]dodecanethioate (3-Ac)

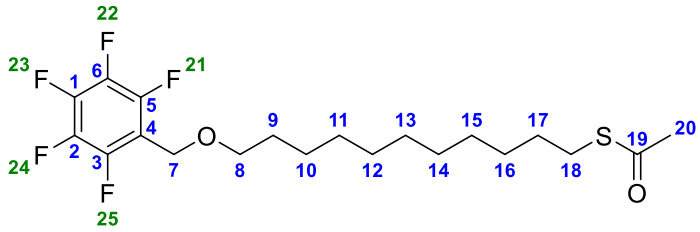

Azobisisobutyronitrile (AIBN) (0.108 g, 0.658 mmol, 0.720 equiv) was added to a dry microwave vial that had been equipped with a stir bar, with (0.320 g, 0.914 mmol, 1 equiv) of **2** dissolved in 6 mL of dry toluene followed by an additional 6 mL of dry toluene. To this mixture, Thioacetic acid (0.470 mL, 36.58 mmol, 7.20 equiv) was added, and the reaction mixture was heated to 60 °C and stirred for 48h. The crude reaction mixture was added to water (20 mL), extracted into EtOAc (80 mL x 3), washed with brine (100 mL), dried over $MgSO_4$ and concentrated on a rotary evaporator. Purification was achieved with flash column chromatography using a gradient (hexane with 0.87-13% EtOAc). The reaction resulted in a clear yellow oil. 0.310 g, Yield 80.0%. **^{1}H NMR** (400 MHz, $CDCl_3$) δ 4.57 (2H, t, *J* = 1.9 Hz, C7-H), 3.48 (2H, t, *J* = 6.6 Hz, C8-H), 2.86 (2H, t, *J* = 7.4 Hz, C18-H), 2.32 (3H, s, C20-H), 1.60 – 1.53 (2H, m, C9-H), 1.37 – 1.22 (16H, m, C10-17-H); **^{19}F NMR** (377 MHz, $CDCl_3$) δ -142.97, -154.08, -162.10; **^{13}C NMR** (101 MHz, $CDCl_3$) δ 196.1, 71.2, 59.5, 30.7, 29.5, 29.4, 29.2, 29.1, 28.8, 26.0 (Solvent $CDCl_3$ Peak 77.2). **HRMS (ESI)** m/z $[M+H]^+$ calcd. for $C_{20}H_{26}F_5O_2S^-$ 425.1579; found 425.1580. **Rf** 0.18 in (10% EtOAc in Hexane).

^{1}H NMR

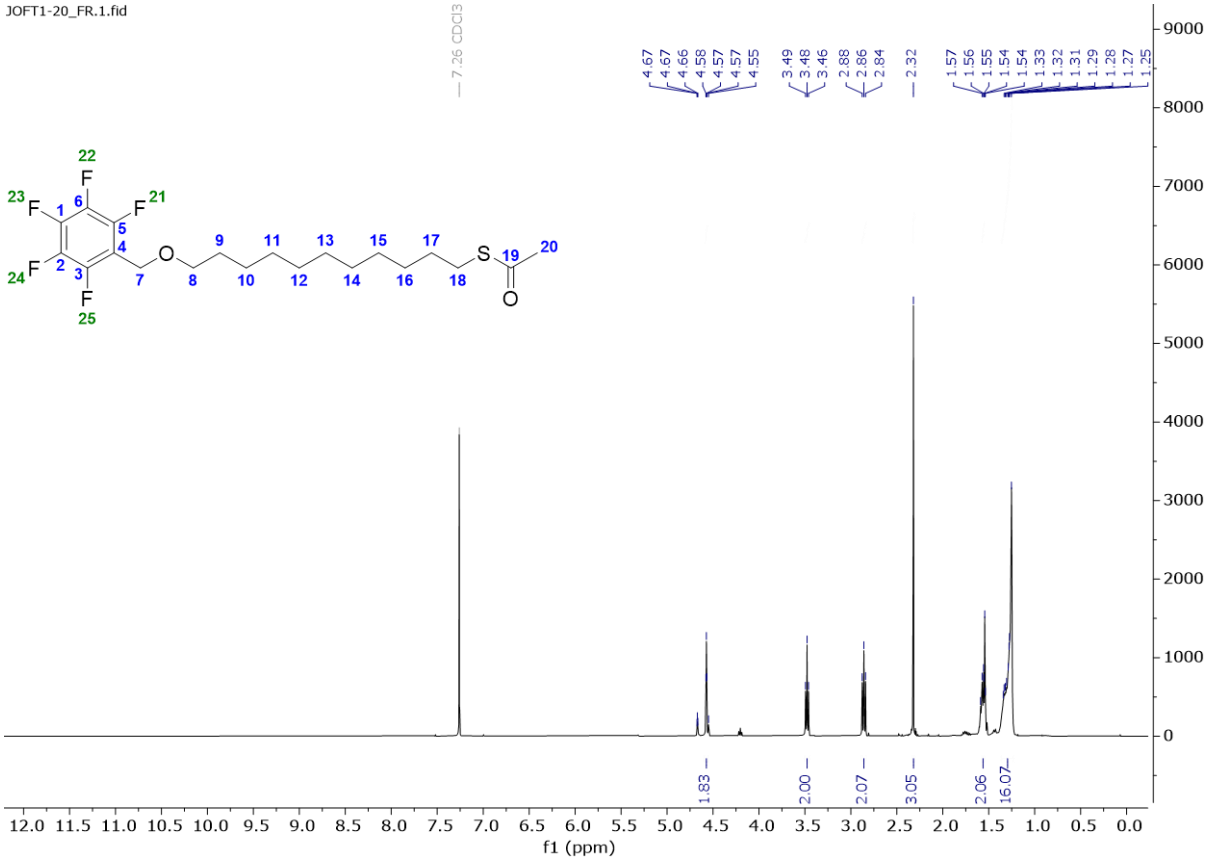

^{19}F NMR

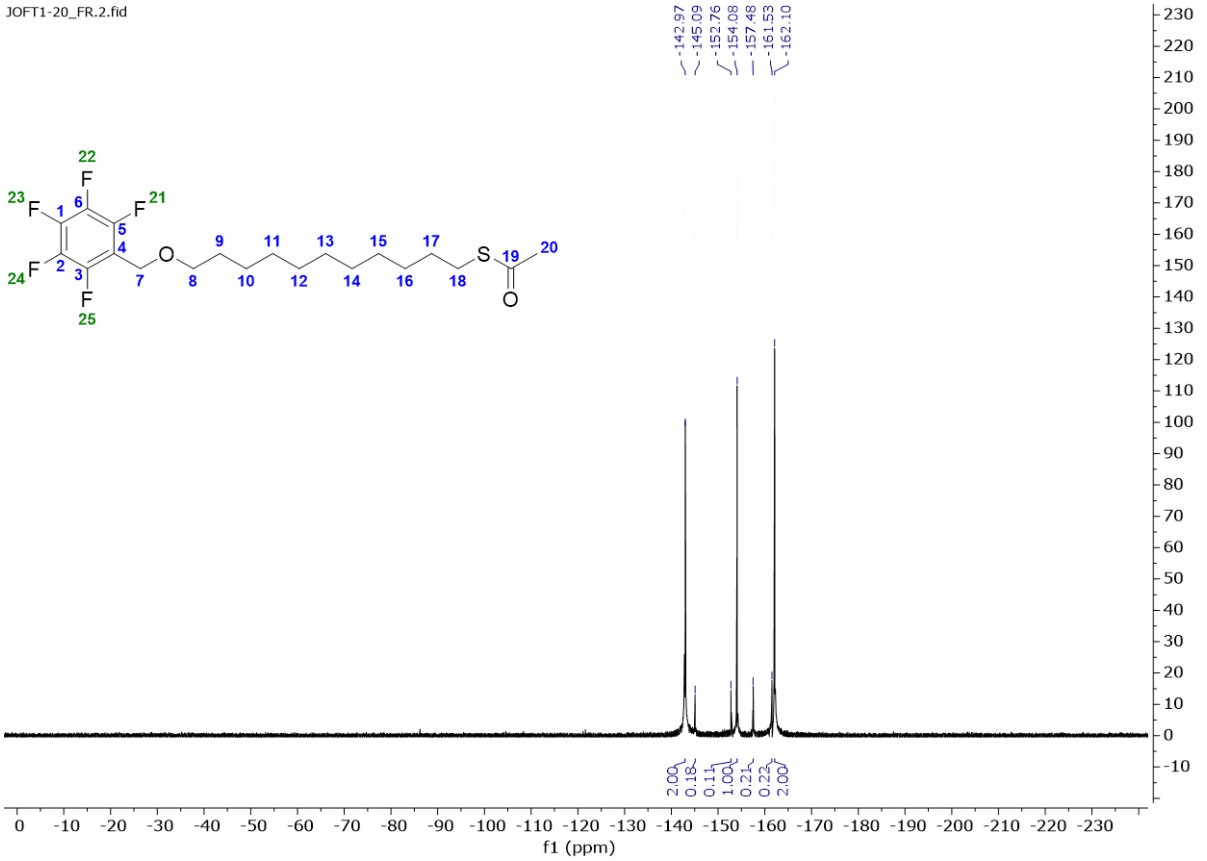

^{13}C NMR

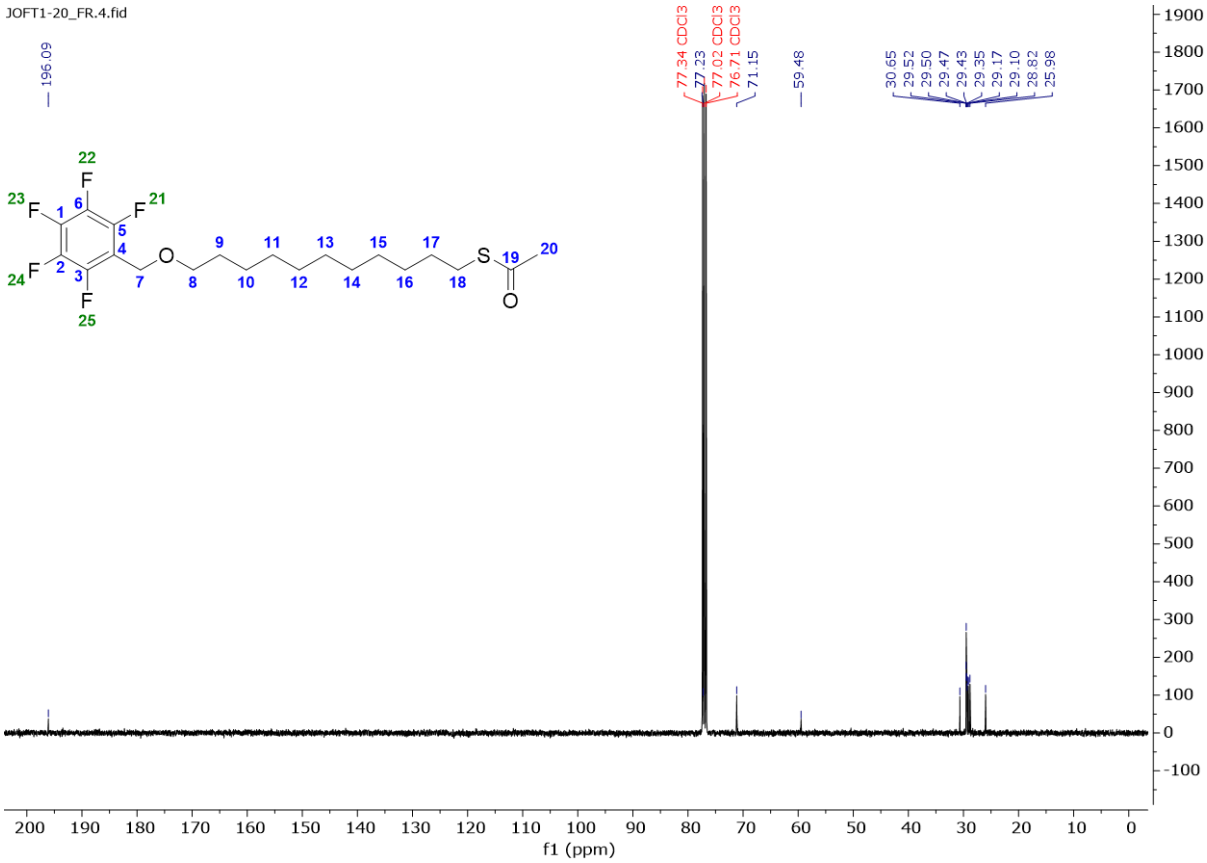
JOFT1-20_FR.4.fid
196.09
77.34 CDCl3
77.23
77.02 CDCl3
76.71 CDCl3
71.15
59.48
30.65
29.52
29.50
29.47
29.43
29.35
29.17
29.10
28.82
25.98
f1 (ppm)

1-(2,3,4,5,6-Pentafluorophenyl)-2,5,8,11,14-pentaoxa-24-pentacosene (4)

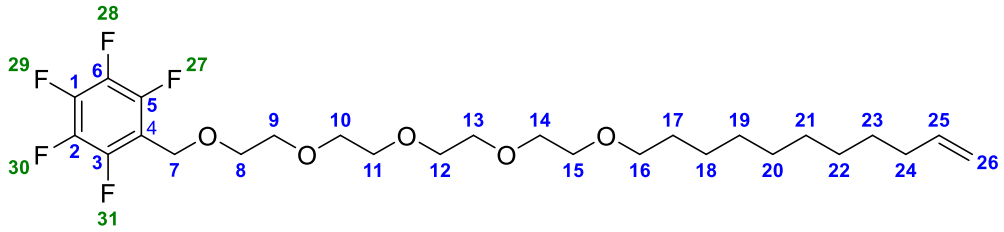

For the synthesis of the **4**, Pentafluorobenzyl bromide (0.278 g, 1.15 mmol, 1.05 equiv) was added to a dry three-necked round bottom flask equipped with a dry stir bar and tetrabutylammonium iodide (0.0202 g, 0.055 mmol, 0.05 equiv) was added. These were then dissolved in THF (2.19 mL), and to this mixture, 3,6,9,12-Tetraoxatricos-22-en-1-ol (0.379 g, 1.09 mmol, 1 equiv) was added via a syringe. The flask was flushed with N_2 and then chilled to 0 °C using a cooling bath. Once the mixture was fully chilled, NaH (0.0460 g, 1.15 mmol, 1.05 equiv) was added portion-wise over 15 minutes, allowing the mixture to react fully and cool before adding more. The mixture was left to stir for 10 minutes, then raised to the temperature of 40 °C and left to stir for 3h. The reaction was quenched with ~4mL of distilled water. The reaction mixture was added to water (20 mL), extracted into EtOAc (80 mL x 3), washed with brine (100 mL), dried over $MgSO_4$ and concentrated on a rotary evaporator. Purification was achieved with flash column chromatography using a gradient (Hexane with 0-10% EtOAc). 0.0859 g Yield 15.0%. **^{1}H NMR** (400 MHz, $CDCl_3$) δ 5.81 (1H, ddt, *J* = 17.0, 10.2, 6.7 Hz, C25-H), 5.04 – 4.88 (2H, m, C26-H), 4.65 (2H, t, *J* = 1.9 Hz, C7-H), 3.68 – 3.57 (16H, m, $(C_2O)_4$-H), 3.44 (2H, t, *J* = 6.8 Hz, C16-H), 2.03 (2H, d, *J* = 7.7 Hz, C24-H), 1.66 – 1.50 (2H, m, C17-H), 1.36 – 1.17 (12H, m, C18-23-H); **^{19}F NMR** (376 MHz, $CDCl_3$) δ -142.66, -153.80, -162.02; **^{13}C NMR** (101 MHz, $CDCl_3$) δ 139.3, 114.1, 71.7 – 70.0 (m), 33.8, 30.8 – 27.9 (m), 26.1. **Rf** 0.51 in (40% EtOAc in hexane).

^{1}H NMR

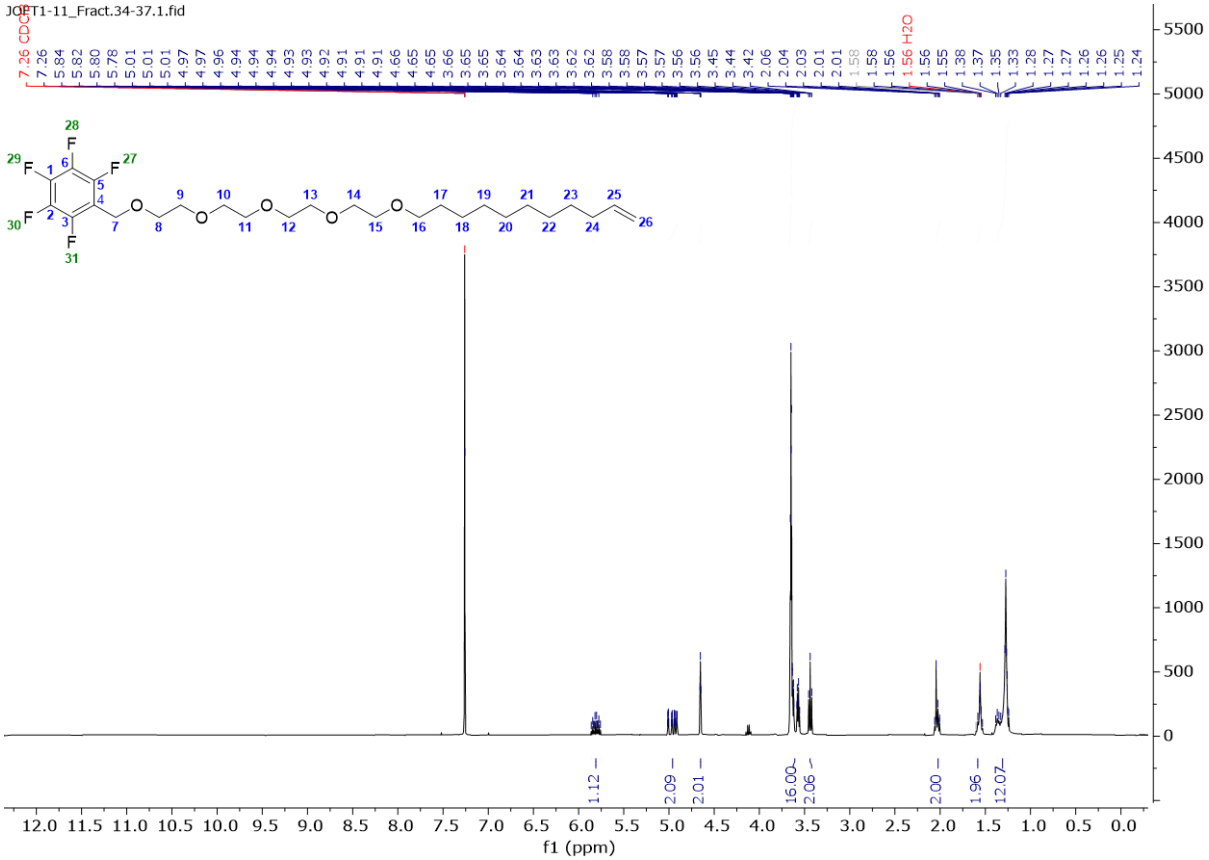

^{19}F NMR

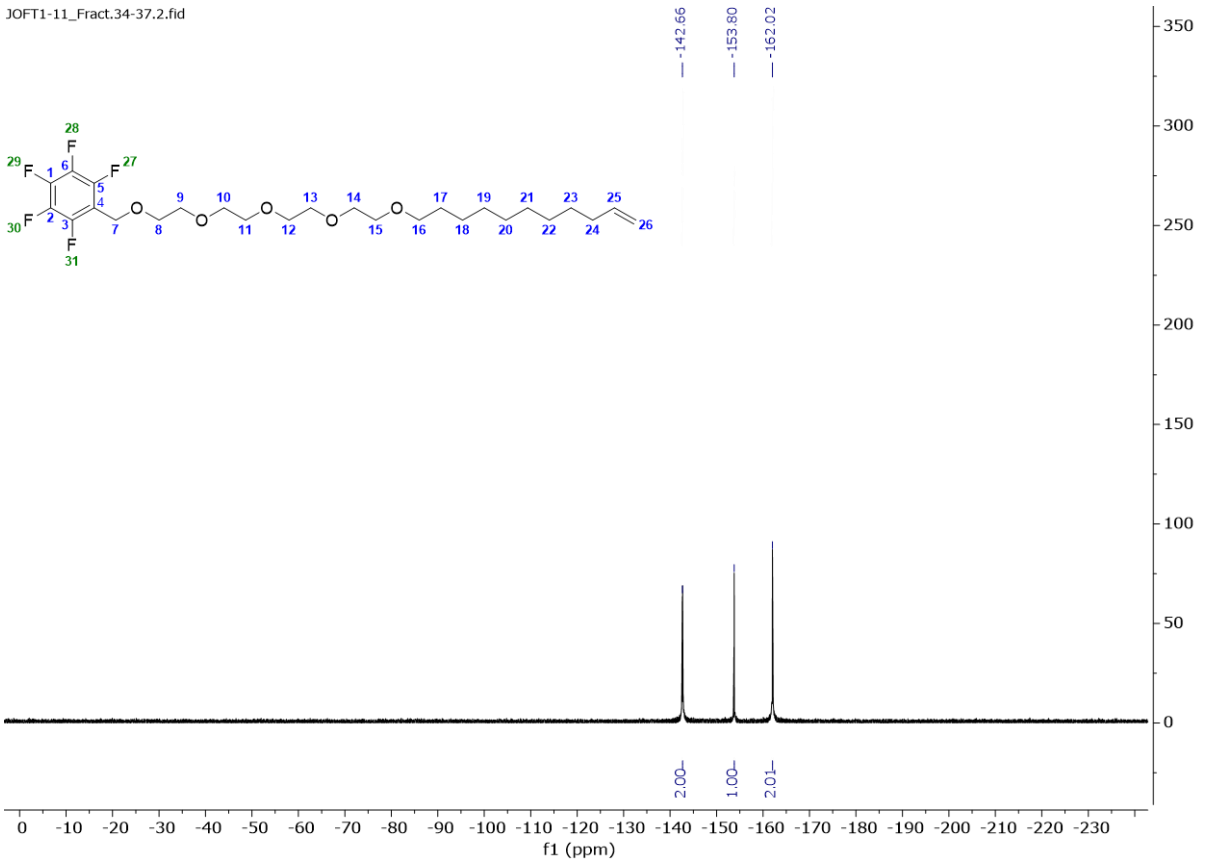

^{13}C NMR

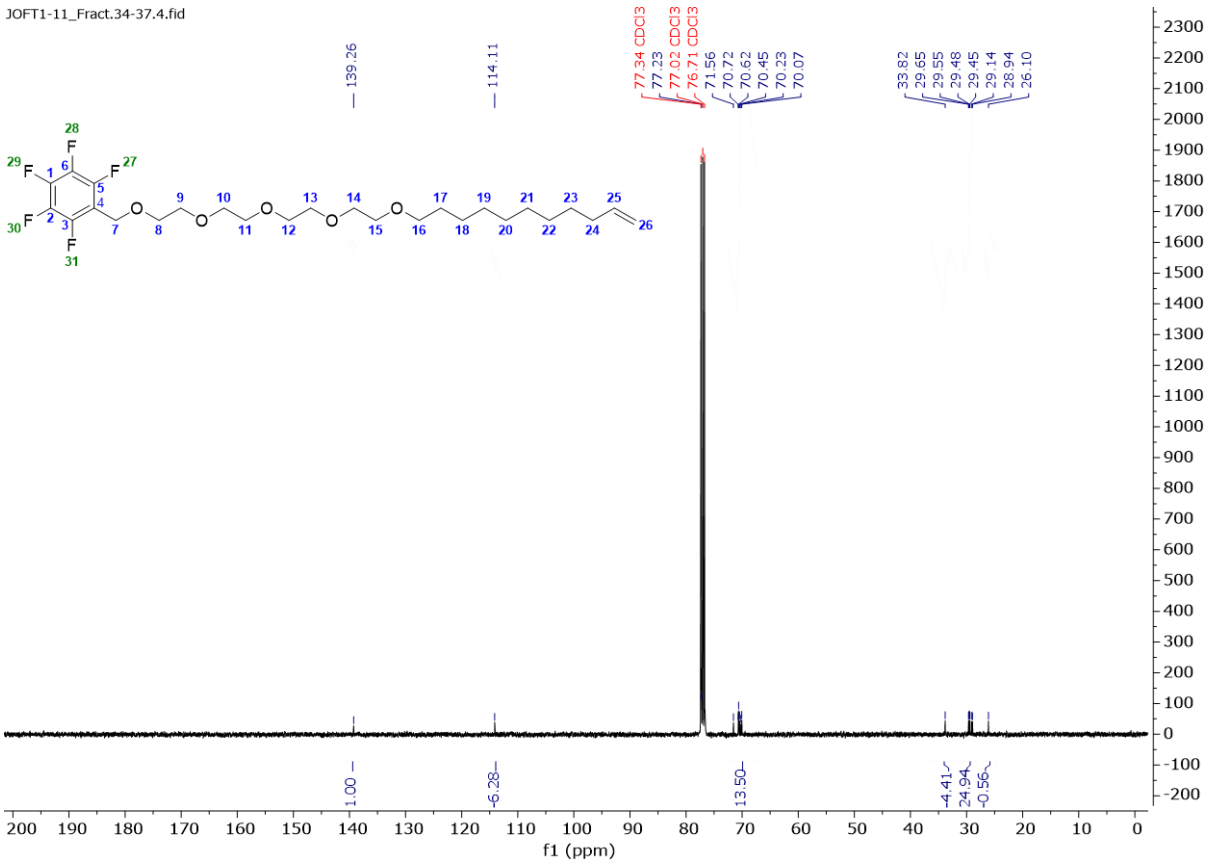
JOFT1-11_Fract.34-37.4.fid
139.26
114.11
77.34 CDCl3
77.23
77.02 CDCl3
76.71 CDCl3
71.56
70.72
70.62
70.45
70.23
70.07
33.82
29.65
29.55
29.48
29.45
29.14
28.94
26.10
1.00
6.28
13.50
4.41
24.94
0.56
f1 (ppm)

***C*-Methyl 26-(2,3,4,5,6-pentafluorophenyl)-13,16,19,22,25-pentaoxahexacosanethioate (5-Ac)**

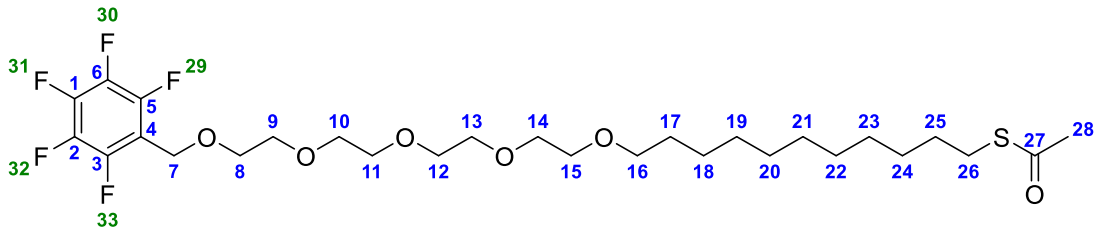

AIBN (0.0161 g, 0.0979 mmol, 0.6 equiv) was added to a microwave vial that had been equipped with a dry stir bar, then **4** (0.0890 g, 0.163 mmol, 1 equiv) was dissolved in 1mL of dry toluene and transferred quantitatively with an additional 0.2ml of dry toluene to the microwave vial. Once mixed, 0.235 ml of thioacetic acid (5 equiv, 0.8156 mmol) was added to the microwave vial. The reaction mixture was then heated to 70 °C and stirred overnight (18h). The reaction mixture was added to water (20 mL), extracted into EtOAc (80 mL x 3), washed with brine (100 mL), dried over $MgSO_4$ and concentrated on a rotary evaporator. Purification was achieved with flash column chromatography (10% EtOAc in hexane). The reaction gave a yellow oil. 0.040 g, Yield 40.7%. **^{1}H NMR** (400 MHz, $CDCl_3$) δ 4.65 (2H, t, *J* = 1.9 Hz, C7-H), 3.64 – 3.57 (16H, m, $(C_2O)_4$-H), 3.43 (2H, t, *J* = 6.8 Hz, C16-H), 2.86 (2H, t, *J* = 7.4 Hz, C26-H), 2.32 (3H, s, C28-H), 1.55 (2H, pd, *J* = 6.7, 4.0 Hz, C17-H), 1.38 – 1.23 (16H, m, C18-25-H); **^{19}F NMR** (377 MHz, $CDCl_3$) δ -142.66, -153.81, -162.02; **^{13}C NMR** (101 MHz, $CDCl_3$) δ 196.1, 71.6, 70.7, 70.6, 70.4, 70.2, 70.1, 60.0, 30.7, 29.6, 29.5, 29.5, 29.2, 29.1, 28.8, 26.0 (Solvent $CDCl_3$ Peak 77.2). **HRMS (ESI)** m/z $[M+H]^+$ calcd. for $C_{28}H_{44}F_5O_6S^+$ 603.2773; found 603.2758. **Rf** 0.61 in (40% EtOAc in hexane).

^{1}H NMR

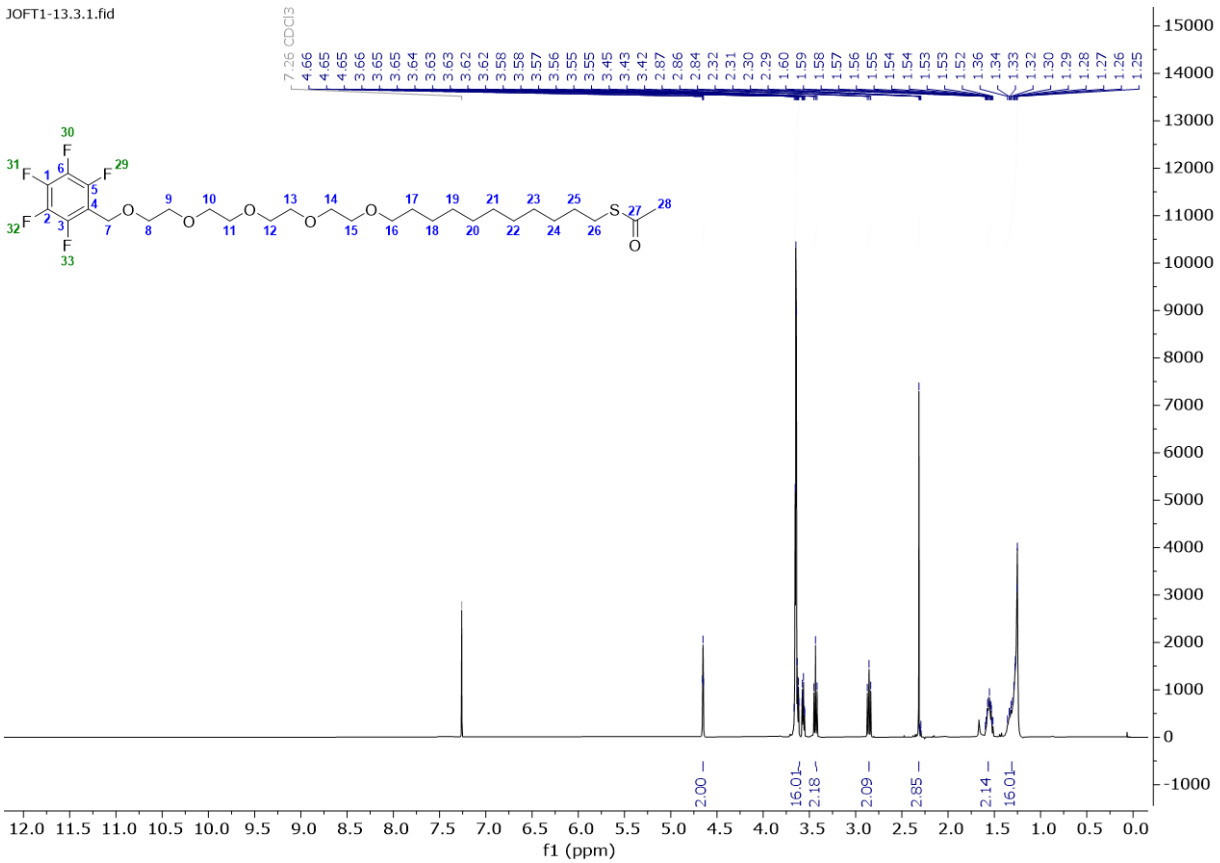

^{19}F NMR

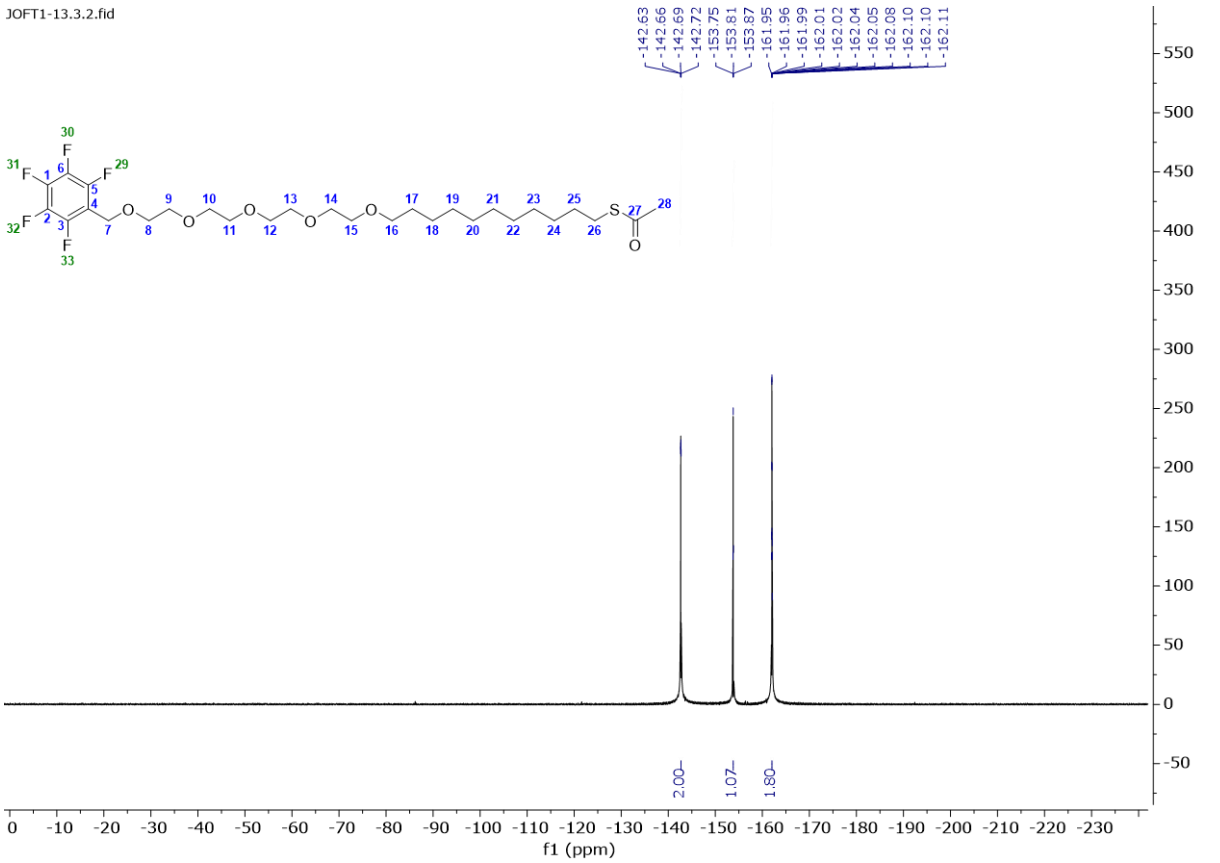

^{13}C NMR

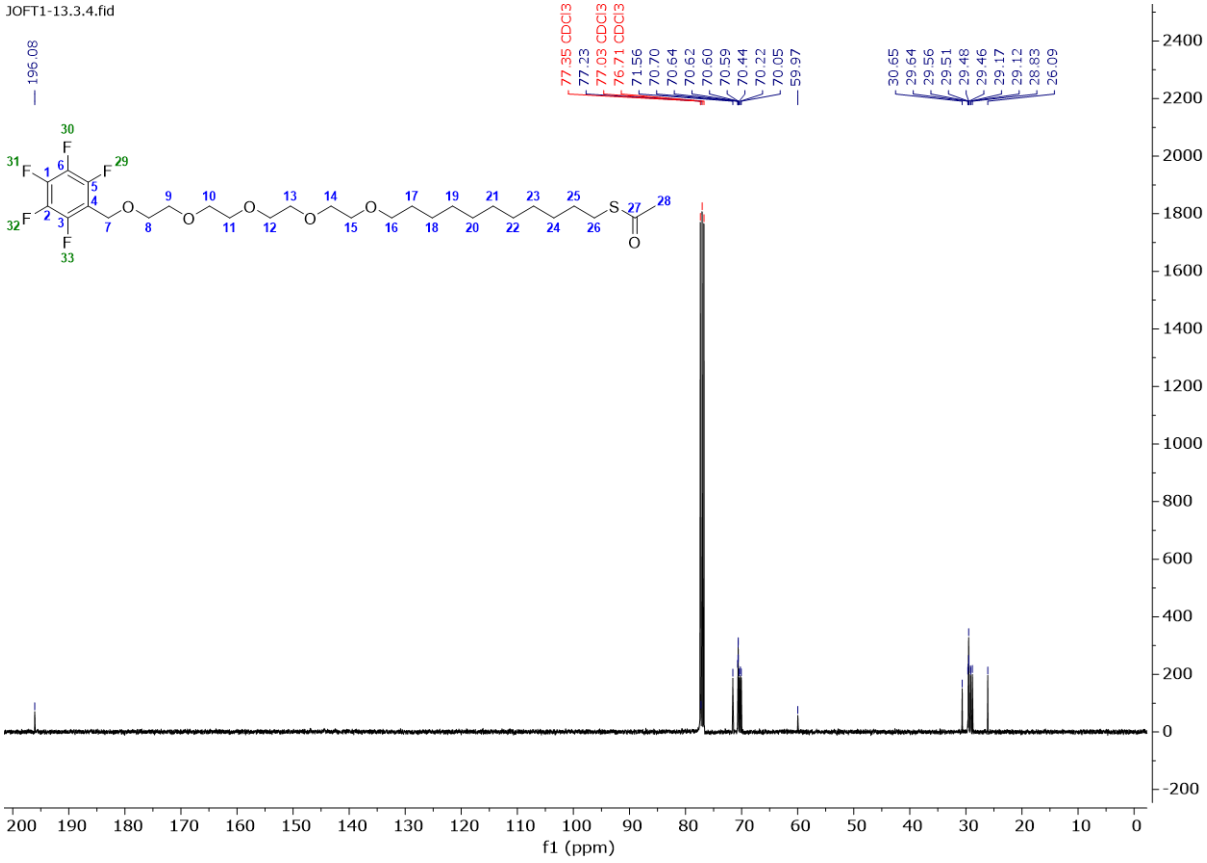

2.1.4 General Thiol Deprotection

For the deprotection of each acetate-protected thiol (**1-Ac**, **3-Ac** and **5-Ac** to **1**, **3** and **5**), the desired amount of the protected thiol, typically 0.040 g, 1 equiv, was placed into a dry microwave vial, followed by the addition of 5 equivalents of methanolic hydrochloric acid (HCl) (1.20 M as supplied), in dry MeOH (0.5 mL). The reaction was stirred at 55 °C for 3 hours. The resulting solution was concentrated via rotary evaporation to yield clean product (>90% yield by NMR) and re-dissolved in ethanol to the desired concentration of 10 mM. These solutions were stored in a fridge and used the next day (18h) to functionalize the Au LSPR sensors.

2.2 LSPR Sensor and Functionalization

The gold nanostructures were created using a standard top-down electron-beam lithography process. The lithography process resulted in a nanoarray consisting of elements that are 130 nm x 130 nm x 50 nm Au individual nanostructures with spacing of 390 nm.

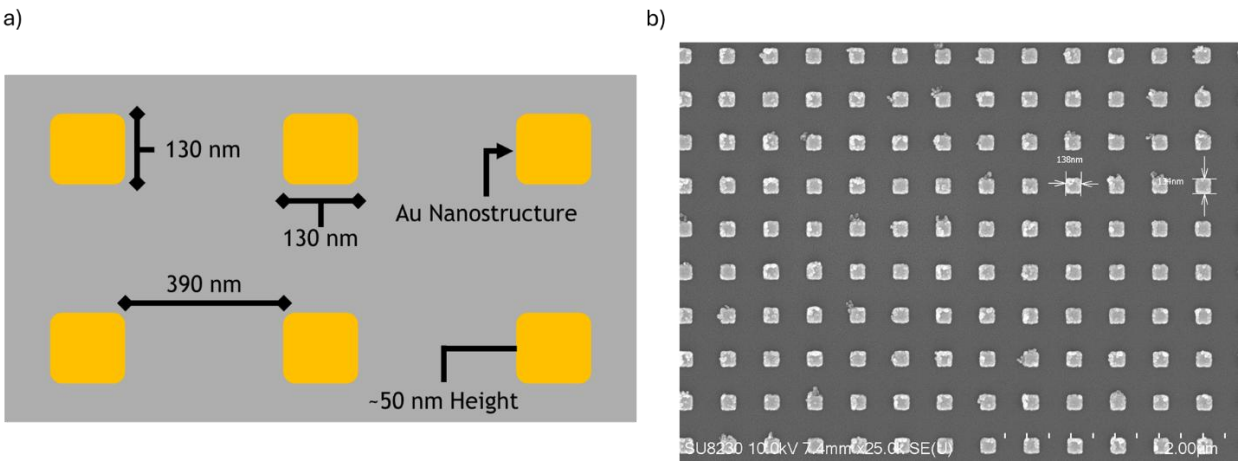

Figure 9. Schematic representation of Au nanostructure design and dimensions. b) Representative SEM of gold nanostructures prepared using the standard top-down electron-beam lithography process, identical to those used in this thesis.

Commercial microfluidic chambers (Microfluidic Chip Shop) were glued to the device. The LSPR flow sensor was composed of individual flow channels that each contained a small grouping of Au nanostructures (Figure 9). All sensing regions were functionalized in parallel.

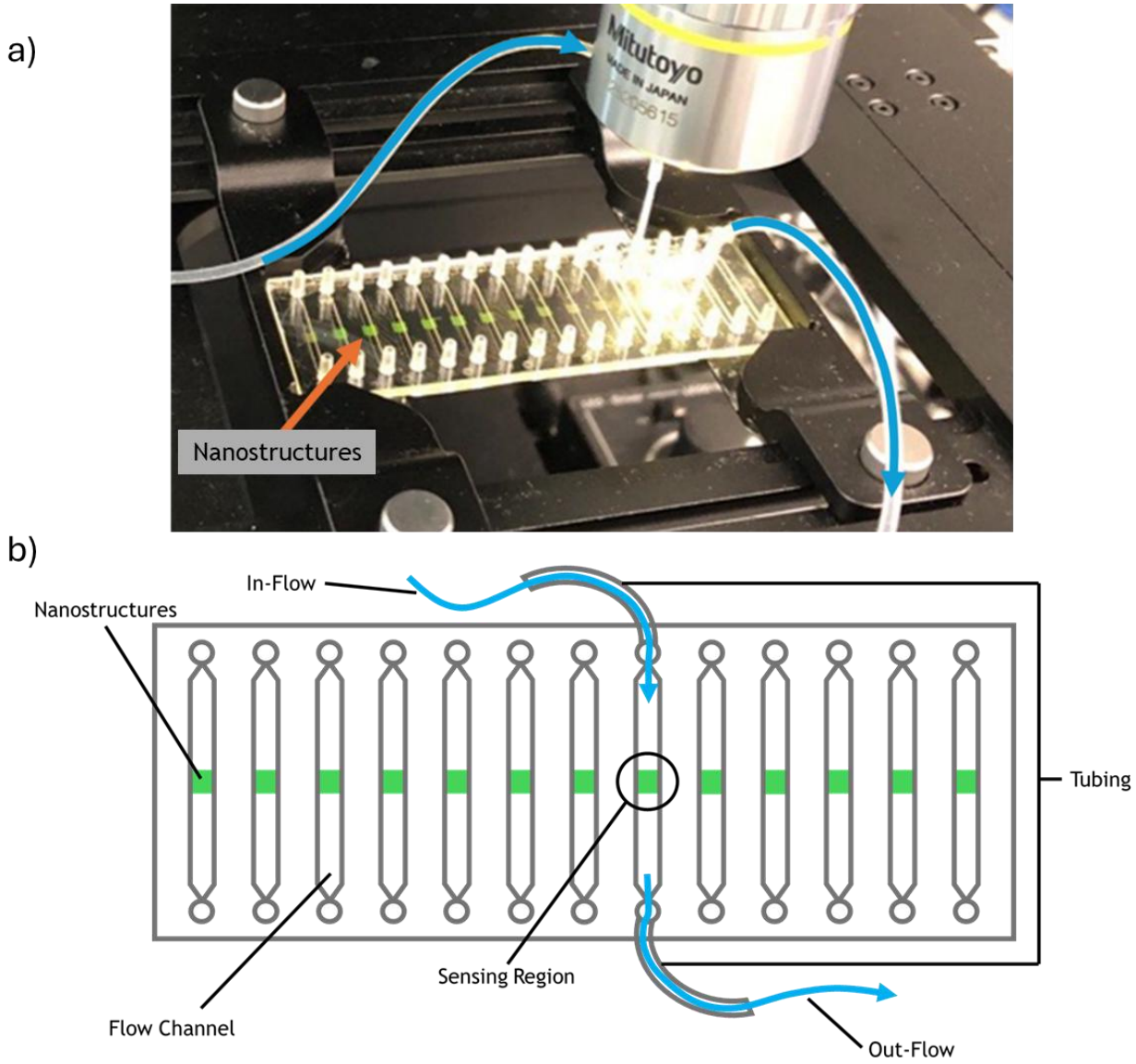

Figure 10. a) LSPR sensor, indicating one of the nanostructures within the sensor and with the blue arrows showing the flowing of a target solution over one of the functionalized sensing regions during a measurement. b) Design of the microfluidic device used.

The senser measured transmission by utilizing a setup which involved a broadband LED light source, a 10x objective, and a Spectrophotometer. The LED light source was a MBB1L3-470-850 nm Mounted Broadband LED, 70 mW (Min), 500 mA, the objective used was a 10x Mitutoyo Objective and the spectrophotometer used was a BLUE-Wave Miniature Spectrometer with a measurement capability in the 200-1150nm wavelength regions and a signal to noise ratio of 1000:1. For all experiments the spectrophotometer acquired spectra over a 500–875 nm wavelength range with a 0.1 nm step size, using a 45 ms integration time and would capture 3 scans in order to average.

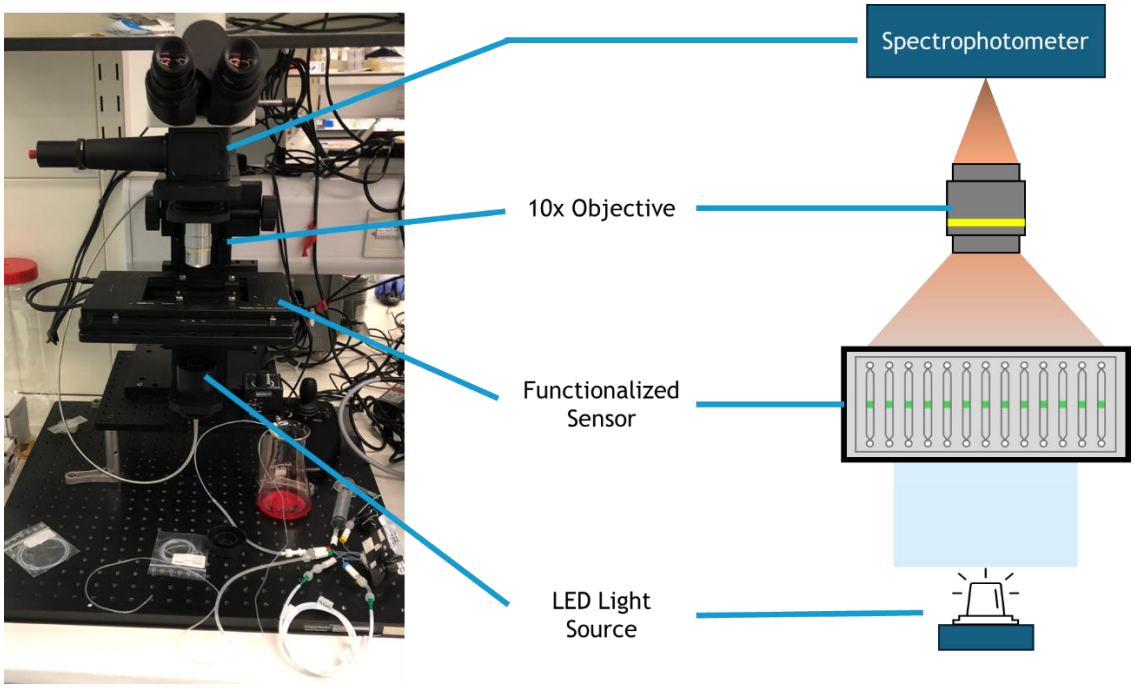

Figure 11. New figure: The experimental set-up used for all LSPR experiments, demonstrated by a photo of the set-up used alongside a schematic representation of the set-up's individual component.

To functionalize thesensing regions, 1 ml of the desired 10 mM thiol-ethanol solution was injected into one of the sensor's flow channels and left to sit for 1 h. This was followed by 0.5 mL of the same thiol-ethanol solution flowing, followed by 1 ml of ethanol, 1 ml of water, and finally 1 ml of phosphate-buffered saline (PBS). The channels after this functionalization were not allowed to dry out, with all sensing regions being kept in solution (PBS) unless otherwise stated.

2.3 Antifouling Experiments

All LSPR measurements were performed using a transmission mode microscope containing an SL1 tungsten halogen light source (focus spot is roughly 45 µm diameter) that acted as a broad-spectrum white light source from under the sensor, and the transmitted light was passed via optical fibre to a spectrometer with a range of 350-1150 nm and resolution of 0.4 nm (StellarNet Inc). All experiments were conducted at room temperature (23°C) in a microfluidic channel (1000 µm wide x 200 µm deep x 18 mm long) connected to Silicone tubing via PTFE tubing (microfluidic ChipShop GmbH). Flow was supplied by LabV1-II peristaltic pump and a MC12 Pump Head (Shenchen).

The process entailed taking the functionalized sensor and flowing PBS over the sensor to test the functionalized surfaces. This was followed by a BSA solution, followed by another rinse of PBS. During this process, the flow rate was set to 200 µL/min for all solutions, and the LSPR

system took spectra at a rate of 1 spectrum per second. During these experiments, multiple solutions were used and switched. The main peristaltic pump would pump PBS, which could be changed to a different solution if needed. The change to a different solution was completed using a 1 mL injection loop (designed by Justin Sperling) (Figure 10).

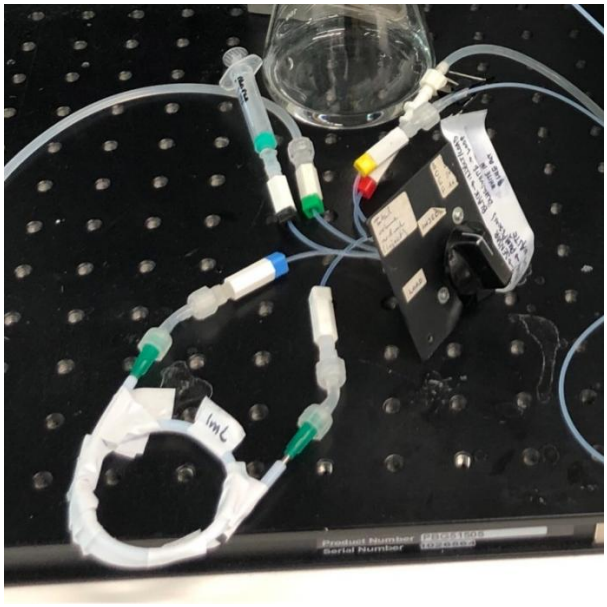

Figure 12. Injection loop used to interchange solutions during experiments.

To load the injection loop, PBS (~1.5 mL) was used to flush and rinse the loop prior to filling it with the BSA test solution. To introduce a new solution in an experiment, the loop was set to the "inject" position, allowing the BSA solution to be delivered into the sensing region. After the designated exposure time, the loop was returned to the "load" position, redirecting the PBS flow back into the sensing region. During PBS flow, the injection loop could be emptied and refilled with a different solution without interrupting the experiment.

To rinse the sensing region, an 80:20 methanol:water (v/v) solution was used. First, the injection loop was flushed with 1.5 mL of PBS, then filled with the methanol solution. When required, the loop was switched to "inject" mode to introduce the methanol solution into the sensing region.

3 Results and Discussion

All designed deprotected antifouling molecules (**1**, **3**, **5**) were evaluated and compared against control surfaces (Figure 11). Two distinct surface types were developed and analysed for specific purposes. The first type was a pure monolayer, intended to assess the antifouling properties of the synthesized molecules. These surfaces were compared to a bare gold sensor and a PEG functionalized reference surface, which served as a standard antifouling benchmark. The second type was a mixed monolayer surface engineered to evaluate the sensing applications of the designed surfaces. The created surfaces were assessed in comparison to pure monolayer versions of the antifouling molecules used in the mixed monolayer surfaces; those were **5**, a PEG functionalized surface, and a carboxyl-terminated molecule incorporating a PEG spacer. These molecules were chosen as they all utilized PEG within them, which would aid in the proper aligning of all the molecules in the SAM (Section 1.3).[61,62] Functionalization of all surfaces was systematically characterized to assess the designed molecules' antifouling and sensing performance.

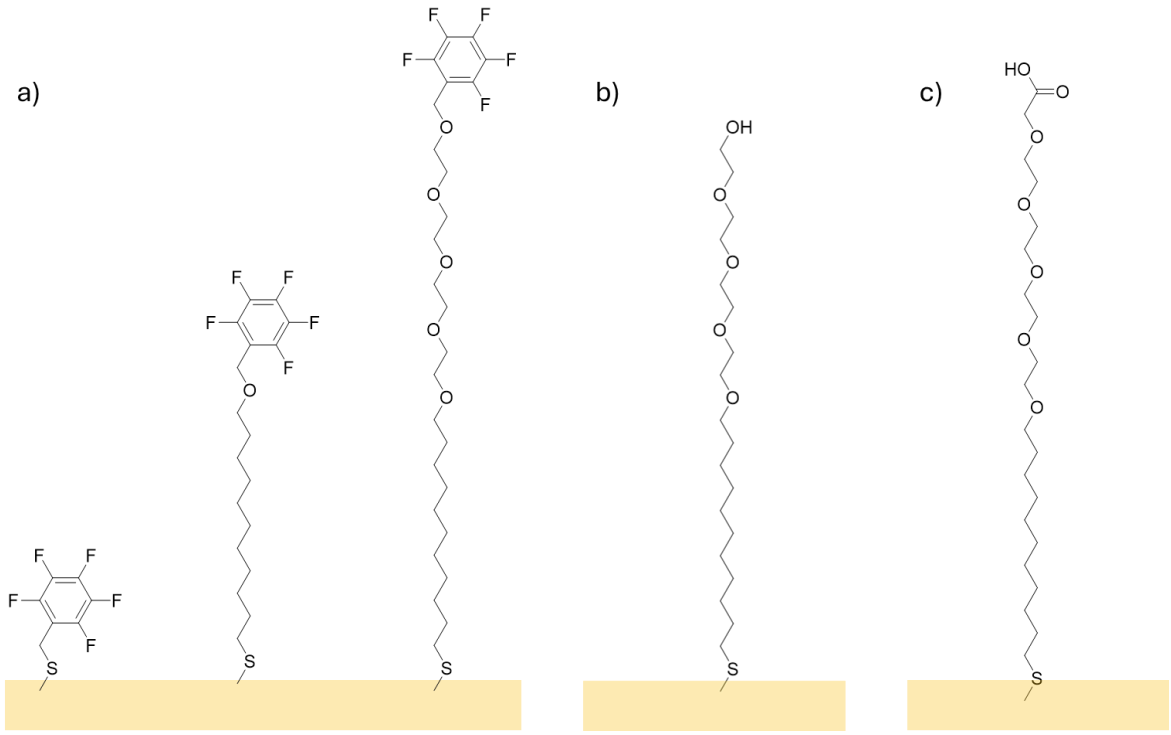

Figure 13. Visual representation of a) designed molecules (1, 3, 5), b) is the PEG based molecule used as a standard in experiments conducted (synthesized by Daniel Osborne at the University of Glasgow) and c) is the carboxyl containing molecule used to functionalize an antibody (synthesized by Daniel Osborne at the University of Glasgow)

3.1 Synthesis

All designed molecules (**1-Ac**, **3-Ac**, **5-Ac**) were successfully synthesized. Originally in the outset of this thesis, a zwitterionic molecule was meant to be designed and synthesized to serve as another control surface. Limited time resulted in the synthetic pathway from Wang

et al. for the zwitterionic molecule to be left incomplete.[88] The use of only PEG as a control surface however provided enough of a reasonable control due to its frequent and prolonged use for antifouling surfaces (Section 1.4).

3.1.1 Synthesis of S-[(2,3,4,5,6-pentafluorophenyl)methyl] ester (1-Ac)

A small antifouling molecule containing only the PFB moiety was designed to evaluate the antifouling efficacy of the PFB group in isolation, without the influence of an alkyl chain. Additionally, the reduced molecular size aimed to provide insight into the impact of chain length on antifouling performance. In order to synthesize the protected thiol in compound **1**, a reaction similar to a Williamson ether reaction, taken from Sohn et al., which used K_2CO_3 to react the pentafluorobenzyl bromide with thioacetic acid was used.[117] This reaction afforded compound **1-Ac** in 40.0% yield (Figure 12).

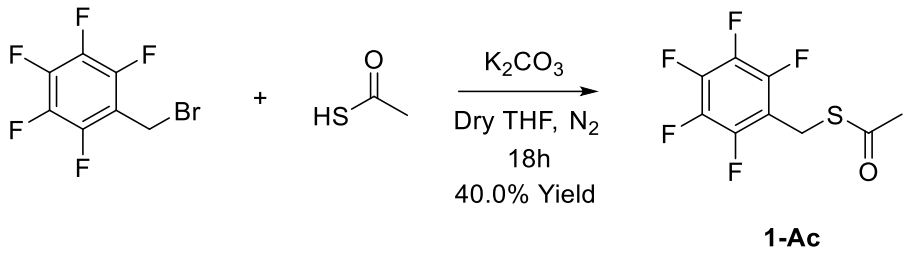

Figure 14. Reaction Scheme for the synthesis of compound 1-Ac

3.1.2 Preparation of the alkyl fluorous antifouling molecule.

A molecule incorporating both an alkyl chain and the PFB moiety was synthesized to assess the antifouling capability of the PFB group, within a SAM governed by alkyl thiol interactions; an established method for generating well-ordered and effective SAMs. In order to incorporate PFB into an alkyl chain initially, a reaction influenced by Molnár et al. was attempted for the creation of both compounds **2** and **4**.[118] This reaction utilized NaH to create the alkoxide, to synthesize an ether. Bu_4NI was used in the reaction to ensure the base would dissolve in the reaction solution. However, this reaction was unable to successfully synthesize **2**. This failure likely resulted from the reaction procedure taken from Molnár et al., in which a formal deprotonation was attempted in the presence of the electrophile. This approach provided the base with multiple off-target sites for deprotonation on the PFB ring via nucleophilic aromatic substitution, reducing the reaction's selectivity and efficiency. An alternative reaction was selected to avoid a formal deprotonation in situ and to employ a base less likely to induce nucleophilic aromatic substitution on the fluorinated ring. A synthetic process adapted from Rakhimov et al. which utilized KOH instead of NaH was used for the synthesis of **2**.[119] The

reaction had the deprotonation occur before the introduction of the pentafluorobenzyl bromide. This improved reaction afforded compound **2** in 52.0% yield (Figure 13).

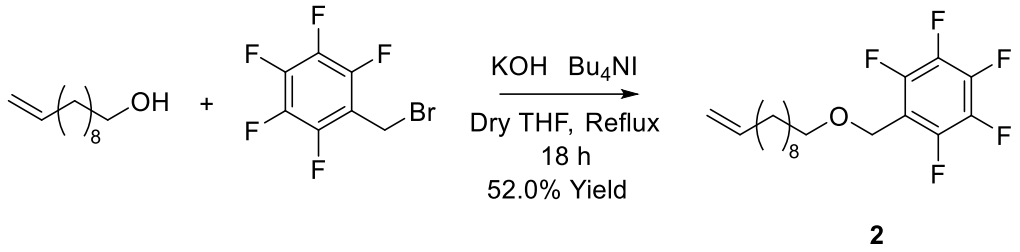

Figure 15. Reaction Scheme for the synthesis of compound 2

3.1.3 Protection of 11-[(2,3,4,5,6-Pentafluorophenyl)methoxy]-1-undecene (2)

In order to add the protected thiol to compound **2**, a thiol-ene click reaction was performed utilizing AIBN as a radical initiator. Due to an error in calculation, the reaction used to synthesize **3-Ac** had a higher ratio of AIBN (0.720 equiv) and thioacetic acid (7.20 equiv). Ideally for an optimal reaction, 3 equivalents of thioacetic acid and 0.30 equivalents of AIBN should have been used. However, this was not an issue, and the reaction afforded a yield of 80.0% of compound **3-Ac** (Figure 14).

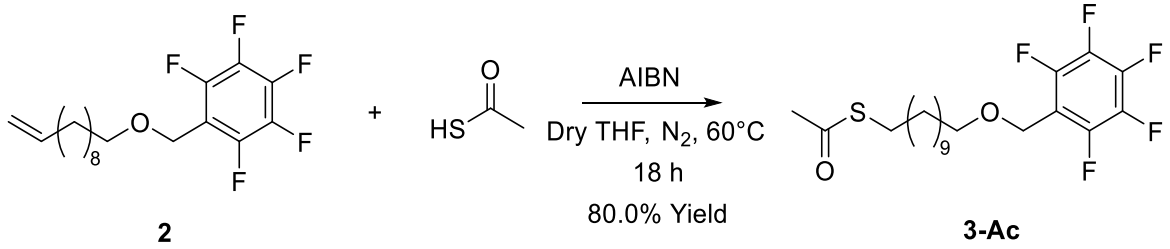

Figure 16. Reaction Scheme for the synthesis of compound 3-Ac

3.1.4 Preparation of the amphiphilic fluorous antifouling molecule

To synthesize an amphiphilic compound, the hydrophobic PFB moiety was integrated into a molecule containing a hydrophilic PEG segment. An 11-carbon alkyl chain was also included to promote the formation of a uniform and well-ordered SAM. The reaction used, which was adapted from Molnár et al., was the same reaction initially used to synthesize compound **2** which utilized NaOH as a base.[118] This process suffered from the same issue seen in Section 3.1.2, reducing the reaction's selectivity and yield. The reaction process afforded a yield of 15.0% of compound **4** (Figure 15). Due to a lack of time, the optimized synthetic pathway used

in Section 3.1.2 to synthesize compound **2** was unable to be used for the synthesis of **4**, but enough material was produced using the initial reaction pathway for further testing.

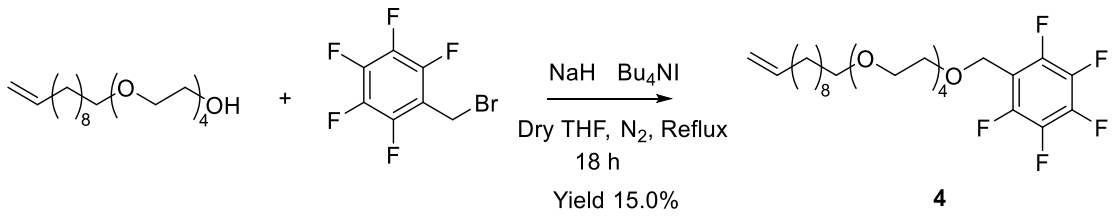

Figure 17. Reaction Scheme for the synthesis of compound 4

3.1.5 Protection of 1-(2,3,4,5,6-Pentafluorophenyl)-2,5,8,11,14-pentaoxa-24-pentacosene (4)

In order to add the protected thiol to compound **4**, a thiol-ene click reaction was performed utilizing AIBN as a radical initiator. This reaction process afforded a yield of 40.7% of compound **5-Ac** (Figure 16).

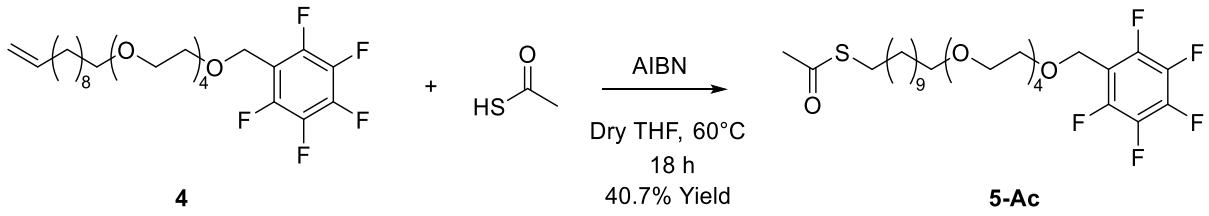

Figure 18. Reaction Scheme for the synthesis of compound 5-Ac

3.1.6 Deprotection process

The process used to deprotect the thiol was adapted from Sohn et al. and utilized HCl in methanol at 55 °C for 3 h to form the free thiol and a volatile methyl acetate by-product (Figure 17).[117] The volatile by-product would be removed via rotary evaporation.

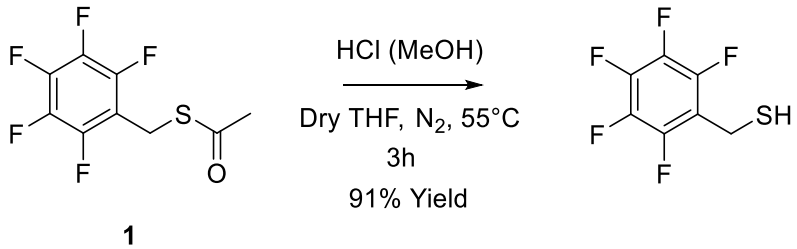

Figure 19. Reaction Scheme for the deprotection of compound 1-Ac to compound 1

Due to the unstable nature of thiol molecules, the yields for all deprotection reactions were assumed to be >90%. This value was determined by ^{1}H NMR analysis of the crude reaction mixture obtained during the synthesis of the deprotected compound **1** (Figure 18) and is further supported by values reported in other studies.[120]

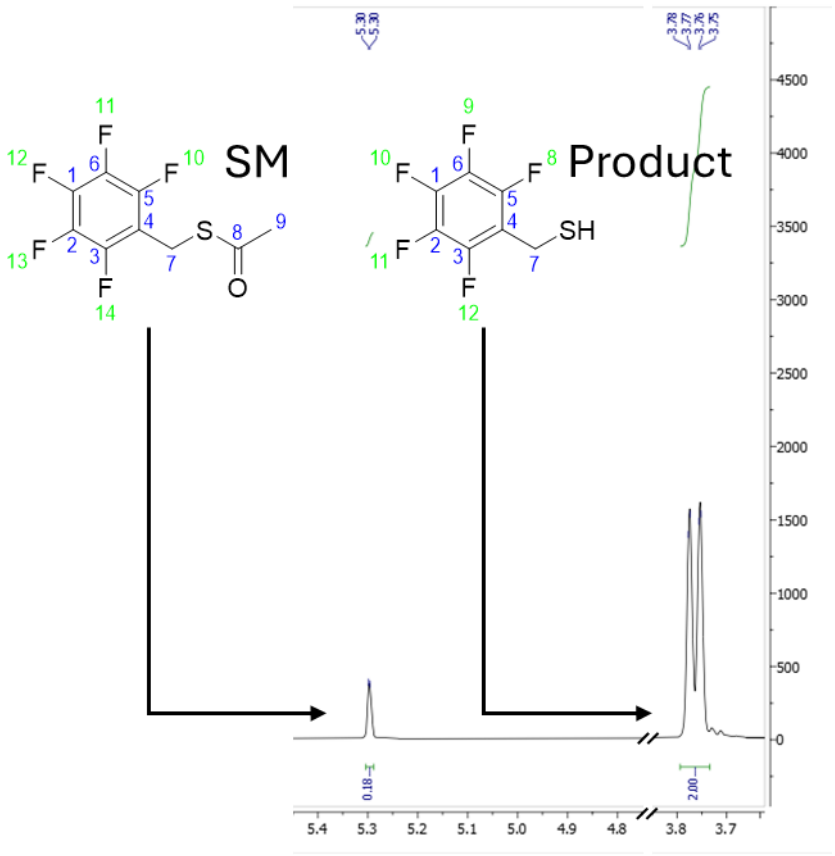

Figure 20. The ^{1}H HMR of the reaction mixture after the deprotection of compound 1-Ac, showing the peak integration for the protons on carbon 7 of the starting material (0.18) and the product (2.00). The ratios between the integration values can be used to determine the yield of the reaction, here 91%.

3.2 Antifouling Ability of Designed Molecules

To determine the antifouling ability of all designed deprotected molecules (**1**,**3**,**5**), each molecule was functionalized onto their own individual sensing region on a LSPR sensor, resulting in the creation of a SAM. Each of these sensing regions were then flowed over with BSA to determine the amount of protein that would foul onto them.

3.2.1 Functionalization

The creation of the SAMs was monitored using LSPR (Figure 19). A singular transmission spectrum was taken of each untreated LSPR sensor in PBS before introducing the ethanolic solution containing the desired antifouling molecule and subsequent rinsing in PBS. The pre-

functionalized transmission minima from the untreated sensor in PBS were compared to the corresponding transmission minima obtained under PBS after sensor functionalization and rinsing. The post-functionalization values were determined by calculating the mean of the last 100 LSPR measurements taken during the initial PBS rinsing step (Figure 21). The difference between the pre-functionalization and post-functionalization transmission minima for a given surface would provide a reasonable approximation of the successful functionalization and the formation of a SAM. However, since only a single transmission spectrum was taken for each untreated sensor surface, the uncertainty of the difference data could not be calculated.

Observing a difference value would demonstrate that the surface environment was changed by introducing the antifouling molecules, indicating that the surface was functionalized and confirming the creation of the SAM.

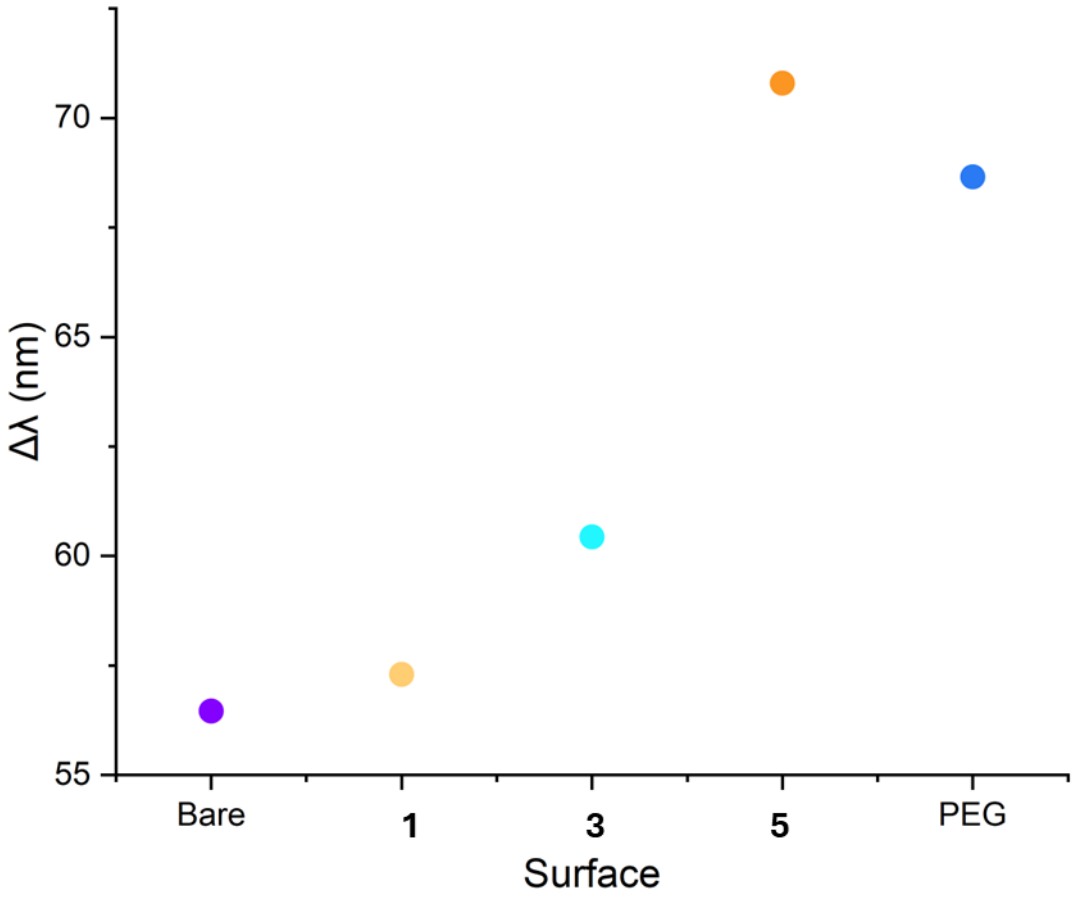

Figure 21. Graph showing the change in LSPR signal before and after surface functionalization with deprotected antifouling compounds 1, 3, 5, and PEG, compared to a bare gold surface. The observed signal shifts serve as a reasonable approximation of functionalization success, indicating the extent of surface modification for each compound relative to the unmodified bare gold surface.

As expected, the bare unfunctionalized surface showed the least difference from the functionalization, as no molecules were added to functionalize the surface. However, the

bare gold, used as the control, had shifted 56.46 nm. It is difficult to determine an exact cause for this disparity; since it was a control surface, little change should have been observed. Two factors were the most likely to create the difference regarding the bare gold. Glue used in the flow channels could have dissolved in the ethanolic solution used to functionalize the surface and could have affected the sensor's surface. In addition, the rinsing of the Au nanomaterials alone may have caused enough of a change to the localized plasmon environment. Though this unexpected difference was observed, a clear pattern between each surface design was seen. Compound **1** shifted 0.84 nm more than the bare sensor. Using the same metric, Compound **3** had a difference of 3.98 nm from the bare sensor, Compound **5** had a shift of 14.34 nm, and PEG shifted 12.20 nm compared to the bare sensor. All surfaces had increased, showing a redshift. A red shift is expected when a surface is functionalized or when any material adsorbs onto the sensor. The size of the shift corresponds to the amount of material adsorbed at the surface. Larger electropositive molecules will cause a greater shift.[121] This pattern is seen in the functionalization data, as the larger molecules PEG and Compound **5** had a larger shift when compared to compounds **1** and compound **3** molecules.

3.2.2 Data acquisition

In order to determine the amount of functionalization, fouling and immobilization, LSPR was utilized. As described in Section 1.2.3 plasmonic measurements are based on the minimum of the transmission spectrum, corresponding to the plasmonic resonance of localized surface plasmons.[27,41] This resonance was identified by determining the wavelength at which the percent transmission reached its minimum (Figure 20). The wavelength would determine the plasmonic resonance of the sensor, and if a change occurred to the wavelength, this would indicate a change to the sensor's surface environment.

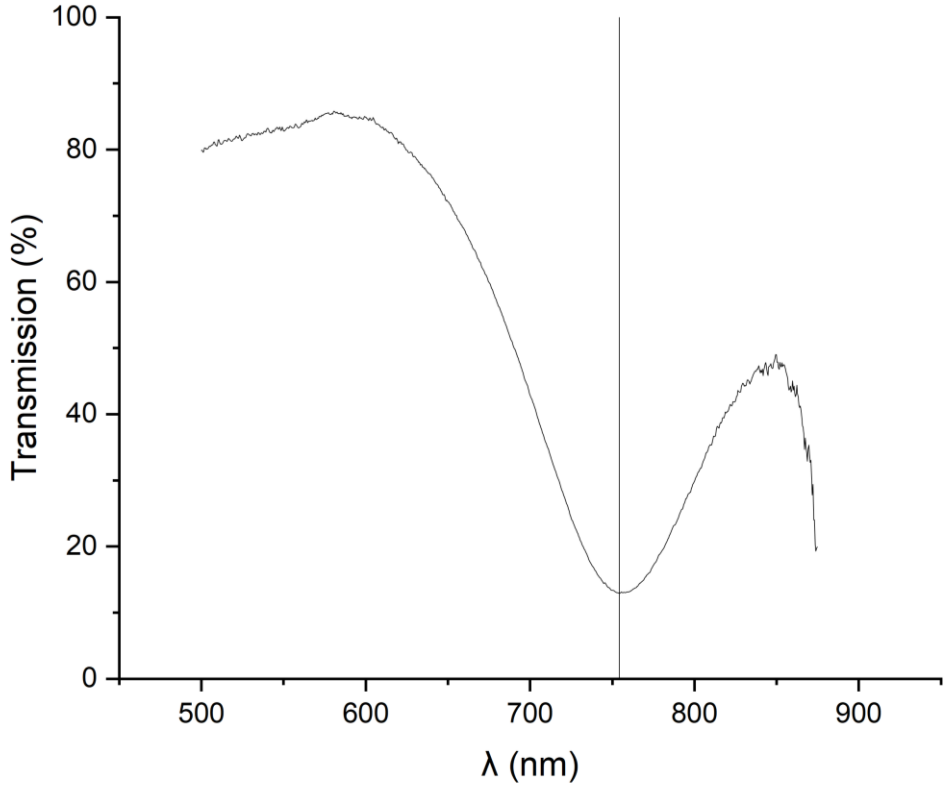

Figure 22. Transmission spectra of unfunctionalized bare LSPR sensor, showing a minimum of transmission caused by localized plasmons resonating at 754.38 nm.

To monitor the change to the surface environment in real time, an LSPR measurement was taken every second. For each spectrum taken, the wavelength value at the minimum transmission was extracted, plotted against time, and then smoothed using 10-point adjacent averaging. This process was done using software developed by Calum Cuthill and Justin Sperling at the University of Glasgow.

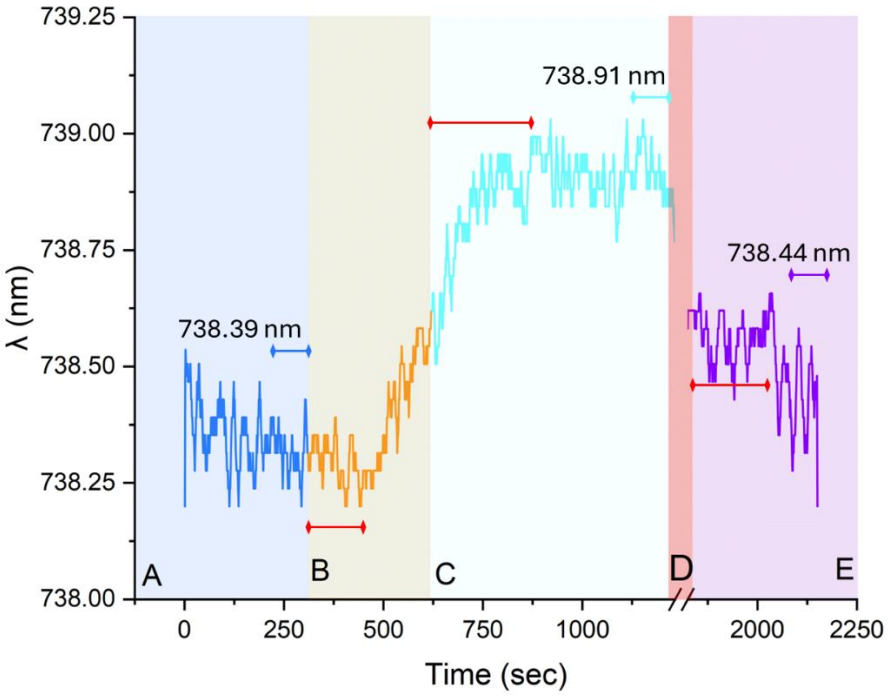

Figure 23. A graph of bare gold, plotting wavelength of the transmission minima vs time. A) Initial rinse of PBS over functionalized surface. B) Introduction of BSA. C) A secondary rinse of PBS used to determine the amount of protein adsorbed onto the surface. D) Methanol solution (ratio 80:20 methanol and water) rinse which was excluded from the plot due to the change in refractive index caused by the change from PBS to methanol which overshadowed relevant data. E) Final rinse with PBS. The portions highlighted by the red arrows within the graph shows the delay that would occur when solutions were changed utilizing the injection loop. The portions highlighted in blue arrows at the end of part A, C, and E, of the plot shows the mean of the last 100 measurements taken for that part of the experiment. This mean is what was used to calculate the difference data.

Capturing a spectrum per second allowed for real-time visualization of how the surface changed when introduced to different environments. This enables an approximation of the amount of BSA that fouls onto a given surface as a function of LSPR peak shift. To determine the amount of fouling, the mean of the last 100 data points taken during the first PBS rinsing process before the introduction of protein and the mean of the last 100 data points taken during the second PBS rinsing process were subtracted from each other (Δλ), with the error being calculated using:

$$\sigma_z = \sqrt{(\sigma_x)^2 + (\sigma_y)^2}$$

where σ_z is the uncertainty, σ_x is the standard deviation of pre-protein rinse data set, and where σ_y is the standard deviation of the post-protein rinse data set. This method allowed for the accurate depiction and comparison of the antifouling ability of the created surfaces.

As shown in Figure 21, when a methanol solution was used, the solution exhibited a refractive index (RI) distinct from that of the PBS solution, resulting in a significant discrepancy in the LSPR data obtained. However, this RI related effect was considered negligible in the case of the BSA solution, as PBS, the same solution used in all baseline measurements, was used as the solvent for all test solutions of BSA.

3.2.3 Antifouling Results and Conclusions

It was found that of the designed antifouling molecules, all were able to prevent fouling when compared to the bare Au. None of the designed molecules were able to antifoul against BSA more efficiently than the control PEG molecule. The PEG unexpectedly had a lower wavelength value after the introduction of the BSA than before. This could mean that an amount of the surface coating had been removed from flowing of the solutions during testing.

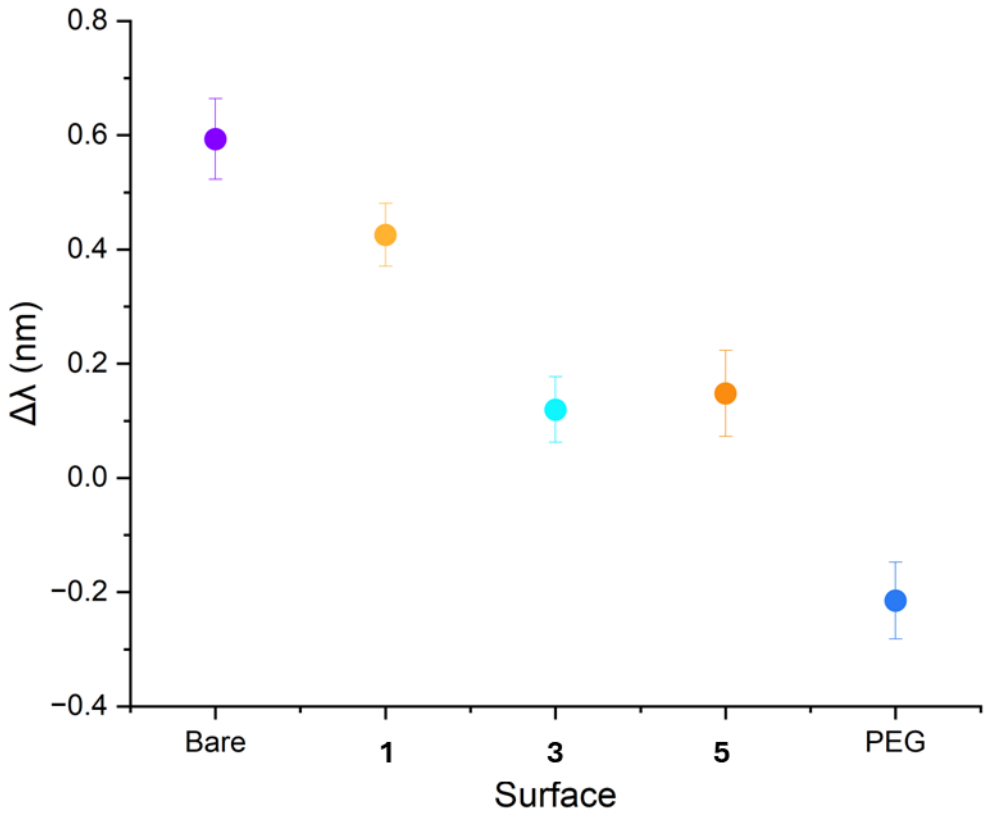

Figure 24. Graph of the difference value the LSPR signal found from before and after flowing of 500 nM BSA over the sensor vs the created surfaces, showing the amount of nonspecific binding (error bars were calculated using the formula mentioned in 3.2.2).

An important note to mention is that much of the data collected has the possibility to be within error as the spectral resolution was 0.4 nm. The concentration of BSA being 500 nM could have been responsible for this low change in wavelength. In future experiments, the

use of a higher concentration, as done in section 3.3.4, may be necessary. In addition, more replicate experiments are necessary to provide more accurate data.

3.3 Mixed Monolayer Surface

The development of a mixed surface, incorporating antibodies onto an antifouling layer, was attempted using a pentafluorobenzyl moiety as part of the surface chemistry. The goal was to create a sensor capable of selectively detecting the target analyte upon exposure, through specific binding to the surface-immobilized antibodies, while effectively repelling non-target (non-antigenic) species due to the antifouling properties. The main difference between the use and creation of the mixed surface when compared to the previous experiment (section 3.2) was the incorporation of the antibody into a SAM. To functionalize the antibody onto the surface, a molecule containing an alkane and PEG spacer, as well as a carboxy head group, had to be incorporated into the monolayer in a ratio of 75:25 antifouling molecule to carboxyl-containing molecules.

3.3.1 Functionalization of Mixed Monolayer Surface

For the creation of the mixed monolayer, which incorporated an antibody to the surface of the sensor, a carboxyl containing molecule incorporating PEG (Figure 11) (synthesized by Daniel Osborne from the university of Glasgow), was used and functionalized on the surface of the sensor. Once the surface had been functionalized, the confirmation of the functionalization of the created surfaces was found by utilizing the same method stated in Section 3.2.1 (Figure 23). A singular transmission spectrum was taken of each untreated LSPR sensor before introducing the ethanolic solution containing the desired antifouling molecule. These values were then compared to the mean of the last 100 LSPR measurements taken during the first PBS rinsing process. However, since only a single transmission spectrum was taken for each untreated sensor surface, the uncertainty of the difference data could not be calculated.

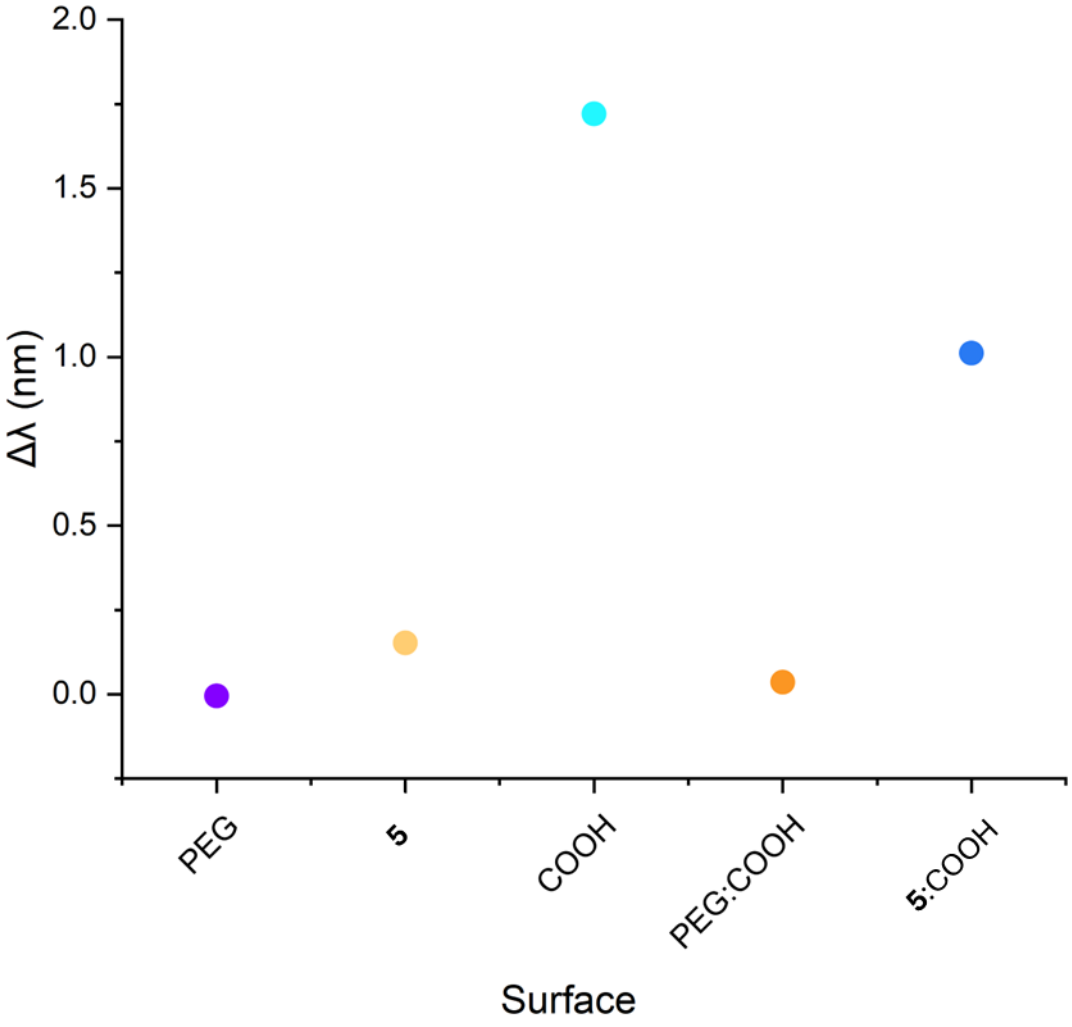

Figure 25. Graph showing the difference in LSPR signal before and after functionalization for each surface. Where COOH refers to the surface modified with a carboxyl-containing molecule; PEG:COOH represents a mixed monolayer surface composed of PEG and the carboxyl-containing molecule; and 5:COOH denotes a mixed monolayer surface incorporating both the carboxyl-containing molecule and compound 5. This graph is showing the relationship that a greater difference value represents a greater change to a given surface.

Contrasting the previous experiment carried out with pure monolayers, there was less evidence that the functionalization of the surfaces was successful. The 100% PEG surface, 100% compound **5** surface and the PEG mixed monolayer surface showed little change in wavelength after introducing the antifouling molecules. The 100% PEGalated carboxyl surface and the **5**:COOH surface were the only surfaces demonstrating a change after the functionalization process. In the future to provide more reliable data, more replicates of this experiment would need to be conducted.

3.3.2 Antifouling Results of Mixed Monolayer Surface

Two different experiments were conducted using the created mixed SAM surface. The first involved flowing the BSA over the surface and measuring the change in fouling before the immobilization of the anti-BSA antibody onto the surface. This first section was done as a control to see how the incorporation of a mixed monolayer would affect the antifouling ability of the designed surfaces (Figure 24).

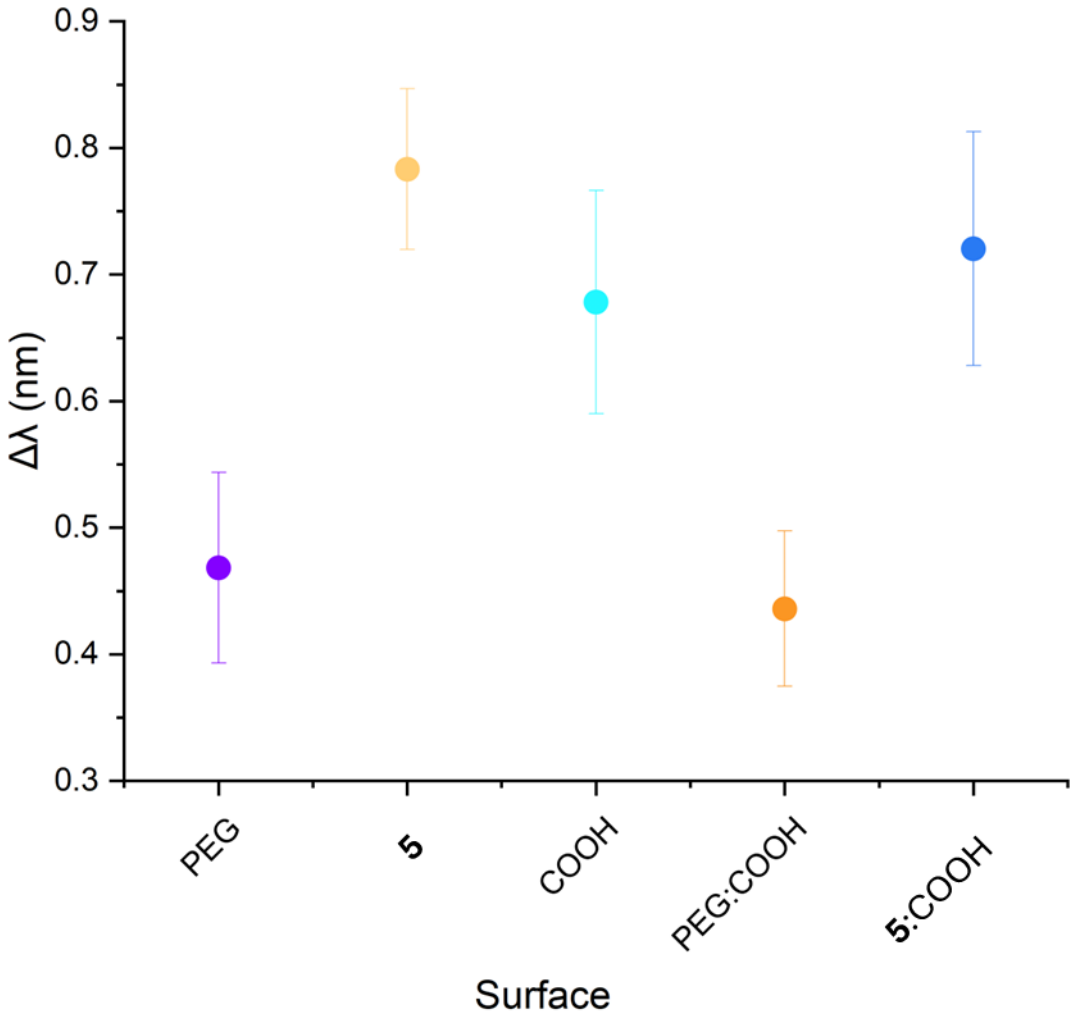

Figure 26. Graph of the difference values of the LSPR signal observed before and after the introduction of 500 nM BSA vs each surface, where COOH is the carboxyl containing molecule, PEG:COOH represents the mixed monolayer surface composed of PEG and the carboxy containing molecule, and where 5:COOH is the mixed monolayer composed of the carboxyl containing molecule and compound 5. Showing the level of fouling on the created mixed monolayer surfaces compared to the non-mixed monolayer equivalents (error bars were calculated using the formula mentioned in 3.2.2).

The results provided information that adding these carboxy-containing molecules did not significantly affect the surface compared to the non-carboxy-containing monolayer. The difference data showed that the fouling on the 100% PEG surface, 100% compound **5** surface and the PEG:COOH mixed monolayer surface mimicked the behaviour shown in the previous

antifouling experiments (Section 3.2.3), as both PEG surfaces outperformed the antifouling ability of compound **5** equivalent. This similarity suggests that even if the functionalization data had evidence of failed functionalization, the repetition of the observed pattern shows that functionalization could have occurred. However, the data used to make this conclusion, much like the data found in Section 3.2.3, could be within error as the spectral resolution was only 0.4 nm. The low concentration of BSA could have resulted in this uncertainty. Additionally, In the future to provide more reliable data, more replicates of this experiment would need to be conducted.

3.3.3 Antibody immobilization

Once the antifouling tests were complete, 1.5 mL of a PBS-based solution composed of 200 mM of EDC, 50 mM NHS and 50 µg/mL of anti-BSA was loaded into the desired flow chambers. This mixture was left to react with the carboxy-containing molecules affixed to the surfaces at RT overnight (18 h). A similar process that determined antifouling ability, as described in Section 3.2.3 and used in Section 3.3.2, was employed to monitor the antibody immobilization. For each surface, the mean of the last 100 LSPR measurements taken during the last PBS rinsing process of the experiment conducted in Section 3.3.2 was found. These values were then compared to the mean of the last 100 LSPR measurements taken after the immobilization process during the experiment to determine the sensing performance of the created surfaces. The error was calculated by the equation used in Section 3.2.2 of the data sets was used to determine the error of the found difference between the mean values.

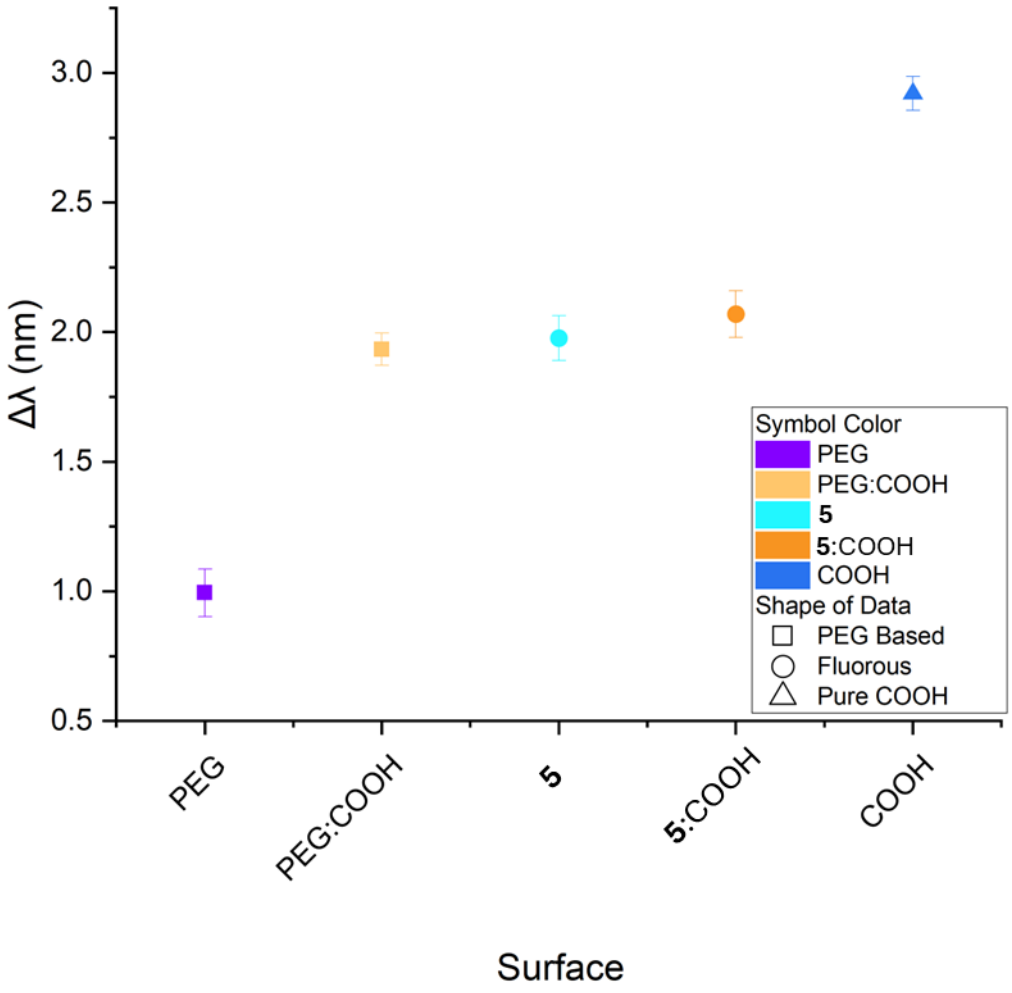

Figure 27. Graph of the difference values of the LSPR signal observed before and after the immobilization of the anti-BSA antibody vs the used surfaces tested, showing the effect and success of the incorporation of the antibody onto each surface, with a larger Δλ indicating a greater immobilization of antibodies on that surface (error bars were calculated using the formula mentioned in 3.2.2).

Successful antibody incorporation onto the mixed monolayer surface would be indicated by a greater signal difference compared to the corresponding non-mixed monolayer (Figure 25). This trend can be seen with the created PEG-Antibody surface, as this surface had a difference value, a 0.939 nm increase compared to the pure PEG monolayer. In addition, the pure monolayer composed of carboxy-containing molecules should have seen the most significant shift, as most antibodies would attach themselves to this surface. This trend is also visualized in the data found, with the pure monolayer containing the carboxy group having an overall difference from the baseline of 2.92 nm, indicating the successful immobilization of the antibody. However, a shift was seen in both PEG and compound **5** after the introduction of the antibody, which is not expected and indicates that an amount of anti-BSA had non-specifically bound to those surfaces. Additionally, much less of a change was seen between the two surfaces which utilized compound **5**, indicating that the introduced antibody was binding to both surfaces equally, meaning that the antibody was binding in a nonspecific manner. The disparity in change could have been caused by the PFB-PEG being less effective

at resisting the specific binding of the antibody to the target COOH molecule incorporated within the monolayer. This effect could have been reduced by incorporating a longer COOH-containing molecule, which would have given larger separation between the surface and targeting group, a concept discussed in section 1.3 that might have help immobilize the antibody more easily.[48]

3.3.4 Surface Sensing Performance

To evaluate the sensing performance of the mixed monolayer, 500 nM BSA was flowed over the sensors (Figure 26), followed by a second flow of 5 μM of BSA (Figure 27).

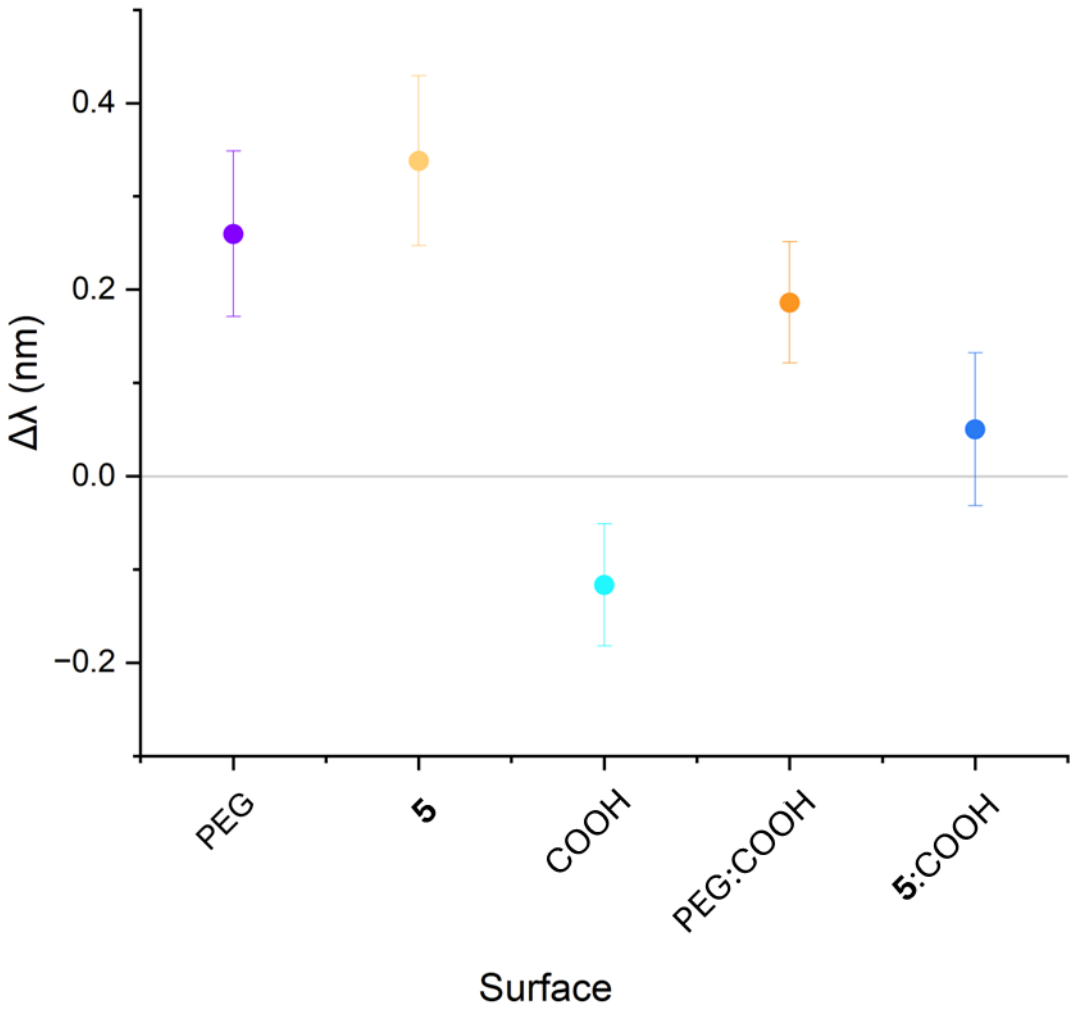

Figure 28. Graph of the difference values of the LSPR signal found from before and after flowing of 500 nM BSA over the sensor vs the created mixed monolayer surfaces, showing the amount of binding onto the antibody, indicating the functionality of the sensor (error bars were calculated using the formula mentioned in 3.2.2).

There was a greater difference between the antifouling surfaces without antibodies than those with incorporated antibodies, which is the opposite of what was expected, as the

antibodies should have caused more BSA to accumulate on the surface. This could be due to the introduction of BSA done in Section 3.3.2 before antibody incorporation. If residual BSA from the testing in Section 3.3.2 was on the sensing surfaces, the antibodies might not have had time to react with the carboxy groups as intended, as their high affinity to their respective target could cause them to bind to any residual BSA on the surface before they had a chance to react and functionalize. This would have resulted in the added antibodies having little to no effect, most likely causing an increase in fouling instead of a decrease. The choice of introducing the BSA before the antibody to determine the antifouling effects on the mixed monolayer surfaces was driven by a limitation of the testing setup used.

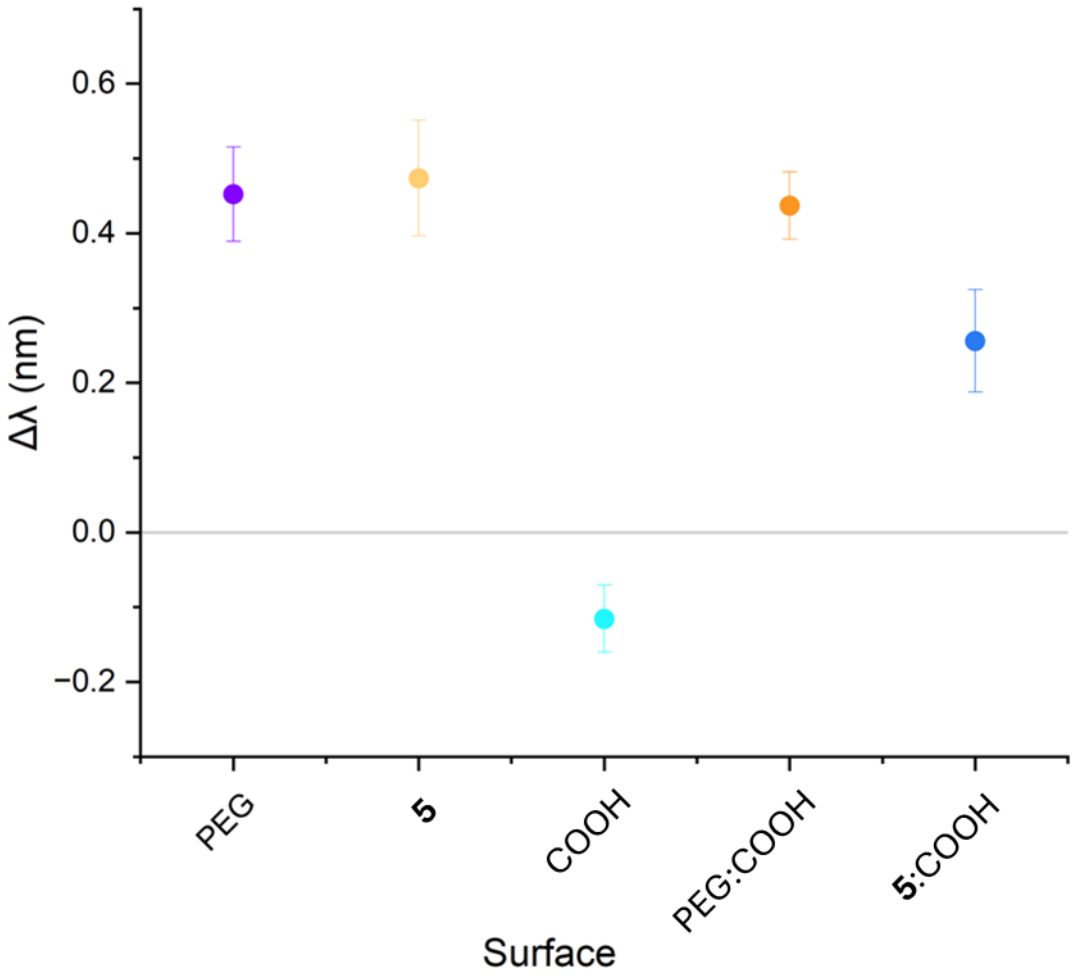

Figure 29. Graph of the difference values of the LSPR signal found from before and after flowing of 5 µM of BSA over the sensor vs the created surfaces, showing the amount of binding onto the antibody, indicating the functionality of the sensor (error bars were calculated using the formula mentioned in 3.2.2).

All LSPR measurements were done consecutively due to the nature of the LSPR device used. This consecutive method resulted in restrictions on the number of trials that could be conducted. This lack of repeated trials significantly decreased the reliability of the results. In addition, due to the consecutive nature of the trials, some of the functionalized sensors

were left in solution longer before testing than others tested beforehand. Despite rigorous washing, this delay may have led to variations in the surface and SAM. To prevent this issue for future testing, instead of utilizing flow channels, a different methodology which allows for the testing of multiple surfaces in parallel could be incorporated. Sperling et al. used an approach that enabled the simultaneous measurement of all plasmonic sensing elements.[122] Parallel measurements were carried out using a plasmonic chip containing 24 nanostructured sensing regions, each aligned with a dedicated slit aperture in the chip's opaque top metal layer. When illuminated from the backside with broadband light, all sensor regions were exposed at once. The transmitted light was then dispersed by a diffraction grating onto a Complementary Metal-Oxide-Semiconductor (CMOS) camera, producing a hyperspectral image in which each aperture generated its own vertical spectral column. This configuration allowed the resonance wavelength of all 24 sensing regions to be extracted from a single camera exposure, enabling true parallel LSPR measurement.

4 Conclusions and Future Work

This thesis explored the development and application of antifouling molecules incorporating a pentafluorobenzyl moiety for label-free chemical sensing, specifically targeting the reduction of nonspecific protein adsorption on gold nanostructures. All synthesized PFB-based molecules demonstrated antifouling capabilities against bovine serum albumin, outperforming bare gold surfaces. Compounds **3** and **5**, which incorporated long alkyl chains (11 carbons long), exhibited behaviour comparable to polyethene glycol, the current "gold standard" in antifouling. The study highlighted the potential of pentafluorobenzyl-functionalized surfaces to resist fouling while maintaining compatibility with plasmonic sensing techniques such as localized surface plasmon resonance. Incorporating PFB into mixed monolayers, combined with antibodies, aimed to create selective sensing surfaces, though the results were inconclusive due to experimental limitations. Despite this, the findings suggest that pentafluorobenzyl-based antifouling strategies offer a promising alternative to traditional methods, particularly in environments where PEG may degrade or fail to repel hydrophilic proteins.

However, the overall reliability of the antifouling and sensing data was constrained by the low spectral resolution of the LSPR spectrometer (0.4 nm), which limited the ability to resolve small wavelength shifts with confidence. Additionally, the lack of experimental replicates, caused by the consecutive measurement design of the LSPR system, prevented meaningful statistical comparison and reduced the robustness of the observed trends. These constraints mean that some of the reported differences between surfaces may fall within measurement uncertainty, underscoring the need for testing with higher concentrations of analyte, higher-resolution instrumentation and parallelized sensing in future work.

Although not directly investigated in this work, studies have addressed the environmental and stability advantages of fluorinated aromatic compounds like PFB, which exhibit biodegradability and reduced toxicity when compared to per- and polyfluoroalkyl substances. This aligns with the growing demand for sustainable antifouling solutions. However, challenges such as inconsistent monolayer formation and the need for optimized antibody immobilization techniques remain areas for future investigation. The study underscores the importance of balancing antifouling performance with sensor functionality. Further work should focus on refining surface chemistries, expanding testing to diverse protein systems, and improving the robustness of mixed monolayers for real-world applications. The immediate next steps to advance the work presented in this thesis involve implementing an alternative methodology that enables multiple LSPR measurements in a time-efficient manner, while also allowing for replicates of each measurement. This approach would facilitate verification of the observed effectiveness of the synthesized materials. Despite of this, overall, this thesis

contributes to advancing antifouling technologies, offering insights into the design of next-generation biosensors with enhanced selectivity and durability.

Bibliography

(1) Choi, Y.; Tran, H.-V.; Lee, T. R. Self-Assembled Monolayer Coatings on Gold and Silica Surfaces for Antifouling Applications: A Review. *Coatings* **2022**, *12* (10), 1462. https://doi.org/10.3390/coatings12101462.

(2) Liu, B.; Liu, X.; Shi, S.; Huang, R.; Su, R.; Qi, W.; He, Z. Design and Mechanisms of Antifouling Materials for Surface Plasmon Resonance Sensors. *Acta Biomater* **2016**, *40*, 100–118. https://doi.org/10.1016/j.actbio.2016.02.035.

(3) Krsmanovic, M.; Biswas, D.; Ali, H.; Kumar, A.; Ghosh, R.; Dickerson, A. K. Hydrodynamics and Surface Properties Influence Biofilm Proliferation. *Adv Colloid Interface Sci* **2021**, *288*, 102336. https://doi.org/10.1016/j.cis.2020.102336.

(4) Cao, Z.; Cao, P. Research Progress on Low-Surface-Energy Antifouling Coatings for Ship Hulls: A Review. *Biomimetics* **2023**, *8* (6), 502. https://doi.org/10.3390/biomimetics8060502.

(5) Delgado, A.; Power, S.; Richards, C.; Daly, P.; Briciu-Burghina, C.; Delauré, Y.; Regan, F. Establishment of an Antifouling Performance Index Derived from the Assessment of Biofouling on Typical Marine Sensor Materials. *Science of The Total Environment* **2023**, *887*, 164059. https://doi.org/10.1016/j.scitotenv.2023.164059.

(6) Zeng, Q.; Zhu, Y.; Yu, B.; Sun, Y.; Ding, X.; Xu, C.; Wu, Y.-W.; Tang, Z.; Xu, F.-J. Antimicrobial and Antifouling Polymeric Agents for Surface Functionalization of Medical Implants. *Biomacromolecules* **2018**, *19* (7), 2805–2811. https://doi.org/10.1021/acs.biomac.8b00399.

(7) Jiang, C.; Wang, G.; Hein, R.; Liu, N.; Luo, X.; Davis, J. J. Antifouling Strategies for Selective *In Vitro* and *In Vivo* Sensing. *Chem Rev* **2020**, *120* (8), 3852–3889. https://doi.org/10.1021/acs.chemrev.9b00739.

(8) Song, G.; Han, H.; Ma, Z. Anti-Fouling Strategies of Electrochemical Sensors for Tumor Markers. *Sensors* **2023**, *23* (11), 5202. https://doi.org/10.3390/s23115202.

(9) McCann, B.; Tipper, B.; Shahbeigi, S.; Soleimani, M.; Jabbari, M.; Nasr Esfahani, M. A Review on Perception of Binding Kinetics in Affinity Biosensors: Challenges and Opportunities. *ACS Omega* **2025**, *10* (5), 4197–4216. https://doi.org/10.1021/acsomega.4c10040.

(10) Busscher, H. J.; Weerkamp, A. H. Specific and Non-Specific Interactions in Bacterial Adhesion to Solid Substrata. *FEMS Microbiol Lett* **1987**, *46* (2), 165–173. https://doi.org/10.1111/j.1574-6968.1987.tb02457.x.

(11) Kalasin, S.; Santore, M. M. Non-Specific Adhesion on Biomaterial Surfaces Driven by Small Amounts of Protein Adsorption. *Colloids Surf B Biointerfaces* **2009**, *73* (2), 229–236. https://doi.org/10.1016/j.colsurfb.2009.05.028.

(12) Chan, K. C.; Lucas, D. A.; Hise, D.; Schaefer, C. F.; Xiao, Z.; Janini, G. M.; Buetow, K. H.; Issaq, H. J.; Veenstra, T. D.; Conrads, T. P. Analysis of the Human Serum Proteome. *Clin Proteomics* **2004**, *1* (2), 101–225. https://doi.org/10.1385/CP:1:2:101.

(13) Contreras-Naranjo, J. E.; Aguilar, O. Suppressing Non-Specific Binding of Proteins onto Electrode Surfaces in the Development of Electrochemical Immunosensors. *Biosensors (Basel)* **2019**, *9* (1), 15. https://doi.org/10.3390/bios9010015.
(14) Dee, K. C.; Puleo, D. A.; Bizios, R. Protein-Surface Interactions. In *An Introduction to Tissue-Biomaterial Interactions: Tissue-Biomaterial*; John Wiley & Sons: Hoboken, NJ, USA, 2002; pp 37–52.
(15) Goovaerts, V.; Stroobants, K.; Absillis, G.; Parac-Vogt, T. N. Molecular Interactions between Serum Albumin Proteins and Keggin Type Polyoxometalates Studied Using Luminescence Spectroscopy. *Physical Chemistry Chemical Physics* **2013**, *15* (42), 18378. https://doi.org/10.1039/c3cp52848k.
(16) Frutiger, A.; Tanno, A.; Hwu, S.; Tiefenauer, R. F.; Vörös, J.; Nakatsuka, N. Nonspecific Binding—Fundamental Concepts and Consequences for Biosensing Applications. *Chem Rev* **2021**, *121* (13), 8095–8160. https://doi.org/10.1021/acs.chemrev.1c00044.
(17) Aydin, S. A Short History, Principles, and Types of ELISA, and Our Laboratory Experience with Peptide/Protein Analyses Using ELISA. *Peptides (N.Y.)* **2015**, *72*, 4–15. https://doi.org/10.1016/j.peptides.2015.04.012.
(18) Peng, P.; Liu, C.; Li, Z.; Xue, Z.; Mao, P.; Hu, J.; Xu, F.; Yao, C.; You, M. Emerging ELISA Derived Technologies for in Vitro Diagnostics. *TrAC Trends in Analytical Chemistry* **2022**, *152*, 116605. https://doi.org/10.1016/j.trac.2022.116605.
(19) Hosseini, S.; Vázquez-Villegas, P.; Rito-Palomares, M.; Martinez-Chapa, S. O. Advantages, Disadvantages and Modifications of Conventional ELISA; 2018; pp 67–115. https://doi.org/10.1007/978-981-10-6766-2_5.
(20) Kim, M. J.; Haizan, I.; Ahn, M. J.; Park, D.-H.; Choi, J.-H. Recent Advances in Lateral Flow Assays for Viral Protein Detection with Nanomaterial-Based Optical Sensors. *Biosensors (Basel)* **2024**, *14* (4), 197. https://doi.org/10.3390/bios14040197.
(21) Sajid, M.; Kawde, A.-N.; Daud, M. Designs, Formats and Applications of Lateral Flow Assay: A Literature Review. *Journal of Saudi Chemical Society* **2015**, *19* (6), 689–705. https://doi.org/10.1016/j.jscs.2014.09.001.
(22) EL-Sharif, H. F.; Aizawa, H.; Reddy, S. M. Spectroscopic and Quartz Crystal Microbalance (QCM) Characterisation of Protein-Based MIPs. *Sens Actuators B Chem* **2015**, *206*, 239–245. https://doi.org/10.1016/j.snb.2014.09.053.
(23) Cheng, C. I.; Chang, Y.-P.; Chu, Y.-H. Biomolecular Interactions and Tools for Their Recognition: Focus on the Quartz Crystal Microbalance and Its Diverse Surface Chemistries and Applications. *Chem. Soc. Rev.* **2012**, *41* (5), 1947–1971. https://doi.org/10.1039/C1CS15168A.
(24) Buchapudi, K. R.; Huang, X.; Yang, X.; Ji, H.-F.; Thundat, T. Microcantilever Biosensors for Chemicals and Bioorganisms. *Analyst* **2011**, *136* (8), 1539. https://doi.org/10.1039/c0an01007c.
(25) Hansen, K. M.; Thundat, T. Microcantilever Biosensors. *Methods* **2005**, *37* (1), 57–64. https://doi.org/10.1016/j.ymeth.2005.05.011.

(26) Petersen, R. Strategies Using Bio-Layer Interferometry Biosensor Technology for Vaccine Research and Development. *Biosensors (Basel)* **2017**, *7* (4), 49. https://doi.org/10.3390/bios7040049.
(27) Qu, J.-H.; Dillen, A.; Saeys, W.; Lammertyn, J.; Spasic, D. Advancements in SPR Biosensing Technology: An Overview of Recent Trends in Smart Layers Design, Multiplexing Concepts, Continuous Monitoring and in Vivo Sensing. *Anal Chim Acta* **2020**, *1104*, 10–27. https://doi.org/10.1016/j.aca.2019.12.067.
(28) Jug, A.; Bratkovič, T.; Ilaš, J. Biolayer Interferometry and Its Applications in Drug Discovery and Development. *TrAC Trends in Analytical Chemistry* **2024**, *176*, 117741. https://doi.org/10.1016/j.trac.2024.117741.
(29) Ronkainen, N. J.; Halsall, H. B.; Heineman, W. R. Electrochemical Biosensors. *Chem Soc Rev* **2010**, *39* (5), 1747. https://doi.org/10.1039/b714449k.
(30) Hammond, J. L.; Formisano, N.; Estrela, P.; Carrara, S.; Tkac, J. Electrochemical Biosensors and Nanobiosensors. *Essays Biochem* **2016**, *60* (1), 69–80. https://doi.org/10.1042/EBC20150008.
(31) Mayer, K. M.; Hafner, J. H. Localized Surface Plasmon Resonance Sensors. *Chem Rev* **2011**, *111* (6), 3828–3857. https://doi.org/10.1021/cr100313v.
(32) Murray, W. A.; Barnes, W. L. Plasmonic Materials. *Advanced Materials* **2007**, *19* (22), 3771–3782. https://doi.org/10.1002/adma.200700678.
(33) Kittel, C.; McEuen, P. *Introduction to Solid State Physics*, 8th ed.; Wiley: New York, 2005.
(34) Ringe, E. Shapes, Plasmonic Properties, and Reactivity of Magnesium Nanoparticles. *The Journal of Physical Chemistry C* **2020**, *124* (29), 15665–15679. https://doi.org/10.1021/acs.jpcc.0c03871.
(35) Yildizhan, Y.; Vajrala, V. S.; Geeurickx, E.; Declerck, C.; Duskunovic, N.; De Sutter, D.; Noppen, S.; Delport, F.; Schols, D.; Swinnen, J. V.; Eyckerman, S.; Hendrix, A.; Lammertyn, J.; Spasic, D. FO-SPR Biosensor Calibrated with Recombinant Extracellular Vesicles Enables Specific and Sensitive Detection Directly in Complex Matrices. *J Extracell Vesicles* **2021**, *10* (4), e12059. https://doi.org/10.1002/jev2.12059.
(36) Bolduc, O. R.; Masson, J.-F. Advances in Surface Plasmon Resonance Sensing with Nanoparticles and Thin Films: Nanomaterials, Surface Chemistry, and Hybrid Plasmonic Techniques. *Anal Chem* **2011**, *83* (21), 8057–8062. https://doi.org/10.1021/ac2012976.
(37) Charbonneau, R.; Lahoud, N.; Mattiussi, G.; Berini, P. Demonstration of Integrated Optics Elements Based on Long-Ranging Surface Plasmon Polaritons. *Opt Express* **2005**, *13* (3), 977. https://doi.org/10.1364/OPEX.13.000977.
(38) Singh, P. SPR Biosensors: Historical Perspectives and Current Challenges. *Sens Actuators B Chem* **2016**, *229*, 110–130. https://doi.org/10.1016/j.snb.2016.01.118.
(39) Singh, A. K.; Sharma, S. C. A Fixed Detector Kretschmann Configuration Optical System to Study Surface Plasmon Excitations. *Opt Laser Technol* **2014**, *56*, 256–262. https://doi.org/10.1016/j.optlastec.2013.08.004.

(40) Sebastian, M. T. Measurement of Microwave Dielectric Properties and Factors Affecting Them. In *Dielectric Materials for Wireless Communication*; Elsevier, 2008; pp 11–47. https://doi.org/10.1016/B978-0-08-045330-9.00002-9.
(41) Homola, J. Surface Plasmon Resonance Sensors for Detection of Chemical and Biological Species. *Chem Rev* **2008**, *108* (2), 462–493. https://doi.org/10.1021/cr068107d.
(42) Kuncová-Kallio, J.; Auer, S.; Spehar, A.; Qu, J. H.; Spasic, D.; Lammertyn, J. Optical and Acoustic Label-Free Instrumentation for Molecular Detection with a Focus on Food. In *Rapid Antibody-based Technologies in Food Analysis*; The Royal Society of Chemistry, 2019; pp 223–255. https://doi.org/10.1039/9781788016322-00223.
(43) Maier, S. A. *Plasmonics: Fundamentals and Applications*; Springer US: New York, NY, 2007. https://doi.org/10.1007/0-387-37825-1.
(44) Li, M.; Liu, M.; Qi, F.; Lin, F. R.; Jen, A. K.-Y. Self-Assembled Monolayers for Interfacial Engineering in Solution-Processed Thin-Film Electronic Devices: Design, Fabrication, and Applications. *Chem Rev* **2024**, *124* (5), 2138–2204. https://doi.org/10.1021/acs.chemrev.3c00396.
(45) Xu, J.; Li, H.-L. The Chemistry of Self-Assembled Long-Chain Alkanethiol Monolayers on Gold. *J Colloid Interface Sci* **1995**, *176* (1), 138–149. https://doi.org/10.1006/jcis.1995.0017.
(46) Ulman, A. Formation and Structure of Self-Assembled Monolayers. *Chem Rev* **1996**, *96* (4), 1533–1554. https://doi.org/10.1021/cr9502357.
(47) Chen, X.; Noy, A. Antifouling Strategies for Protecting Bioelectronic Devices. *APL Mater* **2021**, *9* (2), 020701. https://doi.org/10.1063/5.0029994.
(48) Smith, R. K.; Lewis, P. A.; Weiss, P. S. Patterning Self-Assembled Monolayers. *Prog Surf Sci* **2004**, *75* (1–2), 1–68. https://doi.org/10.1016/j.progsurf.2003.12.001.
(49) Wink, Th.; van Zuilen, S. J.; Bult, A.; van Bennekom, W. P. Self-Assembled Monolayers for Biosensors. *Analyst* **1997**, *122* (4), 43R-50R. https://doi.org/10.1039/a606964i.
(50) Gangula, A.; Chelli, J.; Bukka, S.; Poonthiyil, V.; Podila, R.; Kannan, R.; Rao, A. M. Thione–Gold Nanoparticles Interactions: Vroman-like Effect, Self-Assembly and Sensing. *J Mater Chem* **2012**, *22* (43), 22866. https://doi.org/10.1039/c2jm35279f.
(51) Lee, S. Y.; Tsalu, P. V.; Kim, G. W.; Seo, M. J.; Hong, J. W.; Ha, J. W. Tuning Chemical Interface Damping: Interfacial Electronic Effects of Adsorbate Molecules and Sharp Tips of Single Gold Bipyramids. *Nano Lett* **2019**, *19* (4), 2568–2574. https://doi.org/10.1021/acs.nanolett.9b00338.
(52) Ganesh, V.; Pal, S. K.; Kumar, S.; Lakshminarayanan, V. Self-Assembled Monolayers (SAMs) of Alkoxycyanobiphenyl Thiols on Gold—A Study of Electron Transfer Reaction Using Cyclic Voltammetry and Electrochemical Impedance Spectroscopy. *J Colloid Interface Sci* **2006**, *296* (1), 195–203. https://doi.org/10.1016/j.jcis.2005.08.051.
(53) Käfer, D.; Witte, G.; Cyganik, P.; Terfort, A.; Wöll, C. A Comprehensive Study of Self-Assembled Monolayers of Anthracenethiol on Gold: Solvent Effects, Structure, and Stability. *J*

Am Chem Soc **2006**, *128* (5), 1723–1732. https://doi.org/10.1021/ja0571592.
(54) Schwartz, D. K. Mechanisms and Kinetics of Self-Assembled Monolayer Formation. *Annu Rev Phys Chem* **2001**, *52* (1), 107–137. https://doi.org/10.1146/annurev.physchem.52.1.107.
(55) Xu, S.; Cruchon-Dupeyrat, S. J. N.; Garno, J. C.; Liu, G.-Y.; Kane Jennings, G.; Yong, T.-H.; Laibinis, P. E. *In Situ* Studies of Thiol Self-Assembly on Gold from Solution Using Atomic Force Microscopy. *J Chem Phys* **1998**, *108* (12), 5002–5012. https://doi.org/10.1063/1.475908.
(56) Singh, A.; Lee, I. S.; Kim, K.; Myerson, A. S. Crystal Growth on Self-Assembled Monolayers. *CrystEngComm* **2011**, *13* (1), 24–32. https://doi.org/10.1039/C0CE00030B.
(57) Rozlosnik, N.; Gerstenberg, M. C.; Larsen, N. B. Effect of Solvents and Concentration on the Formation of a Self-Assembled Monolayer of Octadecylsiloxane on Silicon (001). *Langmuir* **2003**, *19* (4), 1182–1188. https://doi.org/10.1021/la025906s.
(58) Yan, D.; Saunders, J. A.; Jennings, G. K. Formation and Stability of Hexadecanethiolate SAMs Prepared in Aqueous Micellar Solutions of $C_{12}E_6$. *Langmuir* **2003**, *19* (22), 9290–9296. https://doi.org/10.1021/la0349471.
(59) Schmitt, F.-J.; Häussling, L.; Ringsdorf, H.; Knoll, W. Surface Plasmon Studies of Specific Recognition Reactions at Self-Assembled Monolayers on Gold. *Thin Solid Films* **1992**, *210–211*, 815–817. https://doi.org/10.1016/0040-6090(92)90412-5.
(60) Kanari, Y.; Shoji, Y.; Ode, H.; Miyake, T.; Tanii, T.; Hoshino, T.; Ohdomari, I. Protein Adsorption on Self-Assembled Monolayers Induced by Surface Water Molecule. *Jpn J Appl Phys* **2007**, *46* (9S), 6303. https://doi.org/10.1143/JJAP.46.6303.
(61) Samanta, D.; Sarkar, A. Immobilization of Bio-Macromolecules on Self-Assembled Monolayers: Methods and Sensor Applications. *Chem Soc Rev* **2011**, *40* (5), 2567. https://doi.org/10.1039/c0cs00056f.
(62) Prime, K. L.; Whitesides, G. M. Self-Assembled Organic Monolayers: Model Systems for Studying Adsorption of Proteins at Aurfaces. *Science (1979)* **1991**, *252* (5009), 1164–1167. https://doi.org/10.1126/science.252.5009.1164.
(63) Billah, Md. M.; Hays, H. C. W.; Hodges, C. S.; Ponnambalam, S.; Vohra, R.; Millner, P. A. Mixed Self-Assembled Monolayer (MSAM) Based Impedimetric Immunosensors for Cardiac Troponin I (CTnI) and Soluble Lectin-like Oxidized Low-Density Lipoprotein Receptor-1 (SLOX-1). *Sens Actuators B Chem* **2012**, *173*, 361–366. https://doi.org/10.1016/j.snb.2012.07.017.
(64) Thomas, R. C.; Sun, L.; Crooks, R. M.; Ricco, A. J. Real-Time Measurements of the Gas-Phase Adsorption of n-Alkylthiol Mono- and Multilayers on Gold. *Langmuir* **1991**, *7* (4), 620–622. https://doi.org/10.1021/la00052a004.
(65) Mrksich, M.; Sigal, G. B.; Whitesides, G. M. Surface Plasmon Resonance Permits in Situ Measurement of Protein Adsorption on Self-Assembled Monolayers of Alkanethiolates on Gold. *Langmuir* **1995**, *11* (11), 4383–4385. https://doi.org/10.1021/la00011a034.
(66) Mandler, D.; Kraus-Ophir, S. Self-Assembled Monolayers (SAMs) for Electrochemical Sensing. *Journal of Solid State Electrochemistry*

2011, *15* (7–8), 1535–1558. https://doi.org/10.1007/s10008-011-1493-6.
(67) Wagner, P.; Hegner, M.; Kernen, P.; Zaugg, F.; Semenza, G. Covalent Immobilization of Native Biomolecules onto Au(111) via N-Hydroxysuccinimide Ester Functionalized Self-Assembled Monolayers for Scanning Probe Microscopy. *Biophys J* **1996**, *70* (5), 2052–2066. https://doi.org/10.1016/S0006-3495(96)79810-7.
(68) Holmberg, A.; Blomstergren, A.; Nord, O.; Lukacs, M.; Lundeberg, J.; Uhlén, M. The Biotin-Streptavidin Interaction Can Be Reversibly Broken Using Water at Elevated Temperatures. *Electrophoresis* **2005**, *26* (3), 501–510. https://doi.org/10.1002/elps.200410070.
(69) Dutra, R. F.; Kubota, L. T. An SPR Immunosensor for Human Cardiac Troponin T Using Specific Binding Avidin to Biotin at Carboxymethyldextran-Modified Gold Chip. *Clinica Chimica Acta* **2007**, *376* (1–2), 114–120. https://doi.org/10.1016/j.cca.2006.07.029.
(70) Kondo, T.; Yamada, R.; Uosaki, K. Self-Assembled Monolayer (SAM). In *Organized Organic Ultrathin Films*; Wiley, 2013; pp 7–42. https://doi.org/10.1002/9783527654666.ch2.
(71) Liu, J. T.; Chen, C. J.; Ikoma, T.; Yoshioka, T.; Cross, J. S.; Chang, S.-J.; Tsai, J.-Z.; Tanaka, J. Surface Plasmon Resonance Biosensor with High Anti-Fouling Ability for the Detection of Cardiac Marker Troponin T. *Anal Chim Acta* **2011**, *703* (1), 80–86. https://doi.org/10.1016/j.aca.2011.07.019.
(72) Tiernan, H.; Byrne, B.; Kazarian, S. G. ATR-FTIR Spectroscopy and Spectroscopic Imaging for the Analysis of Biopharmaceuticals. *Spectrochim Acta A Mol Biomol Spectrosc* **2020**, *241*, 118636. https://doi.org/10.1016/j.saa.2020.118636.
(73) Politano, G. G.; Versace, C. Spectroscopic Ellipsometry: Advancements, Applications and Future Prospects in Optical Characterization. *Spectroscopy Journal* **2023**, *1* (3), 163–181. https://doi.org/10.3390/spectroscj1030014.
(74) McDonagh, P. F.; Williams, S. K. The Preparation and Use of Fluorescent-Protein Conjugates for Microvascular Research. *Microvasc Res* **1984**, *27* (1), 14–27. https://doi.org/10.1016/0026-2862(84)90038-4.
(75) Xing, C.-M.; Meng, F.-N.; Quan, M.; Ding, K.; Dang, Y.; Gong, Y.-K. Quantitative Fabrication, Performance Optimization and Comparison of PEG and Zwitterionic Polymer Antifouling Coatings. *Acta Biomater* **2017**, *59*, 129–138. https://doi.org/10.1016/j.actbio.2017.06.034.
(76) Gudipati, C. S.; Finlay, J. A.; Callow, J. A.; Callow, M. E.; Wooley, K. L. The Antifouling and Fouling-Release Perfomance of Hyperbranched Fluoropolymer (HBFP)−Poly(Ethylene Glycol) (PEG) Composite Coatings Evaluated by Adsorption of Biomacromolecules and the Green Fouling Alga *Ulva*. *Langmuir* **2005**, *21* (7), 3044–3053. https://doi.org/10.1021/la048015o.
(77) Love, J. C.; Estroff, L. A.; Kriebel, J. K.; Nuzzo, R. G.; Whitesides, G. M. Self-Assembled Monolayers of Thiolates on Metals as a Form of Nanotechnology. *Chem Rev* **2005**, *105* (4), 1103–1170. https://doi.org/10.1021/cr0300789.

(78) Lin, P.-H.; Li, B.-R. Antifouling Strategies in Advanced Electrochemical Sensors and Biosensors. *Analyst* **2020**, *145* (4), 1110–1120. https://doi.org/10.1039/C9AN02017A.
(79) Jeyachandran, Y. L.; Mielczarski, J. A.; Mielczarski, E.; Rai, B. Efficiency of Blocking of Non-Specific Interaction of Different Proteins by BSA Adsorbed on Hydrophobic and Hydrophilic Surfaces. *J Colloid Interface Sci* **2010**, *341* (1), 136–142. https://doi.org/10.1016/j.jcis.2009.09.007.
(80) Jachimska, B.; Pajor, A. Physico-Chemical Characterization of Bovine Serum Albumin in Solution and as Deposited on Surfaces. *Bioelectrochemistry* **2012**, *87*, 138–146. https://doi.org/10.1016/j.bioelechem.2011.09.004.
(81) D'Agata, R.; Bellassai, N.; Jungbluth, V.; Spoto, G. Recent Advances in Antifouling Materials for Surface Plasmon Resonance Biosensing in Clinical Diagnostics and Food Safety. *Polymers (Basel)* **2021**, *13* (12), 1929. https://doi.org/10.3390/polym13121929.
(82) Wen, J.; Huang, S.; Hu, Q.; He, W.; Wei, Z.; Wang, L.; Lu, J.; Yue, X.; Men, S.; Miao, C.; He, Z.; Yang, X.; Zhai, G.; Li, J.; Ye, L. Recent Advances in Zwitterionic Polymers-Based Non-Fouling Coating Strategies for Biomedical Applications. *Mater Today Chem* **2024**, *40*, 102232. https://doi.org/10.1016/j.mtchem.2024.102232.
(83) Guerrini, L.; Alvarez-Puebla, R. A.; Pazos-Perez, N. Surface Modifications of Nanoparticles for Stability in Biological Fluids. *Materials* **2018**, *11* (7), 1154. https://doi.org/10.3390/ma11071154.
(84) Bevilacqua, P.; Nuzzo, S.; Torino, E.; Condorelli, G.; Salvatore, M.; Grimaldi, A. M. Antifouling Strategies of Nanoparticles for Diagnostic and Therapeutic Application: A Systematic Review of the Literature. *Nanomaterials* **2021**, *11* (3), 780. https://doi.org/10.3390/nano11030780.
(85) Lowe, S.; O'Brien-Simpson, N. M.; Connal, L. A. Antibiofouling Polymer Interfaces: Poly(Ethylene Glycol) and Other Promising Candidates. *Polym Chem* **2015**, *6* (2), 198–212. https://doi.org/10.1039/C4PY01356E.
(86) Ulbricht, J.; Jordan, R.; Luxenhofer, R. On the Biodegradability of Polyethylene Glycol, Polypeptoids and Poly(2-Oxazoline)s. *Biomaterials* **2014**, *35* (17), 4848–4861. https://doi.org/10.1016/j.biomaterials.2014.02.029.
(87) Li, L.; Chen, S.; Jiang, S. Protein Interactions with Oligo(Ethylene Glycol) (OEG) Self-Assembled Monolayers: OEG Stability, Surface Packing Density and Protein Adsorption. *J Biomater Sci Polym Ed* **2007**, *18* (11), 1415–1427. https://doi.org/10.1163/156856207782246795.
(88) Wang, Y.-S.; Yau, S.; Chau, L.-K.; Mohamed, A.; Huang, C.-J. Functional Biointerfaces Based on Mixed Zwitterionic Self-Assembled Monolayers for Biosensing Applications. *Langmuir* **2019**, *35* (5), 1652–1661. https://doi.org/10.1021/acs.langmuir.8b01779.
(89) Joshi, S.; Pellacani, P.; van Beek, T. A.; Zuilhof, H.; Nielen, M. W. F. Surface Characterization and Antifouling Properties of Nanostructured Gold Chips for Imaging Surface Plasmon Resonance Biosensing. *Sens Actuators B Chem* **2015**, *209*, 505–514. https://doi.org/10.1016/j.snb.2014.11.133.

(90) van Andel, E.; Lange, S. C.; Pujari, S. P.; Tijhaar, E. J.; Smulders, M. M. J.; Savelkoul, H. F. J.; Zuilhof, H. Systematic Comparison of Zwitterionic and Non-Zwitterionic Antifouling Polymer Brushes on a Bead-Based Platform. *Langmuir* **2019**, *35* (5), 1181–1191. https://doi.org/10.1021/acs.langmuir.8b01832.
(91) Cametti, M.; Crousse, B.; Metrangolo, P.; Milani, R.; Resnati, G. The Fluorous Effect in Biomolecular Applications. *Chem. Soc. Rev.* **2012**, *41* (1), 31–42. https://doi.org/10.1039/C1CS15084G.
(92) Santana Vega, M.; Bueno Alejo, C.; Taladriz-Sender, A.; Chaplin, A.; Farrow, C.; Axer, A.; Burley, G. A.; Dominguez, C.; Kara, H.; Paschalis, V.; Tubasum, S.; Eperon, I.; Hudson, A. J.; Clark, A. W. A New Platform for Single Molecule Measurements Using the Fluorous Effect. In *Single Molecule Spectroscopy and Superresolution Imaging XVI*; Gregor, I., Erdmann, R., Koberling, F., Eds.; SPIE, 2023; p 21. https://doi.org/10.1117/12.2647953.
(93) Zhou, L.; Triozzi, A.; Figueiredo, M.; Emrick, T. Fluorinated Polymer Zwitterions: Choline Phosphates and Phosphorylcholines. *ACS Macro Lett* **2021**, *10* (10), 1204–1209. https://doi.org/10.1021/acsmacrolett.1c00451.
(94) Zhou, L.; Yang, Z.; Pagaduan, J. N.; Emrick, T. Fluorinated Zwitterionic Polymers as Dynamic Surface Coatings. *Polym Chem* **2023**, *14* (1), 32–36. https://doi.org/10.1039/D2PY01197B.
(95) Shakeri, A.; Jarad, N. A.; Terryberry, J.; Khan, S.; Leung, A.; Chen, S.; Didar, T. F. Antibody Micropatterned Lubricant-Infused Biosensors Enable Sub-Picogram Immunofluorescence Detection of Interleukin 6 in Human Whole Plasma. *Small* **2020**, *16* (45), 2003844. https://doi.org/10.1002/smll.202003844.
(96) Gentilini, C.; Evangelista, F.; Rudolf, P.; Franchi, P.; Lucarini, M.; Pasquato, L. Water-Soluble Gold Nanoparticles Protected by Fluorinated Amphiphilic Thiolates. *J Am Chem Soc* **2008**, *130* (46), 15678–15682. https://doi.org/10.1021/ja8058364.
(97) Hoque, E.; DeRose, J. A.; Hoffmann, P.; Bhushan, B.; Mathieu, H. J. Chemical Stability of Nonwetting, Low Adhesion Self-Assembled Monolayer Films Formed by Perfluoroalkylsilanization of Copper. *J Chem Phys* **2007**, *126* (11), 114706. https://doi.org/10.1063/1.2566333.
(98) Zenasni, O.; Jamison, A. C.; Lee, T. R. The Impact of Fluorination on the Structure and Properties of Self-Assembled Monolayer Films. *Soft Matter* **2013**, *9* (28), 6356. https://doi.org/10.1039/c3sm00054k.
(99) Pujari, S. P.; Spruijt, E.; Cohen Stuart, M. A.; van Rijn, C. J. M.; Paulusse, J. M. J.; Zuilhof, H. Ultralow Adhesion and Friction of Fluoro-Hydro Alkyne-Derived Self-Assembled Monolayers on H-Terminated Si(111). *Langmuir* **2012**, *28* (51), 17690–17700. https://doi.org/10.1021/la303893u.
(100) Weinstein, R. D.; Moriarty, J.; Cushnie, E.; Colorado, , Ramon; Lee, T. R.; Patel, M.; Alesi, W. R.; Jennings, G. K. Structure, Wettability, and Electrochemical Barrier Properties of Self-Assembled Monolayers Prepared from Partially Fluorinated Hexadecanethiols. *J Phys Chem B* **2003**, *107* (42), 11626–11632. https://doi.org/10.1021/jp035067y.
(101) Pujari, S. P.; van Andel, E.; Yaffe, O.; Cahen, D.; Weidner, T.; van Rijn, C. J. M.; Zuilhof, H. Mono-Fluorinated Alkyne-Derived SAMs on Oxide-Free Si(111) Surfaces: Preparation, Characterization and

Tuning of the Si Workfunction. *Langmuir* **2013**, *29* (2), 570–580. https://doi.org/10.1021/la303403v.
(102) Bensebaa, F.; Ellis, T. H.; Badia, A.; Lennox, R. B. Thermal Treatment of *n* -Alkanethiolate Monolayers on Gold, As Observed by Infrared Spectroscopy. *Langmuir* **1998**, *14* (9), 2361–2367. https://doi.org/10.1021/la9711589.
(103) O'Hagan, D. Understanding Organofluorine Chemistry. An Introduction to the C–F Bond. *Chem. Soc. Rev.* **2008**, *37* (2), 308–319. https://doi.org/10.1039/B711844A.
(104) Panieri, E.; Baralic, K.; Djukic-Cosic, D.; Buha Djordjevic, A.; Saso, L. PFAS Molecules: A Major Concern for the Human Health and the Environment. *Toxics* **2022**, *10* (2), 44. https://doi.org/10.3390/toxics10020044.
(105) Bock, A. R.; Laird, B. E. PFAS Regulations: Past and Present and Their Impact on Fluoropolymers. In *Perfluoroalkyl Substances*; The Royal Society of Chemistry, 2022; pp 1–21. https://doi.org/10.1039/9781839167591-00001.
(106) Ruan, T.; Field, J.; Cousins, I.; Lohmann, R.; Jiang, G. Emerging Contaminants: Fluorinated Alternatives to Existing PFAS. *Environ Sci Technol* **2022**, *56* (10), 6001–6003. https://doi.org/10.1021/acs.est.2c03041.
(107) Carvalho, M. F.; Alves, C. C. T.; Ferreira, M. I. M.; De Marco, P.; Castro, P. M. L. Isolation and Initial Characterization of a Bacterial Consortium Able To Mineralize Fluorobenzene. *Appl Environ Microbiol* **2002**, *68* (1), 102–105. https://doi.org/10.1128/AEM.68.1.102-105.2002.
(108) Wackett, L. P. Strategies for the Biodegradation of Polyfluorinated Compounds. *Microorganisms* **2022**, *10* (8), 1664. https://doi.org/10.3390/microorganisms10081664.
(109) Lejars, M.; Margaillan, A.; Bressy, C. Fouling Release Coatings: A Nontoxic Alternative to Biocidal Antifouling Coatings. *Chem Rev* **2012**, *112* (8), 4347–4390. https://doi.org/10.1021/cr200350v.
(110) Bartels, J. W.; Cheng, C.; Powell, K. T.; Xu, J.; Wooley, K. L. Hyperbranched Fluoropolymers and Their Hybridization into Complex Amphiphilic Crosslinked Copolymer Networks. *Macromol Chem Phys* **2007**, *208* (15), 1676–1687. https://doi.org/10.1002/macp.200700104.
(111) Pollack, K. A.; Imbesi, P. M.; Raymond, J. E.; Wooley, K. L. Hyperbranched Fluoropolymer-Polydimethylsiloxane-Poly(Ethylene Glycol) Cross-Linked Terpolymer Networks Designed for Marine and Biomedical Applications: Heterogeneous Nontoxic Antibiofouling Surfaces. *ACS Appl Mater Interfaces* **2014**, *6* (21), 19265–19274. https://doi.org/10.1021/am505296n.
(112) Gudipati, C. S.; Greenlief, C. M.; Johnson, J. A.; Prayongpan, P.; Wooley, K. L. Hyperbranched Fluoropolymer and Linear Poly(Ethylene Glycol) Based Amphiphilic Crosslinked Networks as Efficient Antifouling Coatings: An Insight into the Surface Compositions, Topographies, and Morphologies. *J Polym Sci A Polym Chem* **2004**, *42* (24), 6193–6208. https://doi.org/10.1002/pola.20466.
(113) Arifuzzaman, S.; Özçam, A. E.; Efimenko, K.; Fischer, D. A.; Genzer, J. Formation of Surface-Grafted Polymeric Amphiphilic Coatings

Comprising Ethylene Glycol and Fluorinated Groups and Their Response to Protein Adsorption. *Biointerphases* **2009**, *4* (2), FA33–FA44. https://doi.org/10.1116/1.3114502.
(114) Gu, Y.; Zhou, S. Novel Marine Antifouling Coatings. In *Functional Polymer Coatings*; Wiley, 2015; pp 296–337. https://doi.org/10.1002/9781118883051.ch11.
(115) Murty, K. V. G. K.; Venkataramanan, M.; Pradeep, T. Self-Assembled Monolayers of 1,4-Benzenedimethanethiol on Polycrystalline Silver and Gold Films: An Investigation of Structure, Stability, Dynamics, and Reactivity. *Langmuir* **1998**, *14* (19), 5446–5456. https://doi.org/10.1021/la980249i.
(116) Kang, H.; Kim, Y.; Hara, M.; Noh, J. Two-Dimensional Ordering of Pentafluorobenzenethiol Self-Assembled Monolayers on Au(1 1 1) Prepared by Ambient-Pressure Vapor Deposition. *Ultramicroscopy* **2010**, *110* (6), 666–669. https://doi.org/10.1016/j.ultramic.2010.02.029.
(117) Sohn, C. H.; Chung, C. K.; Yin, S.; Ramachandran, P.; Loo, J. A.; Beauchamp, J. L. Probing the Mechanism of Electron Capture and Electron Transfer Dissociation Using Tags with Variable Electron Affinity. *J Am Chem Soc* **2009**, *131* (15), 5444–5459. https://doi.org/10.1021/ja806534r.
(118) Molnár, I. G.; Gilmour, R. Catalytic Difluorination of Olefins. *J Am Chem Soc* **2016**, *138* (15), 5004–5007. https://doi.org/10.1021/jacs.6b01183.
(119) Rakhimov, R. G.; Galin, F. Z.; Tomilov, Yu. V.; Le, V. T. Synthesis of Ethophenprox. *Russian Journal of Organic Chemistry* **2002**, *38* (11), 1629–1634. https://doi.org/10.1023/A:1022562101602.
(120) Lin, Y. A.; Chalker, J. M.; Floyd, N.; Bernardes, G. J. L.; Davis, B. G. Allyl Sulfides Are Privileged Substrates in Aqueous Cross-Metathesis: Application to Site-Selective Protein Modification. *J Am Chem Soc* **2008**, *130* (30), 9642–9643. https://doi.org/10.1021/ja8026168.
(121) Unser, S.; Bruzas, I.; He, J.; Sagle, L. Localized Surface Plasmon Resonance Biosensing: Current Challenges and Approaches. *Sensors* **2015**, *15* (7), 15684–15716. https://doi.org/10.3390/s150715684.
(122) Sperling, J. R.; Osborne, D. D.; Aekbote, B.; Perri, A. E.; Setford, R. A.; Gao, H.; Wilson, L. T.; Sipperley, C. M.; Schick, R. J.; Gauchotte-Lindsay, C.; Peveler, W. J.; Clark, A. W. An Integrated Plasmonic Sensing Array for Chemical Fingerprinting and Flavor Profiling in Beverages and Other Liquids. *ACS Sens* **2025**, *10* (10), 7936–7946. https://doi.org/10.1021/acssensors.5c02485.